NUMERICAL MODELING OF PILLAR STRESS REDISTRIBUTION DURING THE RETREAT MINING PROCESS

by

Rahel Dean-Pelikan

A thesis submitted to the Faculty and the Board of Trustees of the Colorado School of Mines in partial fulfillment of the requirements for the degree of Master of Science (Underground Construction and Tunnel Engineering).

Golden, Colorado

Date _____

Signed: _____

Rahel Dean-Pelikan

Signed: _____

Dr. Gabriel Walton
Thesis Advisor

Golden, Colarado

Date _____

Signed: _____

Dr. Wendy Bohrson
Professor and Department Head
Department of Geology and Geological Engineering

ABSTRACT

Retreat mining is a mining method typical to underground room and pillar mines. The process of retreat mining inherently creates an unstable environment as pillars, which are initially left in place to provide support for the mine, are removed. As a result, retreat mining is associated with high risk, safety concerns, and ground control issues. Safety is a critical concern in the mining industry to ensure all workers make it home, safe, every day. As a result, it is important to conduct research to advance the understanding of the mechanics associated with retreat mining and improve the safety of the method.

Previous research regarding to retreat mining in room and pillar mines is limited. Research has mainly focused on modeling individual components of retreat mining (i.e. roof/floor influence, gob development, retreat method). Research has resulted in the overall progression of modern-day pillar mechanics and design, which has resulted in improvement in the design of mines employing retreat operations. However, there is a relative lack of research on investigating the retreat phase of room and pillar mining and how the entire retreat process impacts the global and local stresses in the mine. This thesis aims to contribute to closing this gap.

A preliminary study was performed in order to understand the influences of model type (elastic versus inelastic), pillar width to height (W/H) ratio, and roof properties on the overall retreat mining process. The aim of the study was to constrain how parameters influence stress redistribution during the retreat mining process through the use of numerical modeling. It was found that inelastic numerical models were able to capture the yield propagation within a pillar

array that allows for potential investigation of pillar failure. The W/H pillar ratio and roof properties were seen to influence stress redistribution through the various modeling attempts.

In addition, further investigations on the impacts of retreat mining on global and local scale stress transfer and damage were performed. This was done through the development of a numerical model of Mine C, a room and pillar coal mine in the Western U.S., and the calibration of the numerical model to field data. A calibrated model was established and was found to be in good agreement with the field data. Throughout the retreat process, stress redistribution and yield was most prominent in the pillars near the active mining area. The minimal changes in stress and yield in pillars outside of the active mining area suggest an adequate mine design that was able to isolate the impacts of retreat mining to within the active mining area.

The resulting calibrated model provides a unique opportunity to investigate various components that are unique to retreat operations, such as depillaring sequence, mine design, and support influence. The developed numerical model can be used for future research focused on rock mechanics and ground control in the context of retreat mining.

CO-AUTHORSHIP

The thesis “Numerical modeling of pillar stress redistribution during the retreat mining process” is the product of research conducted by the author, Rahel Dean-Pelikan. The individuals (co-authors) as mentioned below, also had a significant contribution in this research in terms of scientific and editorial feedback. The author has permission from all the co-authors to use the materials (data, figures, text, etc.) as presented in Appendix A.

Dr. Gabriel Walton

Assistant Professor and Thesis Advisor

Department of Geology and Geological Engineering

Colorado School of Mines

Golden – 80401, Colorado, USA

TABLE OF CONTENTS

LIST OF FIGURES

LIST OF TABLES

ACKNOWLEDGEMENTS

The research presented in this thesis has been made possible due to the generous funding by the National Institute for Occupational Safety and Health (NIOSH). The modeling effort for this study was conducted in part using educational licenses of FLAC^{3D} provided by Itasca Consulting, Ltd. I appreciate Itasca's support in this capacity.

I would like to first acknowledge the Colorado School of Mines for allowing me the opportunity to pursue graduate studies and expand my knowledge. I would like to express my sincere gratitude to my advisor, Dr. Gabriel Walton, for accepting me as one of his studies in his research group and all the guidance he has provided throughout my time at the Colorado School of Mines. He provided me great opportunities to further challenge myself and grow as an individual, researcher, and critical thinker. I could not have imagined a better advisor to work alongside.

I am also thankful for Dr. Jürgen Brune and Dr. Jamal Rostami for serving on my M.Sc. committee and providing guidance throughout my research. I would also like to thank Tim Burgess, Dr. Mark Larson, and Samantha Wilson for their technical input. I am extremely thankful for Dr. Sankhaneel Sinha. His guidance and knowledge have made a significant impact on me and my research efforts.

I want to thank all of my professors from the South Dakota School of Mines and Technology that prepared me for graduate school. I would like to specifically thank all of the professors in the Mining Engineering department for inspiring future mining engineers and preparing me for not only higher education but also for my career and life in generally.

I want to express special regards to the wonderful individuals that I have had the pleasure of working alongside: Rami Abousleiman, Caroline Bedwell, Ryan O'Connell, Isabella West, Luke Weidner, Claire Vavrus. These individuals have all made a significant impact through their words of encouragement and own hard work and dedication. I am proud to have worked with such an amazing group of people.

To all the people I have met during my time at the Colorado School of Mines, I thank you for making my graduate experience one I will never forget. I want to thank all the individuals I have had the pleasure of serving on the Graduate Student Government with. You all truly left your mark on my journey during those crazy, unprecedented times. To my amazing friend groups from all over, your constant belief in me and support you provide has meant the world to me. Special shout out to my lovely ladies: Laetitia Galeazzi, Emily Hagge, Kylie Johnson, Savanna Wilkinson, and Sasha Vreugdenhil.

Lastly, I would not be here without my amazing family. My parents, Julie Dean-Pelikan and Louis Pelikan, my brothers, Lajos Pelikan and Tas Pelikan, my sister-in-law, Sujey Pelikan, and to all my cats. Their constant love and support have helped me get through life. They will forever and always be my rock.

DEDICATION

To the family that makes me strive to do better,

To the family that has been the voice of encouragement,

To the family that will always be my #1 fans,

To the Pelikan Squadron, that has made me who I am today,

I would not be here without you all: Julie, Louis, Lajos, Tas, and Sujey.

CHAPTER 1

THESIS INTRODUCTION

1.1 Background

Mining has been a key component in the growth of civilization. The history of mining parallels the history of civilization and is reflected in many important cultural eras: the Stone Age (prior to 4000 B.C.E.), the Bronze Age (4000-5000 B.C.E), the Iron Age (1500 B.C.E to 1780 C.E.), the Steel Age (1780-1945), and the Nuclear Age (1945-present). The materials derived from mining are used in the development of many important goods including tools, weapons, decoration, currency, structures, energy, machinery, electronics, and nuclear fission. Mining has also provided incentives that has led to the settlement of California, Alaska, South Africa, Australia, and the Canadian Klondike. The current world we live in, with our structures, modern technology, modes of transportation, for example, would not be possible without mining (Hartman and Mutmansky, 2002).

There are two types of overarching mining methods: surface and underground. Surface mining is the predominant method of extracting minerals worldwide. Surface mining, typical of massive orebodies, is associated with high productivity, low operating cost, and good safety conditions. When orebodies become more variable or extend to greater depths, underground mining is generally preferred. One of the most advantageous aspects of underground mining is the variety of ore bodies that can be mined using a multitude of mining methods. Disadvantages of underground mining are greater costs and worse safety conditions. Figure 1.1 and 1.2 highlights the number of injuries and injury rate associated with surface and underground mines, as well as the number of fatalities and fatality rate. Sectors included in the statistics are coal, metal, nonmetal, and stone.

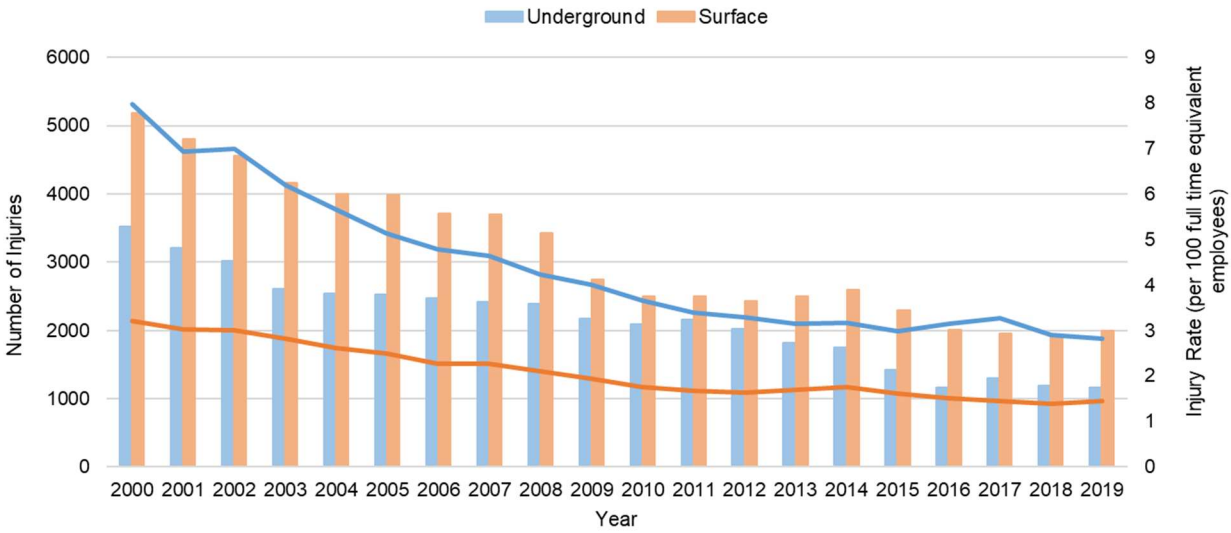

Figure 1.1: Number of injuries (bar graph) and injury rate (line graph) for surface mines in the U.S., excluding office employees, from 2000-2019 (NIOSH, 2021).

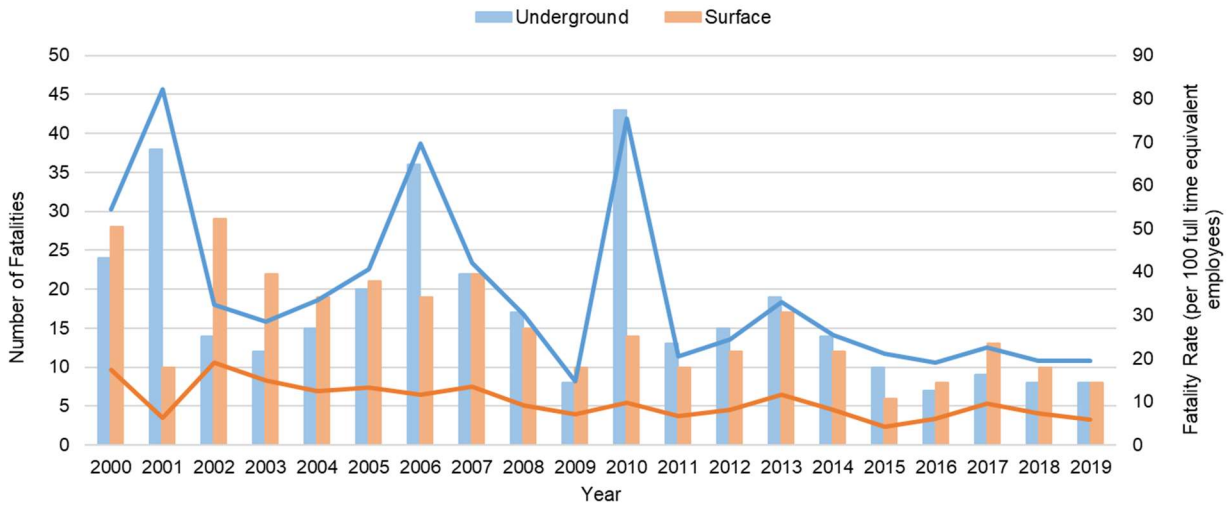

Figure 1.2: Number of fatalities (bar graph) and fatality rate (line graph) for surface mines in the U.S., excluding office employees, from 2000-2019 (NIOSH, 2021).

Figure 1.1 and Figure 1.2 shows that a large number of injuries and fatalities occur as a result of surface mining. However, underground mining has a significantly higher rate of injuries and fatalities. The spikes observed in the number of underground fatalities (Figure 1.2) relate to mine disasters: Jim Walter Resources Blue Creek No. 5 Mine (2001), Sago Mine (2006), Aracoma Alma Mine No. 1 (2006), Darby Mine No. 1 (2006), Crandall Canyon (2007), Upper Big Branch

Mine (2010). It is apparent that an underground worker is more likely to experience an injury or fatality than a surface worker.

1.2 Motivation

Important to the mining industry is safety and ensuring everyone returns home, to their friends and family. The work performed in this thesis is towards ensuring miner safety. The motivation behind this thesis can be understood through a deeper investigation of the safety statistics surrounding underground mining, and specifically retreat mining.

1.2.1 Underground Mining Safety Statistics

As previously mentioned, underground mining has a greater injury and fatality rate than surface mining. When considering the statistics of underground mining specifically, the injury and fatality statistics can be broken down by sector, as shown in Figure 1.3 and Figure 1.4. It is apparent that underground coal mining is less safe than the other sectors. Thus, working in an underground coal mine is associated with more risk. Figure 1.5 highlights the fatality statistics pertaining to underground coal mines. The fatality rate is fairly irregular over time and does not follow a consistent downward trend. In fact, the number of fatalities increased from 2018 to 2019. Figure 1.6 and Figure 1.7 break down injuries and fatalities by accident class. Ground falls are a significant contributor towards injuries and fatalities: third most contributor for injuries and the first for fatalities.

The high number of injuries, injury rate, fatalities, and fatality rate suggests that more work and research needs to be performed to improve the safety of underground coal mining. It is imperative to ensure the safety of all mines and miners, and it is apparent from the entirety of the presented safety statistics that underground coal mines are the most hazardous sector of the mining industry. Additionally, hazards pertaining to ground falls are a significant factor towards

underground safety. As a result, this thesis will focus on underground coal mining.

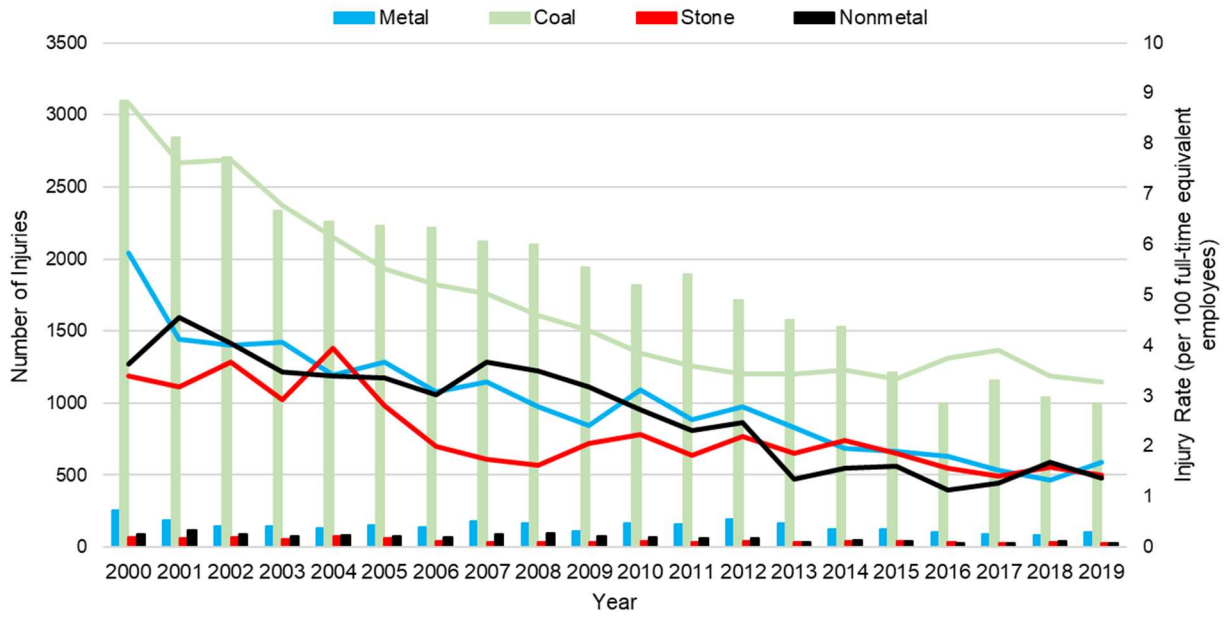

Figure 1.3: Number of injuries (bar graph) and injury rate (line graph) per sector for underground mines in the U.S., excluding office employees, from 2000-2019 (NIOSH, 2021).

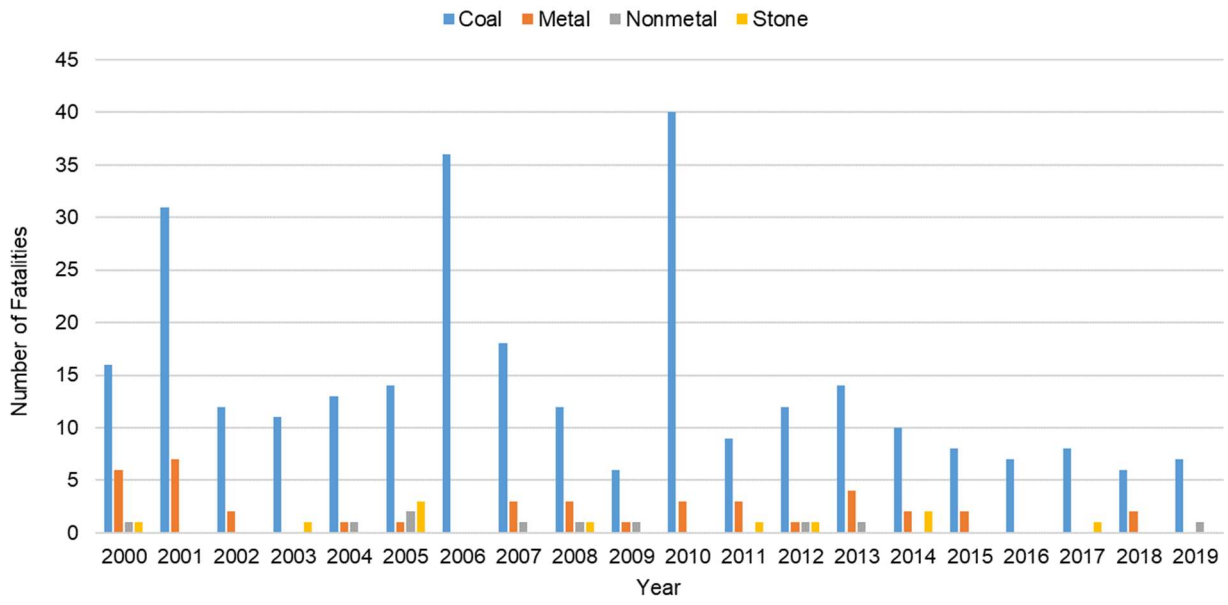

Figure 1.4: Number of fatalities per sector for underground mines in the U.S., excluding office employees, from 2000-2019 (NIOSH, 2021).

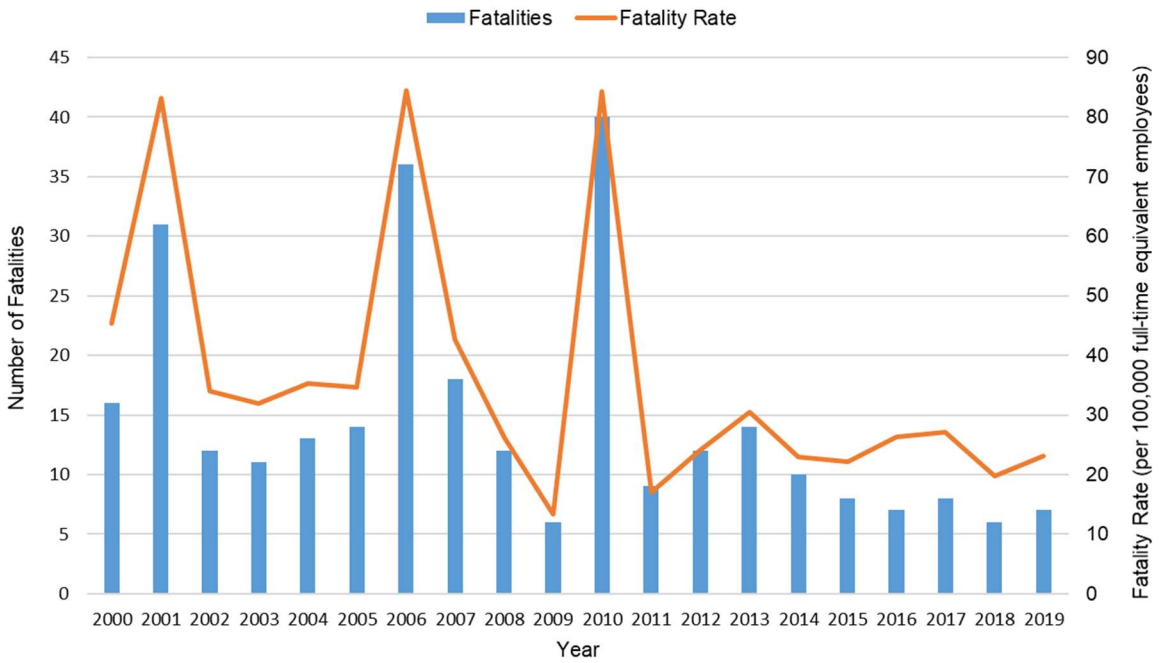

Figure 1.5: Number of fatalities and fatality rate for underground coal mines in the U.S., excluding office employees, from 2000-2019 (NIOSH, 2021).

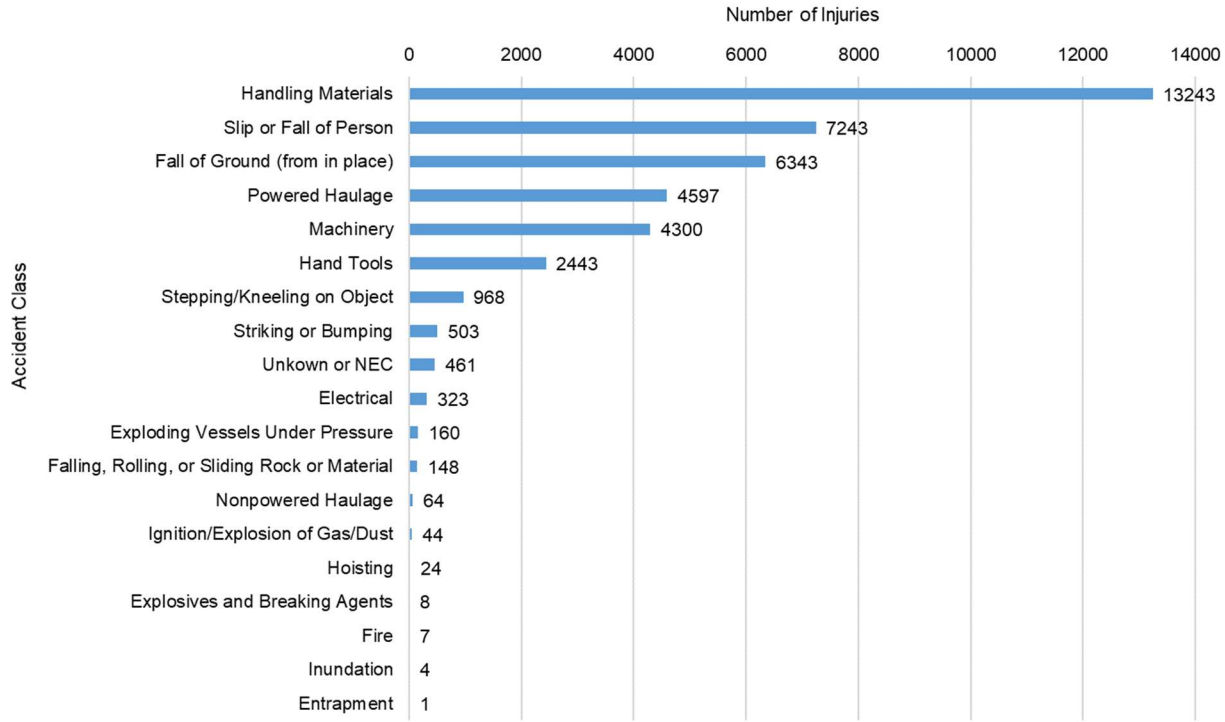

Figure 1.6: Number of injuries for underground coal mines by accident class in the U.S., excluding office employees, from 2000-2019 (NIOSH, 2021).

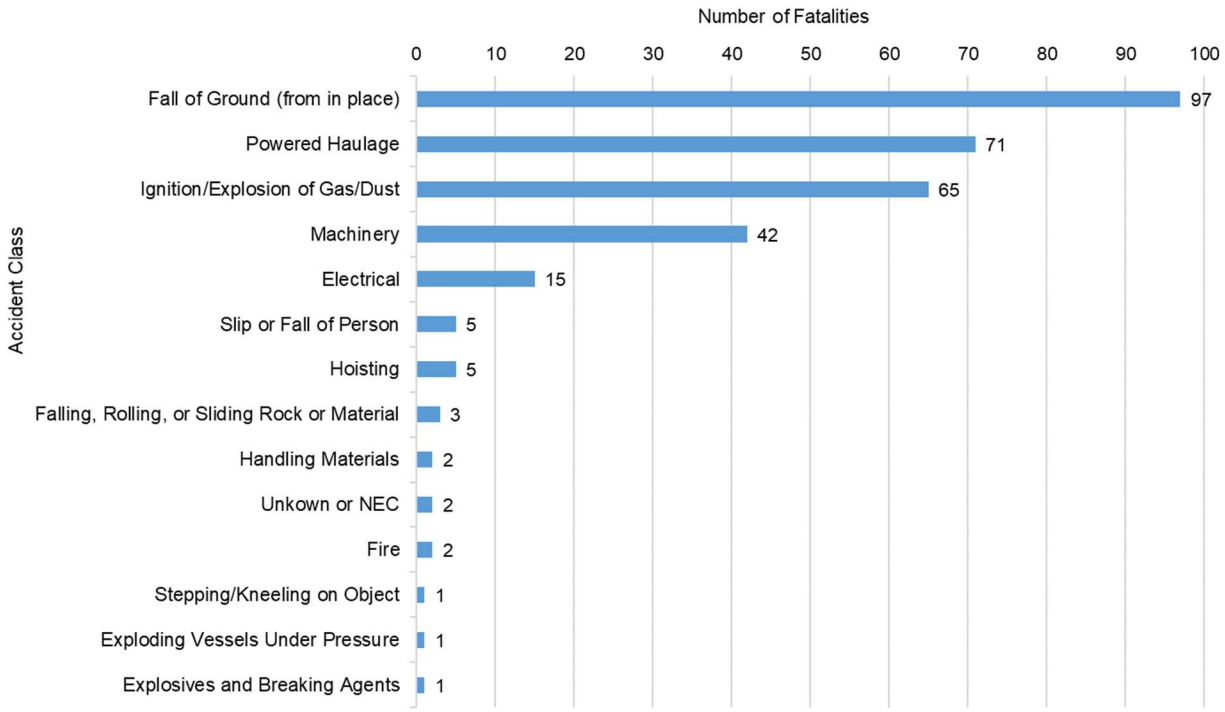

Figure 1.7: Number of fatalities for underground coal mines by accident class in the U.S., excluding office employees, from 2000-2019 (NIOSH, 2021).

Underground coal is generally mined through unsupported and caving methods. The unsupported method most common to coal is the room and pillar mining method. The most common caving method is the longwall mine method. From 1995 to 2008, 112 ground fall fatalities occurred in underground coal mines, in the US. The fatalities were broken down by cause, as seen in Figure 1.8. Only 4% of the fatalities were attributed to longwall mining, whereas retreat mining (associated with room and pillar mining) accounts for 21% of fatalities (Ghasemi et al., 2012). Thus, room and pillar mining is a method that involves more risk than longwall mining.

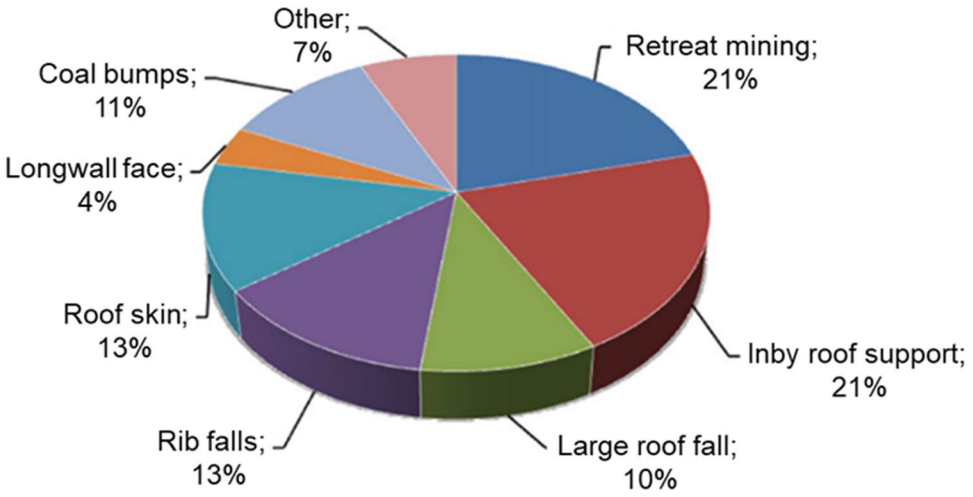

Figure 1.8: Ground fall classifications from 1995-2008 (Ghasemi et al., 2012).

1.2.2 Retreat Mining Safety Statistics

As presented in Figure 1.8, retreat mining accounts for a significant number of fatalities. Retreat mining is a common practice with room and pillar mining, which ultimately creates an unstable environment. The unstable environment creates major safety concerns (Feddock and Ma, 2006). Retreat mining can lead to pillar failure, which results in ground falls (roof and rib). There are three main types of pillar failure that can occur: pillar squeezes, massive collapses, pillar bumps (Mark et al., 2003).

Pillar squeeze occurs when the pillars are too small and as a result are unable to carry the loads applied to them. Loads are gradually transferred, leading to failure of adjacent pillars. The failure can result in severe rib spalling, floor heave, and roof failure.

Massive collapses, otherwise referred to as cascading pillar failure (CPF), are pillar failures that occur rapidly and over a large area (Mark et al., 2003). CPF can have catastrophic results and can have great health and safety implications. An airblast is typical of a CPF. The airblast is caused by the displacement of air during the massive collapse. The airblast can destroy

ventilation stoppings, seals, and fan housings, which completely disrupts the ventilation system. In addition, flying debris can result in injuries or fatalities. Lastly, the CPF may fracture large volumes of rock in the pillars and immediate roof and floor. Depending on the mine, this could cause the sudden release of large quantities of methane into the mine atmosphere and potentially catalyze a methane explosion (Zipf, 2001).

Pillar bumps are a sudden rupture of highly stressed pillars. The rupture causes rock to fly with explosive force which can result in injuries, fatalities, personnel entrapments, and equipment damage (Chase et al., 2002). Retreat mining is associated with 50% of the NIOSH U.S. coal bump database. 95% of the bumps occurred at depths greater than 1,000 ft (Mark et al., 2003). Pillar bumps occur without warning, so it is imperative to determine best design practices for bump prone environments.

It is evident that retreat mining is associated with hazards that can result in severe consequences. Safety statistics surrounding retreat mining have been tracked during various time periods and are summarized below:

- 1986-1996: Retreat mining accounts for about 10% of all US, underground, coal production; however, it has historically accounted for more than 25% of all roof and rib fall fatalities. This trend was also observed in coal mines of Australia and South Africa (Ghasemi et al., 2012).
- 1992-2001: 27% of all US ground fatalities occurred during retreat mining (Mark et al., 2003).
- 1997-2007: On average 2 coal miners died each year from roof fall during retreat mining in the US (Ghasemi et al., 2012).

- 1997-2008: 29 fatalities resulted from roof fall and coal outbursts during retreat mining (Ghasemi et al., 2012).

Note that the statistic from 1992-2001 underestimates the deaths associated with pillar recovery, as deaths can be attributed to other causes that were an indirect result of retreat mining. For example, some deaths classified as "machinery" accidents can actually be attributed to retreat mining as miners were killed by shuttle cars while attempting to flee premature roof collapses. To understand the risk of fatality for a coal miner working in retreat operations versus non-retreat operations, the following statistics are useful:

- A coal miner working in retreat operations is more than 3 times as likely to be fatally injured as a coal miner working in non-retreat operations (Mark et al., 2003).
- A miner working where timber is used as support is about 2 times as likely to be fatally injured as a miner working where MRS is used (Mark et al., 2003).

1.3 Underground Mining Practices

Underground mining consists of three main method classes: unsupported, supported, and caving. Unsupported methods are typically used to extract orebodies that are roughly tabular and associated with strong ore and surrounding rock. Unsupported methods do not use any artificial pillars to help support the openings. Supported methods are generally used in mines with weak rock structure. Artificial pillars of waste are typically utilized to support the roof. Lastly, caving methods are a varied and versatile method that involves caving the ore and/or the overlying rock. This normally results in surface subsidence. This method is most applicable to weak or moderately strong orebodies that readily break up when caved. Overall, underground mining falls under three main method classes that are chosen based on the geology of the deposit and the

degree of ground support necessary to make the methods productive and safe (Hartman and Mutmansky, 2002). The focus of this thesis surrounds room and pillar mining, specifically retreat mining, as the safety statistics suggests that these methods are some of the most dangerous.

1.3.1 Room and Pillar Mining Practices

To better understand retreat mining practices, room and pillar mining must first be understood. Room and pillar mines are developed by driving a series of rooms and leaving pillars, often ore bearing, behind in order to support the roof and prevent collapses. Pillars are supplemented by secondary support systems, such as timbers or mobile roof supports (MRS) (Ghasemi et al., 2012). Room and pillar mining is a very old method often used with horizontal or near horizontal, tabular ore bodies. Common ores extracted from room and pillar mines include coal, potash, sodium chloride, trona, limestone, and any metallic (i.e. lead-zinc) deposits occurring in horizontal seams. The main advantages and disadvantages of room and pillar mining are listed below (Hartman and Mutmansky, 2002):

Advantages:

- Moderately high productivity
- Moderate mining cost
- Moderately high production rate
- Low to moderate dilution
- Suitable to mechanization

Disadvantages:

- Poor recovery (40-60%) without pillar extraction (retreat operations)
- Caving and subsidence occur with retreat operations
- Ground stress and support loads increase with depth

- Potential health and safety hazards exist, especially in coal mines

As noted in the disadvantages, room and pillar mines are associated with safety risks. Room and pillar mines also have poor recovery without the use of retreat operations, which can typically increase the recovery somewhere between 70-90% (Hartman and Mutmansky, 2002). The increased recovery increases the utilization of ore, as well as profits and revenue (Ghasemi et al., 2012).

1.3.2 Retreat Mining Methods

Retreat mining is essential in extracting more reserves beyond the initial development phase. Retreat mining is a process that involves the removal of pillars, which are the main load bearing member in an underground mine. Retreat mining practices utilizes various pillar extraction methods as well as panel extraction sequences. Retreat mining consists of many different sub-methods. There four common retreat mining methods are Christmas Tree, Outside Lift, Split and Fender, and Pocket and Wing. Each method has its advantages and disadvantages as described below:

Christmas Tree (left-right): Cuts are taken from both the left and right of the pillar, and is used when pillars are too wide to take cuts from just one side of the pillar (Ghasemi et al., 2012). Most of the coal on each side of the entry is removed until a chevron type pillar remains. Usually a corner wedge-shaped remnant pillar is left behind (Feddock and Ma, 2006). The main advantage of this method is that no additional roof bolting is required during the retreat (Mark et al., 2003). Figure 1.9 shows a typical Christmas Tree sequence with the use of MRS units.

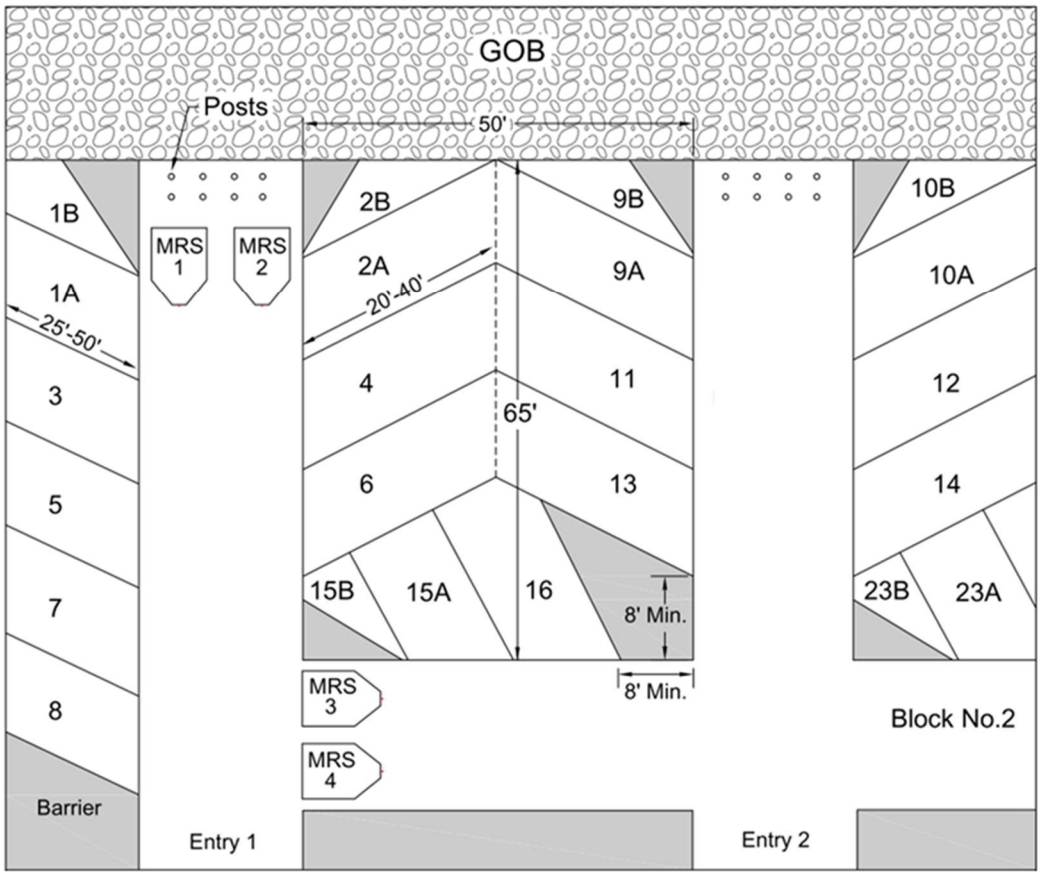

Figure 1.9: Typical Christmas Tree retreat sequence with the use of MRS (after Feddock and Ma, 2006).

Outside Lift: Cuts are taken from one side of the pillar, starting at the gob end and moving toward solid coal (Feddock and Ma, 2006). This method is used in pillars with a width of about 10 m or less (Ghasemi et al., 2012). The main advantages of this method are that no additional roof bolting is required during the retreat and also that operators always have a solid pillar at their back (Mark et al., 2003). Figure 1.10 shows a typical Outside Lift retreat mining sequence with the use of MRS units.

Split and Fender: This method involves multiple cuts, as the pillars are too large to be recovered from cuts taken from the entries (Mark, 2009). The first cut splits the pillar into two

fenders. Cuts are then made through the split cut. This method requires additional roof bolting during the retreat. Roof bolts are added to the roof within the split cut. The main advantage to this method is that multiple pillars can be extracted simultaneously, preventing production delays (Feddock and Ma, 2006). Figure 1.11 shows a typical Split and Fender retreat mining sequence with the use of MRS units.

Pocket and Wing: This method involves multiple cuts for the extraction of large pillars. A cut is extracted at the side of a pillar creating a pocket and wing, allowing for two working areas within the pillar. Cuts are then taken from the pocket. The wing is then split, and cuts are taken from the fender closer to the gob then from the fender away from the gob. This method also allows for multiple pillars to be extracted simultaneously, preventing production delays (Kauffman et al., 1981). Figure 1.12 shows a typical Pocket and Wing retreat mining sequence.

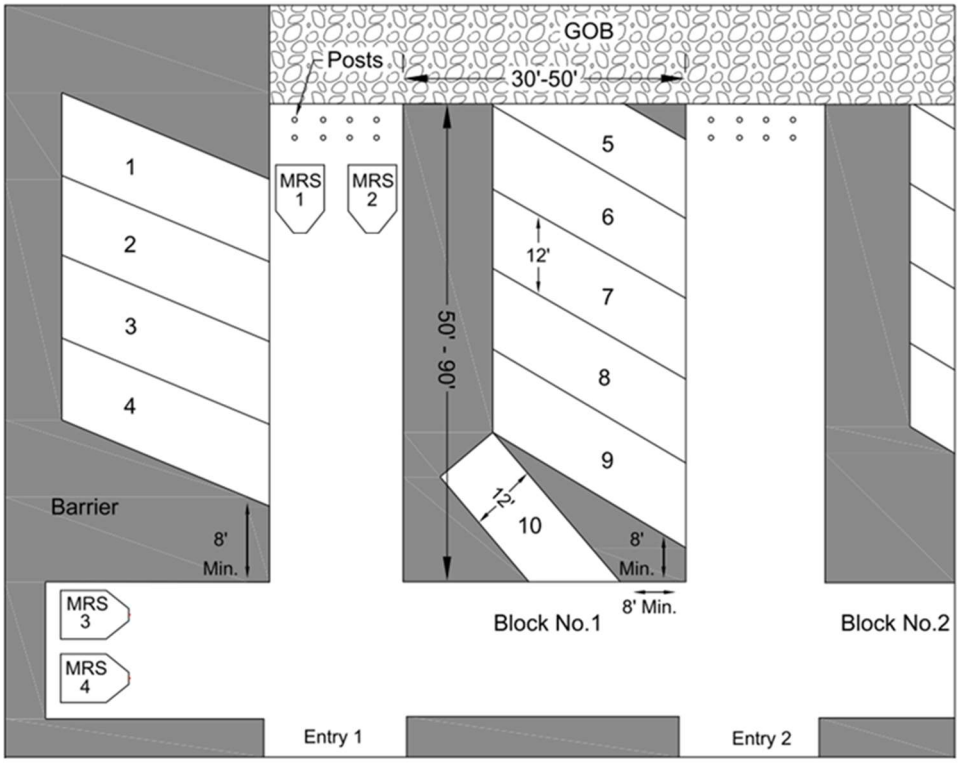

Figure 1.10: Typical Outside Lift retreat sequence with the use of MRS (after Feddock and Ma, 2006).

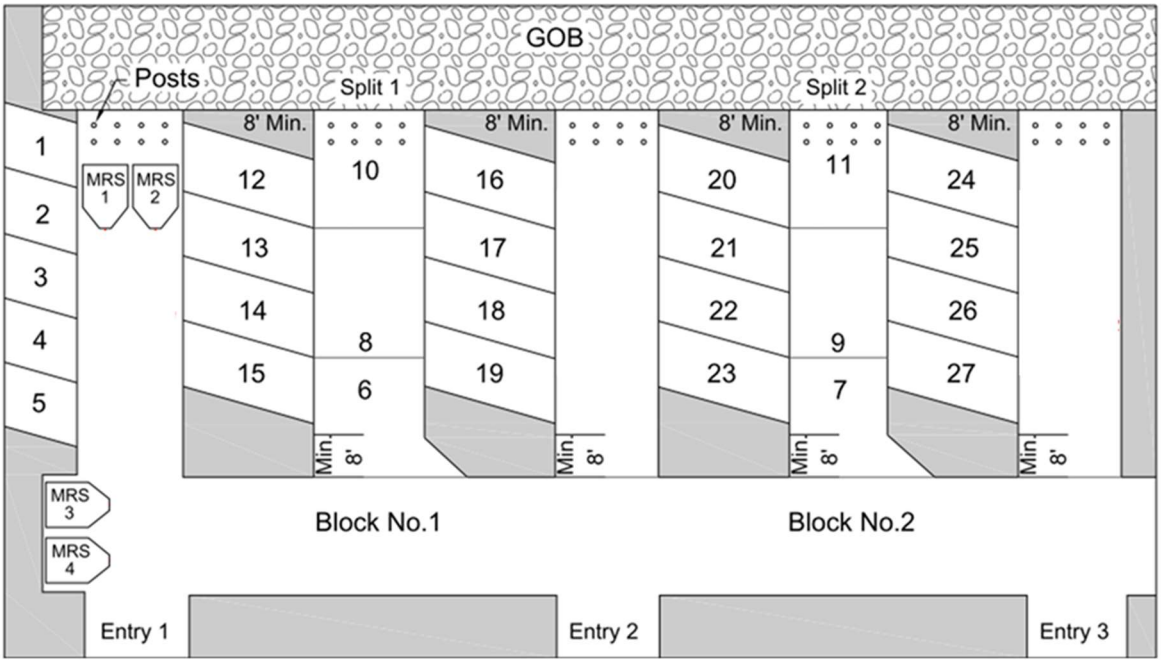

Figure 1.11: Typical Split and Fender retreat sequence with the use of MRS (after Feddock and Ma, 2006).

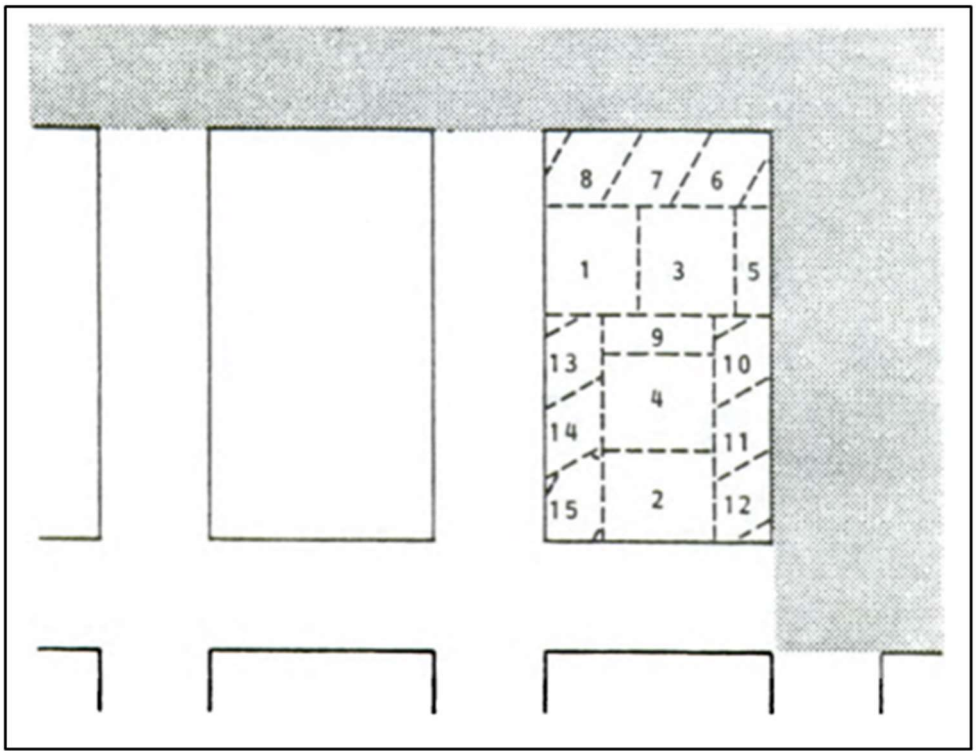

Figure 1.12: Typical Pocket and Wing retreat sequence (Kauffman et al., 1981).

The National Institutes for Occupational Safety and Health (NIOSH) estimates that about 60% of retreat mines use the Christmas tree method, 35% use the Outside Lift method, and 5% using some form of Split and Fender (including Pocket and Wing) (NIOSH, 2010). In addition, the differing methods can be combined and used for retreat operations (i.e. Christmas Tree and Outside Lift method). The Christmas Tree and Outside Lift combination is typically used for pillar systems developed with continuous haulage. An older study conducted in Kentucky (Feddock and Ma, 2006) of 34 retreat mines had findings consistent with NIOSH (2010). The Kentucky study examined a total of 165 pillar recovery plans and found that 55% of the plans utilized the Christmas Tree method, and 32% of the plans utilized the Outside Lift method (Feddock and Ma, 2006). Figure 1.13 shows the breakdown of the recovery plans and associated retreat method.

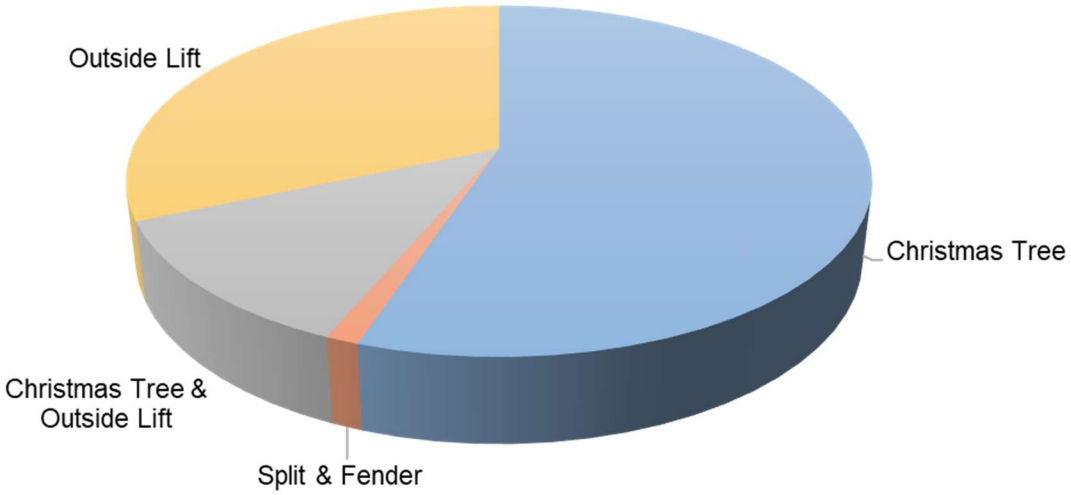

Figure 1.13: Breakdown of retreat methods utilized in the pillar recovery plans from the 34 mines studied in Kentucky (after Feddock and Ma, 2006).

1.3.3 Retreat Mining Excavation Sequences

Extraction sequences of a retreat panel are influenced by a multitude of factors (pillars designed for extraction, seam thickness, in situ stress field etc.). Extraction sequences can be generalized into two categories (Galvin, 2016):

- Extraction of pillars that were formed during the primary development of the mine. These pillars are referred to as standing pillars.
- Extraction of pillars that were mostly formed as part of a secondary extraction process. These pillars are referred to as green pillars. Thus, green pillars are formed as a result of cuts taken from the main development.

When extracting standing pillars, extraction sequences typically follow a 45° extraction line or a 90° extraction line (Figure 1.14). Following a 45° extraction line is popular in some counties (i.e. India) and has its advantages over the 90° extraction line. Advantages include increased protection from abutment stress, large gob spans, and gob ingress at the acute end of the extraction line (Galvin, 2016). The major disadvantage of the 45° extraction line is coal haulage and conveyor belt considerations, making the 90° extraction line approach more common in the United States. As important in determining the extraction line, proper mine design is essential. A proper mine design would be one that took into consideration subsequent pillar extraction: not doing so results in suboptimal layouts and dimensions—increasing risk. Additionally, standing pillars are associated with a large number of intersections, which elevates risk due to extraction (Galvin, 2016).

Extraction of green pillars is a result of pillar extraction layouts that minimize primary development, intersections and standing pillars in the process of accessing the inby end of the panel. Figure 1.15 shows the generic layouts of extracting green pillars. Extraction typically

follows either a single side or double side extraction. In the single side extraction, extraction workings occur only on one side of the main development, whereas, double-sided extraction occurs on both sides of the main development. One or more longs splits are excavated from the main development. Immediately after the splits are excavated, the green pillar (created as a result of the split) is extracted (Galvin, 2016).

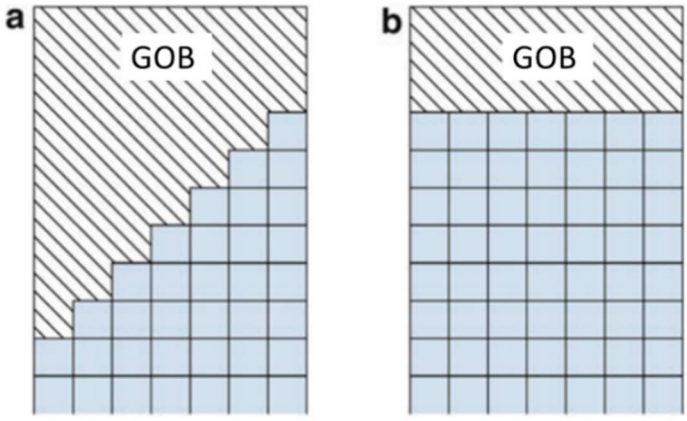

Figure 1.14: General extraction sequencing for standing pillars. (a) 45° extraction line. (b) 90° extraction line (Galvin, 2016).

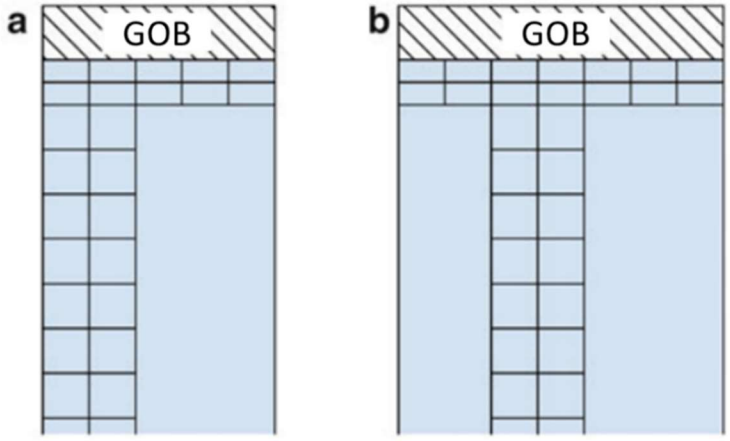

Figure 1.15: Generic layouts for extracting green pillars. (a) Single side extraction. (b) Double sided extraction (Galvin, 2016).

1.3.4 Ground Fall Contributing Parameters During Retreat Mining

It is important to note that majority of the ground falls have been found to be due to poor design of support systems, poor performance of support elements, unknown nature of the stress regime, weak roof rock, not recognizing and controlling hazardous conditions, and/or not following the site's approved roof control plans (Ghasemi et al., 2012; Mark et al., 2003). To manage this risk, it is important to understand the parameters that contribute to ground fall and improve the safety of retreat mining. Ghasemi et al. (2012) determined the major contributing parameters for ground falls during retreat mining through case histories and relevant literature. The parameters are divided into three categories: geological, design, and operational (Ghasemi et al., 2012). Each category is associated with its own sub parameters, as seen in Figure 1.16.

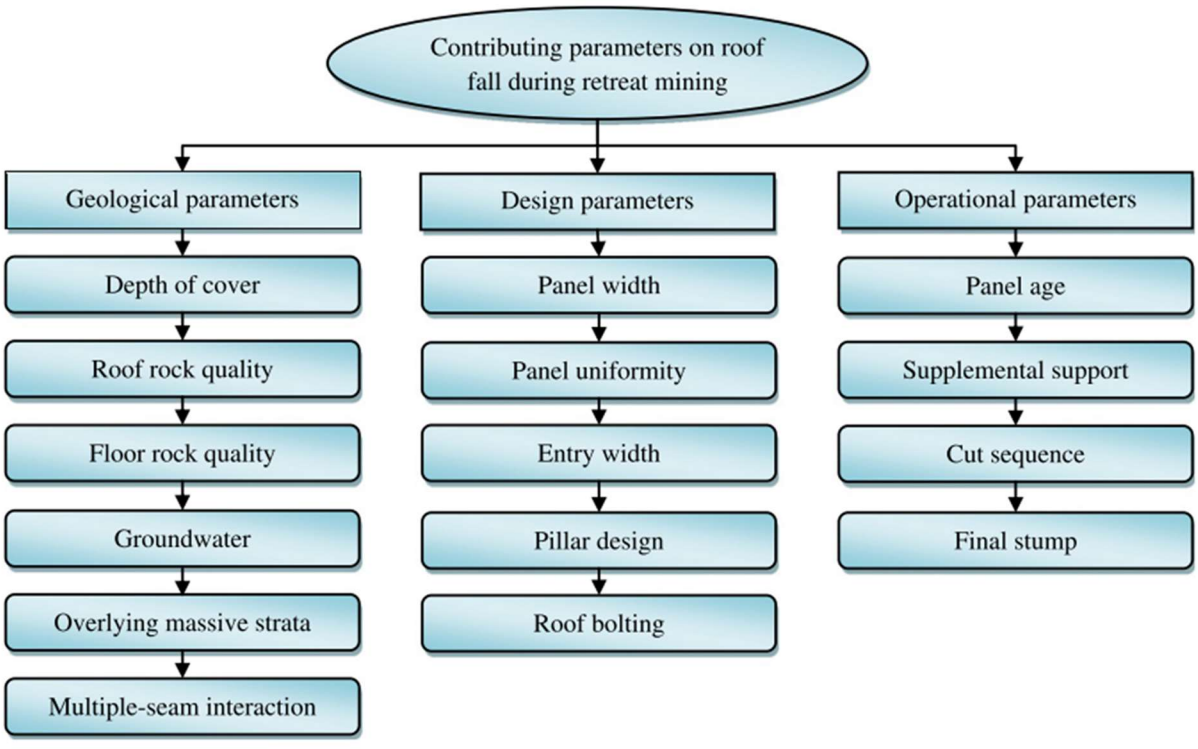

Figure 1.16: Major parameters that contribute to ground fall during retreat mining (Ghasemi et al., 2012).

Proper planning that considers all relevant parameters is important. For instance, it was found that intersections are 8 to 10 times more likely to collapse than the equivalent length of entry or crosscut. This is attributed to abutment loads on the intersections during retreat mining, which requires extra support (Ghasemi et al., 2012). The contributing parameters and associated research that has previously been performed will be discussed in greater detail in Chapter 2.

1.4 Research Objectives

To continue to improve planning and design of retreat mines, numerical modeling will be utilized. Specifically, a finite difference software (FLAC^{3D}) will be used. Using FLAC^{3D} allows the actual geometry of retreat mining operations to be modeled as well as complex geomechanical behaviors. Essentially, a model can be created in order to produce predictions of stress transfer behaviors that occur in response to retreat mining. In addition, complex pillar behavior (i.e. post-peak behavior) can be modeled, which has a direct effect on stress redistribution, whereas simplistic models are unable to do so. A more realistic model will ultimately help improve the safety of the mining method through providing results that more closely approximate reality. Accordingly, designs can be improved through alteration of design components such as extraction ratio, pillar geometry, and extraction sequence.

The ultimate goal of this study is to advance the understanding of retreat mining and improve the safety of the method, through the use of numerical modeling. To achieve the goals of the study, the following objectives were pursued:

1. Conduct a preliminary study of a generic room and pillar coal retreat mine to demonstrate the impact of inelastic pillar material behavior on stress redistribution compared to the conventional elastic approach.

2. Develop a numerical model of Mine C (a coal room and pillar mine in the Western US) in FLAC^{3D} and compare model results to pillar displacement measurements made in-situ. Calibrate the numerical model to realistically match Mine C.

1.5 Thesis Outline

This thesis has been organized into four chapters as outlined below:

- Chapter 1: Introduction. This chapter provides a brief background on the mining industry and methods that relates to the relevant to the thesis research. It outlines the overall goal of the research as well as the specific objectives pursued to achieve the overall research goal.
- Chapter 2: Literature review and preliminary modeling. This chapter presents a technical literature review pertinent to the overall research. This chapter includes preliminary modeling to examine factors that influence stress redistribution during retreat mining.
- Chapter 3: Mine C case study and model calibration. This chapter presents the methodology used to create a numerical model for simulating retreat mining operations at a room and pillar coal mine in the Western US, as well as the process of model calibration and modeling results.
- Chapter 4: Conclusions and Recommendations. This chapter summarizes the work presented in chapters 2 and 3 and provides recommendations for future research.

CHAPTER 2

LITERATURE REVIEW AND PRELIMINARY MODELING

2.1 Introduction

In order to perform the research required to accomplish the main objective of this thesis, a comprehensive literature review was performed and a preliminary numerical modeling study was conducted. The purpose of the literature review is to understand the progression of research that has occurred pertaining to the subject matter of the thesis. The literature review is not only used to build upon knowledge relevant to the research area, but also justify the research as a whole as well as components incorporated into the thesis. In the case of this thesis, literature review was conducted to understand what research has previously been performed in an attempt to improve retreat mining as a whole. Additionally, through the performed literature review, a case for the use of numerical models is made. In addition to the literature review, a preliminary numerical modeling study was conducted. The purpose of this study is to utilize numerical modeling to further understand stress re-distribution during the retreat mining and identify how certain parameters influence the stress redistribution. The preliminary study also makes a case for the use of inelastic models for modeling retreat mining rather than elastic models.

2.2 Literature Review

As highlighted in Chapter 1, retreat mining is associated with high risk, safety concerns, and ground control issues. Retreat mining is associated with the room and pillar method of primary extraction, where pillars are initially left unmined in order to provide support for the mine. Mine stability and ground control are directly influenced by proper mine design, and in particular pillar design. Adequate pillar design becomes especially critical when retreat operations commence.

As a result, pillar design has been a large focus in ground control research. Significant advances in pillar design have resulted from research in the past 70 years. In addition to the advancement pillar design, extensive research has been performed on underground mining and retreat mining as a whole. Research relevant to pillar stability and retreat mining has employed experimental, analytical, empirical, and numerical methods. Presently, empirical methods are among the most common methods to develop a mine design and determine the stability of a mining operation. The primary limitation of empirical methods is that they tend to simplify the observed phenomena to their basic components; while this is often desirable from a practical design perspective, it does limit the degree to which empirical approaches can be used to advance beyond the current state of practice. In contrast, numerical models have the capability of explicitly considering complex mine geometries, geology, and material behavior. Thus, numerical models have the potential to minimize the discrepancies between predicted and observed (site specific) behaviors relative to existing empirical approaches.

2.2.1 Pillar Design

In the past 70 years, substantial progress has been made in pillar design, especially for coal mines. This progress can be attributed to the creation of large databases of case studies that provide information on pillar performance in a multitude of settings. This information has been crucial to the improvement of empirical methods of pillar design. Additionally, the development of computing technology has led to the ability for numerical models to be used for pillar design, which have the potential to more accurately simulate pillar behavior, ultimately leading to improved pillar design (Esterhuizen et al., 2010a, 2010b; Mark, 2007; Mohamed et al., 2018; Tulu et al., 2017).

The evolution of pillar design began based on trial and error approaches, intuition, and established rules of thumb and progressed to pillar design formulas based on laboratory testing (Das, 1986; Sheorey et al., 1986), full-scale pillar testing (Mark and Barton, 1996), and back-analysis of case histories (Chase et al., 2002; Mark and Chase, 1997; Tuncay et al., 2020) to sophisticated numerical models that can simulate the pillar behavior (Esterhuizen et al., 2010b; Ghasemi and Shahriar, 2012; Mohamed et al., 2018; Su and Hasenfus, 1999; Tulu et al., 2017; Tuncay et al., 2021).

The "classic" method of pillar design consists of three steps: 1. Estimate the pillar load 2. Estimate the pillar strength 3. Calculate the pillar stability factor (Mark, 2007). The "classic" method of pillar design is limited to the development phase (prior to retreat mining) of a room and pillar mine. Pillar design that is directly applicable to retreat mining builds upon the methodologies used for pillar design under development loads, and is presented in the subsequent sections.

2.2.1.1 Step 1 – Estimate the Pillar Load

The pillar load is estimated in terms of average pillar stress, typically using tributary area theory (TAT). TAT assumes each pillar to uniformly support the weight of the overlying overburden and one-half the width of the entry on each side of the pillar (Ghasemi and Shahriar, 2012). TAT is a simplification and assumes the following: mined area is very large relative to the pillar size, all pillars have the same dimensions, and pillars at the edge of a panel have the same stresses as those in the middle (Galvin, 2016). One limitation of this approach that it ignores the potential for stress redistribution within the pillar array due to local inelastic deformation (loss of load-carrying capacity), although in practice this limitation is not significant if pillars are designed to high factors of safety. Additionally, in reality, the pillars at the center of the panel

have higher induced stresses than pillars along the edge of the panel (Zipf, 2001). This is because it is possible for the immediate roof to transfer load to the stiffer barriers (stiffness being proportional to the cross-section area), reducing the load on the smaller pillars relative to that predicted by TAT. This means that TAT only predicts the maximum load, so the maximum load is assumed on all the pillars despite representing a conservative assumption. However, the historical use of this assumption in estimating pillar strengths based on stress estimates derived from TAT means that commonly adopted pillar strength formulae may have the potential to overestimate pillar strength in some cases (Frith and Reed, 2017).

2.2.1.2 Step 2 – Estimate the Pillar Strength

Pillar strength is defined as the maximum resistance of a pillar to axial compression (Brady and Brown, 1993). Based on empirical evidence, the strength of a pillar is related to both its volume and its shape (Brady and Brown, 1993; Ghasemi and Shahriar, 2012; Salamon and Munro, 1967). As rock volume increases, rock strength may be adversely affected due to increase of discontinuities (i.e. natural fractures) (Steed et al., 2003). As pillar width-to-height ratio (W/H) increases, the pillar strength will increase. This is because as the W/H increases, the pillar cross-section area increases providing more confinement due to the friction at the coal roof and coal floor interfaces (Du et al., 2008). In addition to their differences in peak strength, lower W/H pillars behave in a more brittle manner than high W/H pillars (Zipf, 2001; Esterhuizen et al., 2010b).

Many formulae have been developed to estimate the pillar strength in coal mines to account for the size and shape effect. The most applicable empirical strength formulas for coal pillars have been developed by Salamon and Munro (1967), Bieniawski (1984), Sheorey et al. (1987) Madden (1991), and Mark and Chase (1997) (the so-called “Mark-Bieniawski” formula).

Each of the formulas share two common variables width to height (W/H) ratio and in-situ coal strength (Ghasemi and Shahriar, 2012).

2.2.1.3 Step 3 – Calculate the Pillar Stability Factor

Pillar Stability Factor (SF) can be determined by comparing the pillar strength (determined using one of the pillar strength equations) with the pillar load (primarily determined by TAT), as seen in Equation 2.1. Potential errors in estimated pillar stability factor may from the assumptions and limitations inherent in the methodologies for determining pillar strength and load (maximum load assumption). The resulting pillar stability factor could be higher than what is realistic and result in an under-design of the pillar which could lead to potential failure (Steed et al., 2003).

$$SF = \frac{Pillar\ Strength}{Pillar\ Load} \tag{2.1}$$

The SF is an important design consideration, as typically a pillar has to last throughout the life of the mine (i.e. main pillar) will require a higher SF. Conversely, pillars designed for short-term applications (i.e. panel pillars) are assigned a lower SF. Generally, in the US, a SF of 2 is required for main pillars and a SF of 1.5 for panel pillars (Mark and Chase, 1997).

2.2.2 Pillar Mechanics

As noted above, the "classic" pillar design approach consists of three steps. Of the three steps, determination of pillar strength has arguably been the most significant point of contention, as there have historically been a variety of schools of thought in the field of coal mechanics (pertinent in estimating coal pillar strength). At the second Workshop on Coal Pillar Mechanics and Design, a unified theory of coal pillar mechanics was developed via different groups of researchers utilizing different approaches that reached similar conclusions (Mark, 2007). It was

observed that not only does pillar strength vary depending on the pillar shape but also pillar behavior. Three pillar categories were identified for expected pillar behavior and failure mode: slender pillars, intermediate pillars, squat pillars.

Slender pillars correspond to W/H values of less than about 3 or 4. When loaded to the pillar's maximum capacity, the pillar fails completely and sheds close to its entire load. A sudden, massive collapse and airblast can occur as a result of failure of multiple slender pillars used over a large area (Zipf and Mark, 1997; Zipf, 2001; Mark, 2007).

Intermediate pillars (yield pillars) fall between slender and squat pillars, falling in a W/H range between about 4 and 8. When intermediate pillars fail, they do not shed their load nor take on more load. Intermediate pillars deform until the overburden transfers load away from the pillar, depending on its flexural rigidity. Failure of intermediate pillars is non-violent pillar "squeeze". The squeezing of the pillar can take anywhere from hours to weeks. With pillar squeeze, large roof to floor closures can occur, which may result in hazardous ground conditions and entrap equipment (Mark, 2007).

Squat pillars exceed a W/H of 8. These large pillars can take on very large loads, as pillar behavior may even be strain-hardening such that the pillar will continue to take on load and deform once they "fail". Pillar design with squat pillars is not without potential concern. With squat pillars, failure may occur as excessive stress is applied to the roof, rib, or floor. Additionally, squat pillars can carry excessive amounts of energy (as the pillar continues to take on more load) and the release of this energy can cause a pillar bump (explosive collapse of a pillar). The strength of squat pillars is variable and is dependent on geologic factors (i.e. soft partings, weak roof, floor interfaces) (Mark, 2007). This entire range of pillar behavior can be observed in the stress-strain data of Das (1986). Although those tests were done on laboratory

specimens and as such is not a true representation of reality, the results are still a useful analogue for understanding how pillar behavior might change as a function of W/H ratio.

2.2.2.1 Empirical Research Regarding Pillar Mechanics and Pillar Design

The majority of the classic pillar design methods (prior to 1990) were derived from data obtained from laboratory or in-situ testing. Salamon and Munro (1967) developed their pillar strength formula based on statistical analysis of case histories in South Africa after the 1960 Coalbrook Colliery disaster. Salamon and Munro's (1967) formula transformed past experience into a practical and verifiable pillar strength formula that can be used by mine planners (Mark, 2007). Additionally, the concept of utilizing case histories to develop pillar design methods became well accepted.

The Analysis of Longwall Pillar Stability (ALPS) became the first method to employ a large case history database to develop a pillar design method. Vital to the usage of ALPS is identifying the proper SF to use for pillar design. A major difficulty in the universal usage of ALPS was the difficulty of incorporating rock strength into the design. However, the development of the Coal Mine Roof Rating (CMRR) allowed for quantitative measurement of the structural competence of the coal mine roof. The inclusion of the CMRR into ALPS led to an 85% success rate in predicting the outcome of individual case histories. ALPS indicated that under stronger roofs, the design SF could be lower (as low as 0.7), and under weaker roofs, the design SF needs to be higher (at minimum 1.3) (Mark, 2007).

The aforementioned pillar design methodologies have been improved over time. However, the methods are best used for room and pillar mines under development loads. Retreat operations are not taken into consideration, and as a result, the methods provide minimal guidance when designing pillars for mines that will undergo retreat operations. Retreat mining

adds complexities (e.g. abutment loads) that need to be considered when designing pillars. Retreat mining adds additional load on the pillars adjacent to the pillar line during retreat operations (Van Der Merwe, 1990). The additional load is a result of the abutment load that forms during retreat operations and the creation of a mined out gob (Ghasemi and Shahriar, 2012). The exclusion of these abutment loads in pillar design can lead to failure during retreat operations. Thus, it is important to develop a pillar methodology that can be directly applied to retreat practices. To do so, the Analysis of Retreat Mining Pillar Stability (ARMPS) program was developed to ensure pillars were adequately sized for future extraction (Mark and Chase, 1997). Similar to the ALPS methodology, ARMPS was developed from case histories and aims to prevent pillar failures resulting from squeezes, collapses, and bursts (Mark, 2010). ARMPS evaluates pillar stability in preliminary and secondary stages through parameter (pillar width, panel width, depth of cover, etc.) inputs (Ghasemi and Shahriar, 2012). ARMPS was able to distinguish the transition of pillar squeeze and pillar collapse. Pillar collapses occurred when the W/H was less than 3 with a SF less than 1.5. This aligns with Salamon and Munro's (1967) observations. A major limitation of the ARMPS program was its difficulty predicting success and failure for cases that had a cover depth greater than 750 ft. Success and failure cases both occurred at SF values well under 1.5 making it difficult to separate successes from failures and limiting the applicability of the ARMPS program based on depth cover. To help improve the limitation of ARMPS, Chase et al. (2002) added 100 more deep-cover cases to the ARMPS database. The study concluded the pillar strength for squat pillars under deep cover was more variable than slender pillars in shallow conditions (Mark, 2007). Continued research is necessary to further improve and address the limitations of the ARMPS program, as is further discussed in Section 2.2.2.2.

Despite improvements to empirical pillar design that account for pillar extraction, ground falls have continued to occur in recent decades. The most notable was the Crandall Canyon (deep cover retreat mine) disaster (August 6, 2007), where widespread pillar failure occurred, leading to coal bursts and mine collapse. Ten days after the initial collapse event, a second major collapse occurred. The overall disaster resulted in multiple fatalities. It was reported that "pillar dimensions were not compatible with the deep overburden and high abutment loading that existed in the South Barrier section" resulting in the "stress level exceed[ing] the strength of a pillar of group of pillars near the pillar line, and that local failure initiated a rapid and widespread collapse that propagated outby through the large area of similar sized pillars." This disaster exemplifies the need for continual improvement in regards to pillar design, especially in deep cover mines.

Based on the conceptual framework of ARMPS, Ghasemi and Shahriar (2012) proposed a new pillar design method for coal mines that includes all anticipated loading conditions that result from retreat operations. The new pillar design method is based on the following principles (Ghasemi and Shahriar, 2012):

- Calculating the maximum load (development and abutment) applied on the pillars in the active mining zone (AMZ). The active mining zone includes all of the pillars on the extraction front (pillar line) and extends out by the pillar line a distance of 5 times the square root of the depth of cover.
- Calculating the overall load-bearing capacity of the pillars in the AMZ.
- Selecting an appropriate safety factor.
- Calculating the pillar width.
- Correcting the pillar width to find the optimum pillar width.

The proposed method helps decrease pillar failure risk by ultimately determining the optimum pillar width accounting for the overall applied loads (Ghasemi and Shahriar, 2012). The main advantage of this method is that pillar failure risk is decreased, especially massive pillar collapses. A limitation of this method is the potential need for new data to be required for the calculations to be performed. In order to utilize the method, the following are required: depth of cover, pillar height, entry width, in-situ coal strength, mean unit weight of the overburden, abutment angle, panel width, CMRR (Ghasemi and Shahriar, 2012). Appropriate results are dependent on the accuracy of the data collected. In some cases, the data might not be readily available, preventing use of this methodology.

2.2.2.2 Numerical Research Regarding Pillar Mechanics and Pillar Design

Numerical modeling is an increasingly common tool that has been used to augment empirical methods (ARMPS, 2010) and improve overall understanding of ground response to mining operations. The benefit of numerical modeling is that complex geology and mine geometries can be examined, and stress re-distribution (as a result of mine operations) can be better understood.

Numerical modeling has contributed to the understanding of coal pillar mechanics via the ability to incorporate the following considerations into analyses (Mark, 2007):

- Simulation of post-failure processes.
- Assessment of shear, tensile, and bedding plane failure within the material with the effect of joints and structural weakness.
- Simulation of material properties and stress distributions of the ground.

- Simulation of failure of the pillar roof and floor and the correct stress path within the pillar system.

Numerical models can be used simulate realistic rock behaviors and interactions between distinct mine system components. Numerical models can be used to perform mine-specific investigations based on calibration to field data and observations. A calibrated numerical model is a powerful tool that can be used to test what conditions may reasonably manifest during mining, and therefore provides the capacity to improve understanding of physical processes relevant to underground mining.

Notable advances in the study of pillar mechanics achieved through the use of numerical modeling result were developed by Su and Hasenfus (1999), Gale (1996, 1998), and Gale and Hebblewhite (2005). Su and Hasenfus (1999) utilized finite element models (FEM) to understand the effect geologic conditions have on pillar strength. Significant findings include evaluation of the influence of a rock parting versus a clay parting and weak floors on pillar strength. The parting and weak floor influences were found to become more significant for pillars with W/H greater than 5. It was also observed that uniaxial coal strength had a limited effect on pillar strength. Field observations that the strength of squat pillars is variable depending upon geological factors rather than coal strength parameters support the modeling results (Chase et al., 2002; Mark, 2007). Gale utilized numerical models to investigate the interactions between coal and the surrounding rock. Investigations between the coal and surrounding rock lead to Gale's observation that pillar strengths fall into two categories: strong roof and floor rock, and weak rock or bedding planes. In the strong roof and floor rock case, it was found that pillar confinement was easily generated. In cases with weak rock or bedding planes, pillar confinement was limited, which limited the strength of the pillar system. Gale's (1996, 1998) continued

research further demonstrated how the strength of squat pillars can be influenced by three main factors: (1) The presence of weak materials or bedding planes in the pillar, at roof and floor interfaces, or in the immediate roof and floor; (2) The stress field, mainly as a result of reduced confining stress; (3) The pillar's ability to limit entry deformation (Mark, 2007). Gale and Hebblewhite (2005) noted that in pillars with a W/H less than 4 or 5, the pillars ability to develop confinement is reduced, resulting in low post-yield load capacity. This occurs regardless of the surrounding rock, and as a result, the pillar mechanics are more dependent on the actual coal properties.

As previously mentioned, the ARMPS program had difficulties determining adequate pillar design under deep cover. As a result, ARMPS was re-evaluated, expanded, and updated with almost 450 new case histories. ARMPS 2010 (ARMPS V6.0) improved design criteria for deep cover retreat mines that confirmed the findings of Chase et al. (2002) as well as the "pressure arch" theory (Holland, 1973; Hill et al., 2008), which was confirmed through the use of numerical modeling (LaModel and FLAC^{3D}) (Mark, 2010).

LaModel, a boundary element program, simulates a laminated overburden as a stack of frictionless plates (Heasley, 1998). Within the seam, coal and gob areas are represented by elements that can be assigned various stress-strain behaviors. Displacements and loads are calculated throughout the modeled area by using the stiffness behavior of the seam elements and the prescribed flexure of the overburden (Tulu et al., 2010). LaModel can simulate vertical stresses and displacements during both development and retreat mining (Klemetti et al., (2017). Mark (2010) used LaModel to determine the loads applied to the active mining zone (AMZ) of 29 deep cover retreat case studies. On average, loads were about 25% lower than those predicted from the ARPMS program. Loads were more accurately depicted in LaModel, as it is able to

model realistic pillar softening as increased load is applied. Additionally, FLAC^{3D} was used to further investigate the development of the pressure arch. Mark (2010) found overburden strength and the mining geometry to be the two main factors for the development of a pressure arch. When the overburden is weak, pillar loads can be approximated using TAT. However, in the case of strong overburden, a pressure arch is better formed, significantly reducing loads. In comparison to the ARMPS calculations, developmental loads were 9% less and loads during retreat mining were 28% less (Esterhuizen and Mark, 2009; Esterhuizen et al., 2010a). The use of LaModel and FLAC^{3D} was vital to the improvement of the ARMPS program to better analyze deep cover mines (Mark, 2010).

Tulu et al. (2010) found LaModel to better match case study observations than ARMPS 2010 and ARMPS. The study concluded further research into load shedding during retreat mining was required to help improve the ARMPS programs. The modeling of strain-softening/strain-hardening material behavior was determined to improve model results, thus better reflecting reality (Tulu et al., 2010). Zhang et al. (2013) developed ARMPS-LAM program to implement the laminated overburden model (from LaModel) into the ARPMS program. ARMPS-LAM improved the accuracy by 71% relative to the original ARMPS program as opposed to the 63% improvement achieved by ARMPS 2010 (Zhang et al., 2013).

Numerical methods have the potential to build upon the empirical and analytical methods. Initially these approaches were used independently, as there was not a direct correlation between them all, making it difficult to compare results from each method. It wasn't until Mark and Iannacchione (1992) demonstrated that each empirical formula implies a non-uniform stress distribution within a pillar that systems comparisons of results obtained using different methods were made. Specifically, pillar stress distributions can be compared to those

determined from numerical models or pillar design formulas. This comparison led to the development of the Mark-Bieniawski formula for rectangular pillars, in addition to the identification of strength parameters for use in boundary element models. This allowed for increased confidence in modeling pillar strengths that are close to real world behavior while accurately analyzing complex mining situations (i.e. multiple seams and realistic pillar layouts). Ultimately, a synthesis between empirical and numerical approaches was created and has improved the overall understanding of pillar mechanics and pillar design. Despite these advances, more research is required pertaining to pillar mechanics and design to better understand the mechanics of squat pillars as well as pillar interactions with the roof and floor (Mark, 2007).

2.2.3 Numerical Modeling of Retreat Mining

Retreat mining has also been examined through various individual case studies (Klemetti et al., 2017; Mark et al., 2003; Steed et al., 2003) to optimize pillar design and retreat operations, and to understand the stress redistribution process. Steed et al. (2003), using Map3D (elastic analysis), found pillar size to influence stress re-distribution, whereas mining direction impacts roof and pillar stability, without structural influences on the roof. Steed et al. (2003) also used NFOLD, a displacement discontinuity stress analysis method, to calibrate a model to field observations and ultimately determine optimal retreat operations and backfill design to improve overall operations of a thick seam metal mine (Steed et al., 2003). Klemetti et al. (2017) used LaModel and Phase2 to examine stress re-distribution due to the topographical relief, multiple-seam interactions, and full extraction mining. Mark et al. (2003), using a boundary element numerical model (BESOL), determined the impact of retreat methods on ground stability. The model results were found to be consistent with fatality reports (Mark et al., 2003) and the

findings of Ghasemi et al. (2012). Mark et al. (2003) confirmed, through numerical modeling, the observations that the Outside Lift method promotes the most stable ground conditions followed by the Christmas Tree method, leaving Split and Fender and Pocket and Wing as significantly more risky methods, and is able to provide quantitative evidence as to the impact of each method on ground stability. Yaghoobi et al. (2019) also investigated the impact of retreat methods during retreat operations at the Tabas Central Coal Mine (TCM), through FLAC^{3D}. Through numerical investigations, the shortwall mining method was determined to be more optimal than the modified split and fender method (planned retreat method for the TCM). Yaghoobi et al. (2019) was able to utilize a calibrated model to understand the direct impacts the retreat method selected had on a specific site.

Zingano and Weiss (2019) studied the behavior of the coal seam and overburden in a room and pillar retreat mine using ARMPS and Plaxis 3D. The study considered a coal room and pillar mine that performs partial pillar recovery through traditional blasting practices. Rapid pillar squeeze was observed on-site and Zingano and Weiss (2019) wanted to determine the cause. Through the course of their study, it was found that an increased pillar recovery rate resulted in greater pillar deformation and roof displacement. From the initial empirical ARMPS analysis, Zingano and Weiss (2019) determined that blasting practices reduced pillar strength by about 20%, as the pillar is weakened by the blast shock wave, and this was identified as the root cause of pillar failure. Through the numerical investigation using Plexis 3D, it was found that the irregular shape of size of the remaining pillars in conjunction with the blast damage contributed to the observed pillar failure. Ultimately, Zingano and Weiss (2019) demonstrated the benefits of numerical modeling, as the empirical method employed was unable to capture all aspects of what was occurring in the field.

Maleki (2017) utilized FLAC^{3D} to understand depillaring-induced horizontal stresses. The main roof and floor were modeled as elastic, and the coal seam and immediate roof and floor were simulated using the strain-softening Mohr-Coulomb (MC) plasticity model. The importance of incorporating the strain softening behavior is that pillars are able to yield, dilate, and ultimately transfer stresses to other elements of the mining system. The pillar can continue to take on load up to its point of peak strength, at which point load will be transferred to the surrounding pillars and abutments. Using their models, Maleki (2017) concluded that significant increase in horizontal stress in the pillar and immediate roof was caused through pillar cuts during depillaring. Increased horizontal stresses can lead to failure and differential movement of the immediate roof. This model highlighted the potential for bump-induced roof falls when the immediate roof buckles as a result of pillar punching (Maleki, 2017).

Pillar behavior depends on two mine system components— the roof/floor (loading system) and the pillar. Realistic behaviors for roof/floor and coal pillars can be simulated using numerical models. Bai et al. (2014) conducted a case study that highlighted the importance and application of numerical modeling in analyzing the behavior of the roof and coal pillars. Through this, Bai et al. (2014) was able to replicate the failure modes and spalling (failure) depths that were consistent with field observations. This ability to replicate observed failure modes is one of the key advantages of numerical modeling. Sinha and Walton (2020) investigated how best to capture the failure modes observed in coal pillars. Ultimately, Sinha and Walton (2020) found the progressive S-shaped yield criterion as a promising strength criterion for capturing realistic behavior in coal pillars. Numerical models have proven to be a realistic representation of what occurs onsite, as well as improving how material properties (i.e. coal) are modeled.

Of importance in retreat mining is appropriate modeling of the gob. Gob response has been examined by Esterhuizen et al. (2010b) and Su (1991) in the context of longwall mining, and these studies presented a model that determines gob behavior based on the parameters a and b (gob stress at b/2 and maximum vertical strain, respectively). Esterhuizen et al. (2010) implicitly modeled the gob by modifying the zone properties to obtain a hyperbolic behavior in the gob (not simulating the rock breakage, collapse, or compaction processes explicitly). Multiple gob stress-strain curves were developed through model calibration and laboratory tests representative of different gob strengths (Esterhuizen et al., 2010b). The extent over which the gob is modeled is important and should reflect reality. Typically the caving height of the gob is considered to be about three times the mining height (Tuncay et al., 2021). Tuncay et al. (2020), building off the work of (Esterhuizen et al., 2010b), was able to accurately model the gob response and successfully calibrate a 3D model of a longwall retreat mine. Lastly, the influence of the roof and floor interface on coal pillar performance is also important to overall mine behavior. Perry et al. (2013) found pillar strength to be heavily influenced by the roof and floor interface and only minimally influenced by the mechanical properties of the roof and floor using FLAC^{3D} (Iannacchione, 1990).

2.2.4 Research Needs

Despite the extensive research to further understand pillar strength, pillar and roof and floor interactions, gob development, extraction methods etc., there is minimal research that examines rock mechanical aspects specific to room and pillar retreat mining. Research performed mainly utilized numerical models to individually look at pillar roof systems. Further research is needed that utilizes numerical models to perform investigations that examine the intricate interactions of the entirety of retreat mining operations (i.e. roof/floor, gob, depillaring sequences, support).

One of the objectives of this thesis was to develop a numerical model and calibrate to match field observations at Mine C. This model was then used to examine the stress redistribution processes occurring at the mine, and in future could be used to simulate "what-if" scenarios, including alternative depillaring sequences. In order to run a model at the mine scale a continuum model is necessary and allows for reasonable model run times. A finite element model is not able to consider complex inelastic behavior and a boundary element method does not consider inelasticity. As a result, a finite difference model was considered due to its capability of easily incorporating any complex behavior needed (considers inelasticity) and its explicit solution scheme. FLAC^{3D} was specifically used for modeling purposes due to its ability to successfully perform large deformation analysis, which is important in mine scale investigations.

2.3 Objective 1: Preliminary modeling of a generic coal room and pillar mine

TAT and simplified (elastic) models are the conventional methods to determine pillar stresses. These conventional approaches have limitations that tend to lead to conservative results, which may lead to an overestimation of the pillar strength, an overconfidence in a pillar's ability to support the overburden, and an under-design of supplemental support (Frith and Reed, 2017). An unintentional consequence is the creation of unsafe mining conditions.

To better understand realistic pillar stresses and more accurately estimate the pillar strength, a model was created using FLAC^{3D}. A representative coal room and pillar was modeled with realistic geomechanical behaviors, panel layouts, and de-pillaring sequencing. The models were used to examine the stress redistribution on pillars during the retreat mining process. In this preliminary study, variable width to height ratios and extraction ratios, material properties, and mining sequences were modeled to understand how the various parameters impact the stress

concentrations on the pillars and how inelastic behavior differs in stress concentration trends from those predicted by conventional elastic models. Previous research investigating the aforementioned properties were based on case studies and/or utilized more simplistic model. There is limited research that investigates the general behavior of a mine as a result of various parameters modeled with inelastic properties.

2.3.1 Model Layout and Sequencing

The hypothetical retreat mine in this case is modeled based on a typical layout and includes a bleeder entry, as shown in Figure 2.1. The pillar panel considered follows a 6 x 10 grid pattern. The pillar length and width are dependent on the pillar width to height ratio (W/H), which was varied as part of this study (3 and 6). The pillar height is 3 m. Figure 2.2 and 2.3 shows the pillar naming convention as well as the difference in pillar size between the W/H cases of 3 and 6. The pillars in the x direction are labeled i1 through i6, while the pillars in the y direction are labeled j1 through j10.

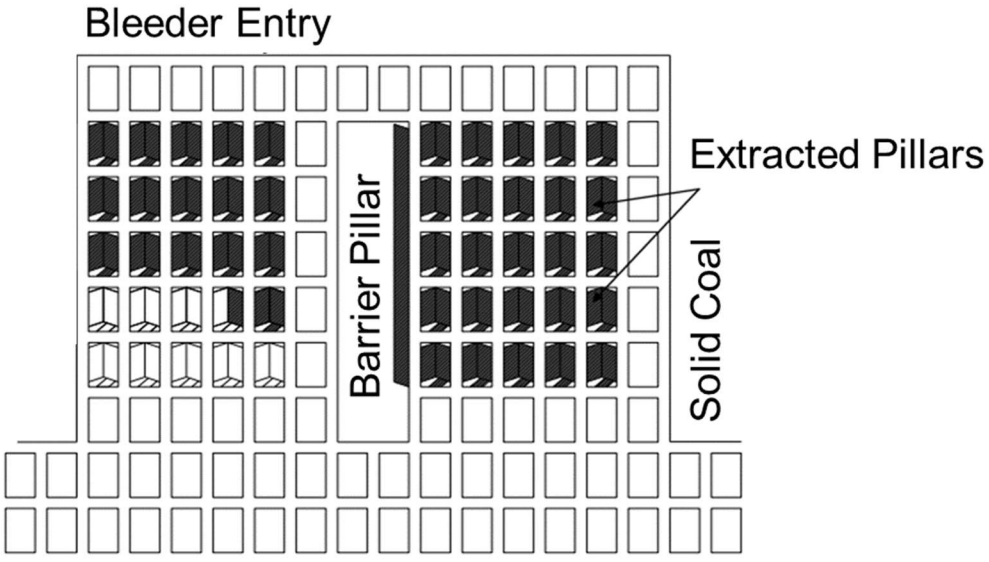

Figure 2.1: General layout of a retreat room and pillar mine (after NIOSH, 2010).

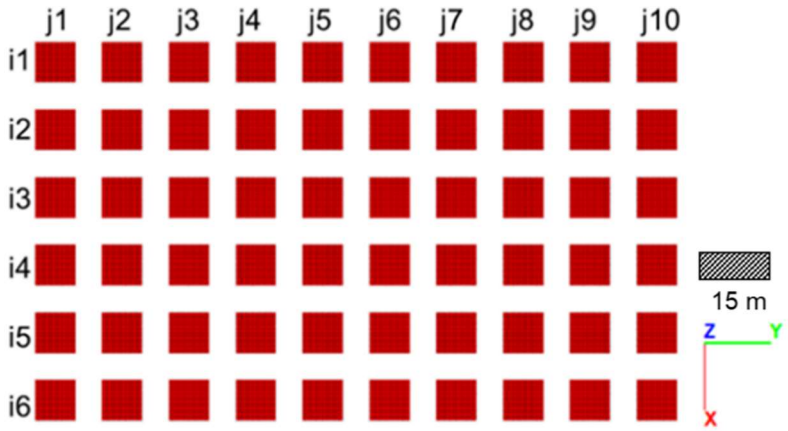

Figure 2.2: Pillar naming convention for W/H = 3 case.

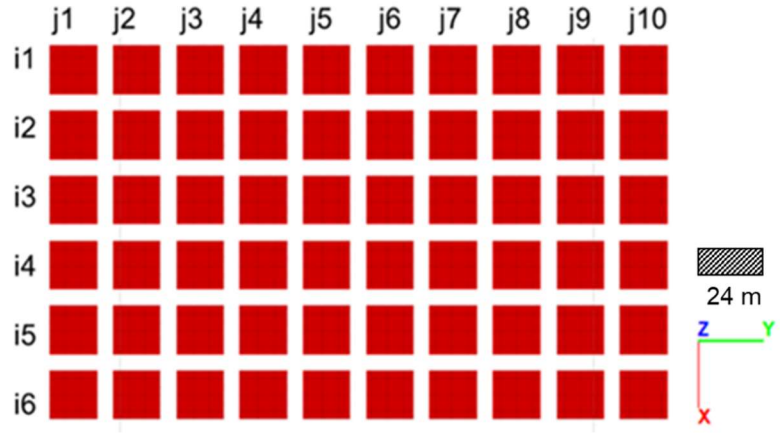

Figure 2.3: Pillar naming convention for W/H = 6 case

Pillars in row i6 and column j1 were not removed, as these pillars are part of the bleeder entry. Accordingly, the panel of pillars to be removed matches the typical layout of a retreat room and pillar mine as shown in Figure 2.1.

In this study, two similar mining sequences are considered: two pillars extracted simultaneously and a single pillar extracted at a time. These two approaches broadly approximate the “Christmas Tree” and “Outside Lift” methods, respectively. In both cases, the pillar removal proceeds from top-left (i1,j2) to bottom right (i5,j10) by first removing pillars in a given column

(top to bottom) and then advancing to the adjacent column (left to right). In the first extraction method (two pillars at a time), the final pillar in each column was removed individually.

2.3.2 Model Set Up

NIOSH visited 30 retreat coal mines, located in Utah, Colorado, West Virginia, Virginia, and Kentucky and a majority of these mines were found to be operating at a depth between 300 m to 500 m (NIOSH, 2010). Accordingly, the adopted coal mine layout has a seam thickness of 3 m with 6 m drifts (Zipf, 2001) at a depth of 400 m below the surface. The model extends up to 200 m below the surface and 74 m below the mining seam (Z depth 200 m to 453 m). The in-situ vertical stress at the top of the coal seam (400 m) is 8.83 MPa. The k ratio was fixed at 1.

As previously mentioned, two W/H ratios were modeled: 3 and 6. The resulting pillar dimensions for W/H=3 and W/H=6, in plan view, are 9 m x 9 m and 18 m x 18 m, respectively. The width and length extents of the model are dependent on the pillar W/H ratios. As the W/H ratio increases, the mining panel area also increases. In addition, a 50 m abutment surrounding the pillar panel was added to the model.

2.3.3 Mesh Size

The mesh size varies throughout the model. Esterhuizen et al. (2010) states that a mesh size of 0.3 m to 0.33 m is typically satisfactory in modeling coal pillars. Accordingly, a mesh size of 0.33 m was used in the depth (Z) range 399 m to 404 m (1 m on either side of the coal seam). The mesh size was doubled to 0.66 m for the abutment area. The mesh size was increased to 1.3 m, 4 m, 8 m, and 12 m for regions further away from the coal seam. Figures 2.4 and 2.5 show how the mesh size varies throughout the model.

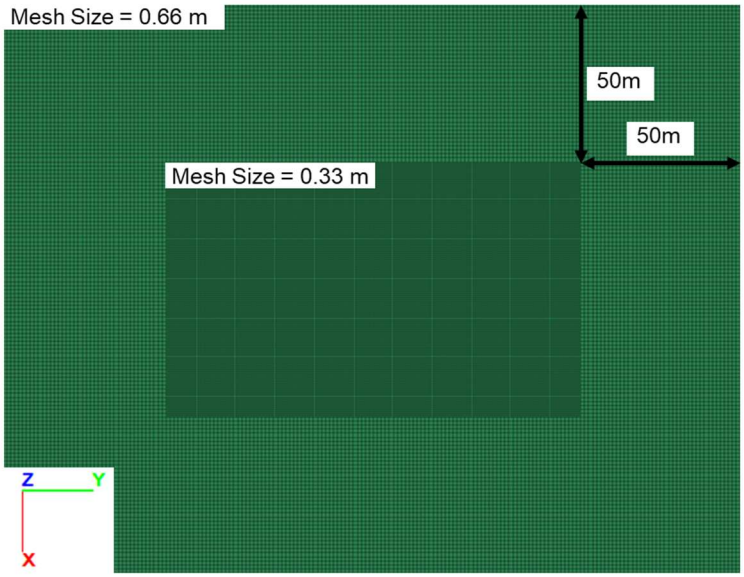

Figure 2.4: Assigned mesh sizes from depth 399 m to 404 m.

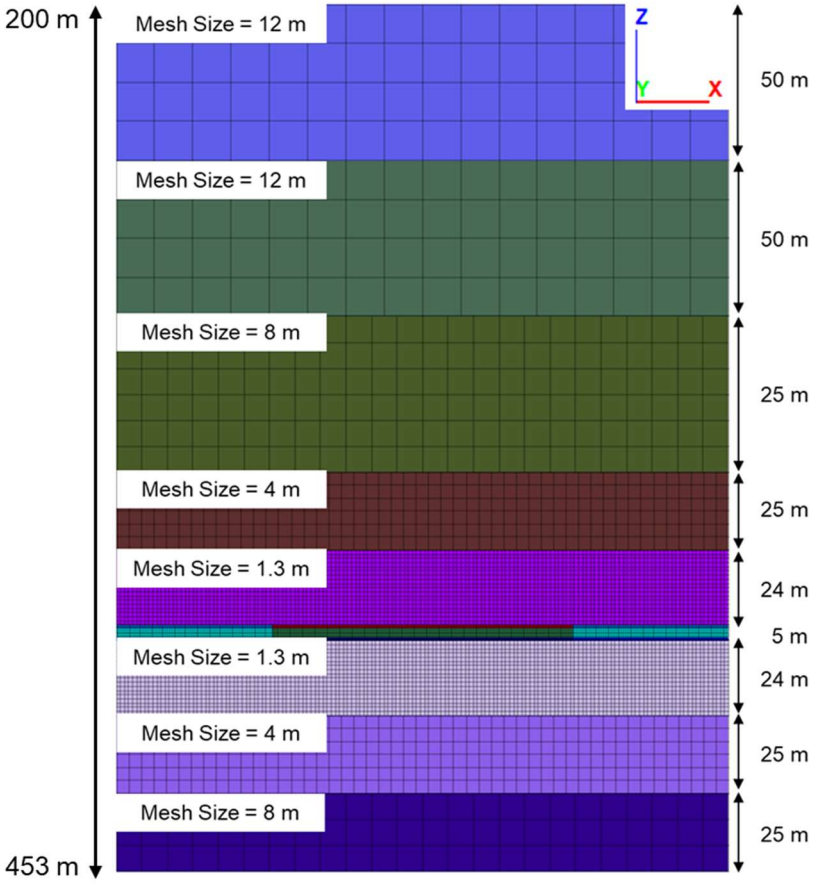

Figure 2.5: Assigned mesh sizes to the model outside of 399 m and 404 m.

2.3.4 Input Parameters

A sensitivity analysis was performed in this study. Specifically, four parameters were considered: retreat method (one or two pillars extracted at a time), W/H ratio, Young's Modulus of the overburden, and pillar material properties. The effect of roof strength was not investigated in this chapter, but was tested in the context of Mine C, which is presented in Chapter 3.

Two overburden Young's Modulus values were considered due to the variable ranges of Young's Modulus reported in the literature (Kumar et al., 2018). End-member values of 10 GPa (stiff roof) and 1 GPa (soft roof) were used in this study.

Two sets of pillar material properties were considered: elastic and strain-softening. The results of the strain-softening cases were then compared to the corresponding elastic model results. In the strain-softening case, only the coal seam was modeled as inelastic, using the elasto-plastic strain-softening model; the surrounding material was modeled as elastic. The elastic properties used in the models are listed in Table 2.1 (Kumar et al., 2018).

Table 2.1: Base model parameters and elastic properties (based on Kumar et al., 2018).

Material	Young's Modulus (GPa)	Density (kg/m3)	Poisson's Ratio
Ore	3	1400	0.25
Host Rock	1 or 10	2250	0.25

Strain-softening parameters for the pillars were based on those from Esterhuizen et al. (2010), (see Table 2.2), who calibrated parameters to match an empirical pillar strength equation (Bieniawski, 1984):

$$\sigma_v(\mathrm{x}) = S_1(0.64 + 0.36\frac{x}{h}) \tag{2.2}$$

where, S_1 is the in-situ coal uniaxial strength, S_p is the coal stress at a distance x from the pillar edge, and h is the height of the pillar.

One deviation from the parameters of Esterhuizen et al. (2010) is that the UCS value was reduced from 20 MPa to 16 MPa in order to model weaker properties; this was done to promote more pillar yield to simulate an upper bound in terms of difference from the elastic models. Additionally, the residual parameters shown in Table 2.2 were also reduced from those suggested by Esterhuizen et al. (2010). Specifically, the residual Hoek-Brown m and s parameters were reduced by 75%. The critical plastic shear strain was also reduced (to 0.02) and is half of the value that corresponds to that suggested by Esterhuizen et al. (2010) after correction for the mesh size dependency of this parameter.

Using a lower critical plastic shear strain results in a greater rate of strength degradation, and simulates more brittle material. A higher critical shear strain of 0.06 was also tested in a limited number of cases to highlight the sensitivity of the model results to this parameter. σ_3^{cv} (a parameter that demarcates the confinement above which a constant-volume flow rule is followed) was assigned a value of 0. With σ_3^{cv} set to 0, the dilation angle is effectively 0^o (Itasca, 2016). Esterhuizen et al. (2010) found that non-zero values for σ_3^{cv} caused large distortions of the yielding elements which were deemed excessive.

The eight cases examined to determine the influence of elasto-plastic strain-softening pillar material behavior on the stress concentration trends predicted through the elastic approach are summarized in Table 2.3.

Table 2.2: Strain-softening Hoek-Brown parameters applied to the ore seam for the elasto-plastic strain-softening cases.

Parameter	Value
UCS (MPa) (lab scale)	16
m-value	1.47
s-value	0.07
a-value	0.65
m-residual	0.25
s-residual	0.00025
Plastic Shear Strain	0.02
σ_3^{cv} (MPa)	0

Table 2.3: Naming convention for the models in this study.

Parameters	Elastic	Inelastic
W/H = 3 ; Soft Roof	Case 3E Soft	Case 3I Soft
W/H = 3 ; Stiff Roof	Case 3E Stiff	Case 3I Stiff
W/H = 6 ; Soft Roof	Case 6E Soft	Case 6I Soft
W/H = 6 ; Stiff Roof	Case 6E Stiff	Case 6I Stiff

2.3.5 Results

The results of the study are presented as percent differences in average pillar stresses between the inelastic (elasto-plastic strain-softening) and elastic model case. Positive percentage differences indicate that the stresses in the strain-softening model are less than those in the corresponding elastic model.

Before comparing the elasto-plastic strain-softening and elastic model cases, two strain-softening models with different critical plastic shear strain values (0.02 and 0.06) were compared. Case 3I Stiff with individual pillar extraction was considered for this test. In this case, positive percentage difference values correspond to higher average stresses in the 0.06 critical plastic shear strain case.

2.3.5.1 Critical Plastic Shear Strain Sensitivity Analysis

The critical plastic shear strain parameter controls the rate of strength degradation following the onset of yield. This parameter essentially determines whether the material acts in a brittle or ductile manner. Lower critical plastic shear strain simulates more brittle material and higher critical plastic shear strain simulates a more ductile material. Values below (0.02) and above (0.06) the recommended typical value for coal (0.04) according to Esterhuizen et al. (2010) were tested in this sensitivity analysis.

The results of the initial sensitivity analysis considering different values of the critical plastic shear strain shows that the pillar stress re-distribution process is notably influenced by the brittleness of the pillars. Figure 2.6 shows the percent difference between the stresses as a result of the critical plastic shear strain.

The development load condition is not shown in Figure 2.6, due to minimal differences in predicted stresses (< 0.5% average pillar stress). Once the retreat operations begin, the critical plastic shear strain impacts the behavior of the pillars. The percent difference jumps from less than 0.5% (development load condition) to over 400% in some pillars. The large discrepancy is due to the fact that the critical plastic shear strain influences the degradation of the pillars. These pillars experience less damage and are able to continue to take on more load after initial yield. In the case of the critical shear strain of 0.02, the pillars carry less stress as there is greater yielding in the pillars, causing them to shed stresses to the abutments.

2.3.5.2 Comparison of Elasto-Plastic Strain-Softening and Elastic Models

Comparison of the models is presented as the % average stress difference for each pillar. The % average stress difference was calculated using the average vertical stress through the pillar in the elasto-plastic strain-softening material model relative to its corresponding elastic

material model. A positive % average stress difference reflects greater predicted average vertical stress in the pillar under elastic conditions.

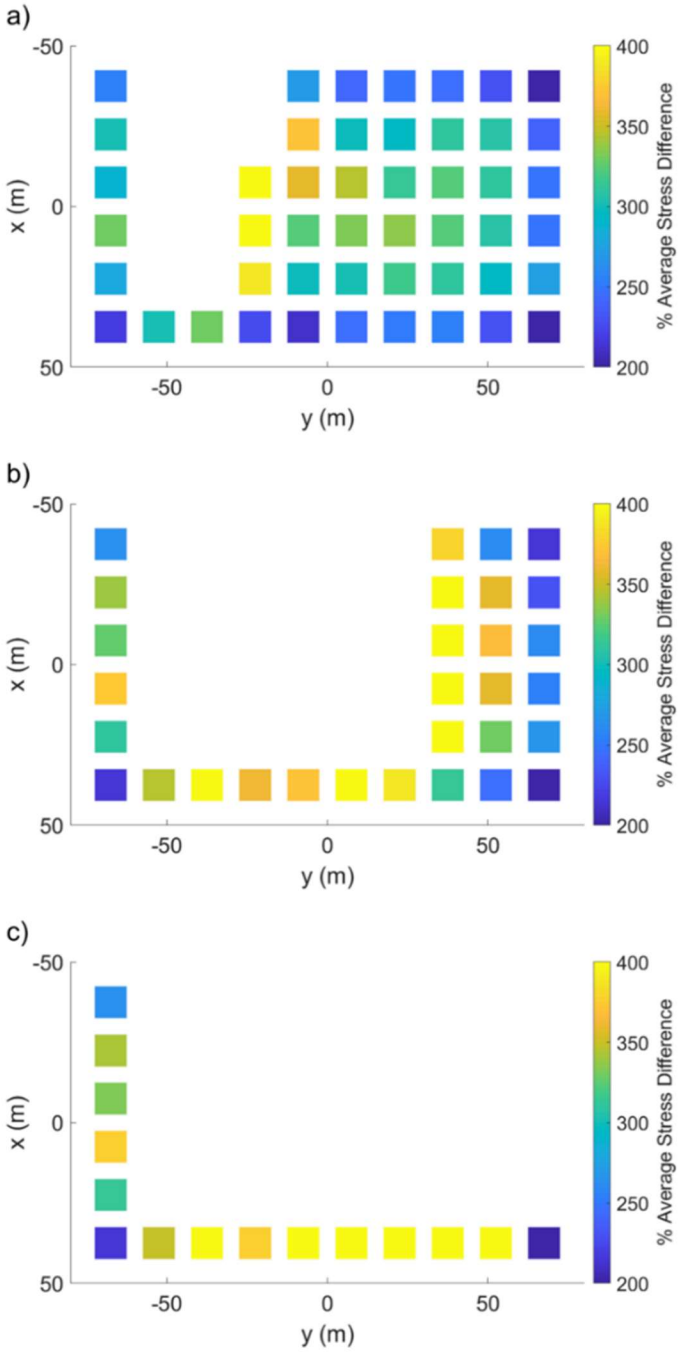

Figure 2.6: Stress comparison between a critical plastic shear strain of 0.2 and 0.06. (a) Percent difference for pillar removal at stage i2j4. (b) Percent difference for pillar removal at stage i5j7. (c) Percent difference after all pillars are removed from the panel.

2.3.5.2.1 W/H of 3

In the W/H = 3 case, upon examining the average stress difference as a result of the sequencing of the pillar removal (one at a time versus two at a time), it was found that there was minimal impact on the model results. Because of this, more detailed results focused on the influence of pillar removal sequence are not presented. All results shown correspond to the case where one pillar was removed at a time.

Figure 2.7 represents the percent difference between Case 3I Stiff and Case 3E Stiff. Figure 2.8 shows the same results for Case 3I Soft and Case 3E Soft.

In both the stiff and soft roof models, the development load conditions (initial room and pillar) is relatively insensitive to the use of an elasto-plastic strain-softening constitutive model; this is because the initial development loading condition doesn't induce high enough stresses to generate significant yield in the pillars.

During the retreat process, stresses in Case 3I Stiff and Soft differ upwards of 80% from those in the Case 3E Stiff and Soft. The stress difference is due to the yielding of the pillars adjacent to the excavated area in the elasto-plastic strain-softening model. As pillars are removed, the adjacent pillars take on more load. As the load on the pillars increases, the pillars experience more yield. The pillars continue to yield until they have reached their residual state and have shed most of their load. As a result, the pillars closest to the excavated area have the greatest % average stress difference. The % average stress difference then reduces moving towards the outer boundary, where pillars experience less stress difference.

Comparing the results of the stiff versus soft roof case, it is apparent that yield extends further away from the excavated area in the soft roof case. However, this is not typical of what has been observed in the field for less extreme conditions. Mark (2000) found that stiffer roofs

lead to less stress shedding and can therefore support smaller pillars. This is because with a stiffer roof, load can be transferred greater distances, and as a result more load is transferred to the abutments than to just the adjacent pillars once de-pillaring starts. It should be expected that stresses should be localized in the pillars around the active mining area with a soft roof and will be spread out further with a stiff roof (limited yield in the soft roof case allows the stresses to remain localized. Thus, an investigation as to why the model results appear to contradict this phenomenon was performed, and the results are presented in Section 2.3.6.

Examining the model in FLAC^{3D} confirms the observation and the yielding of pillars with a W/H=3. At the i2j4 retreat extraction stage, almost all the pillars have yielded through their cores. The plastic shear strain values within the pillars are very similar, with minimal difference, between the soft and stiff roof cases. The resulting plastic shear strains of the soft roof case is shown in Figure 2.9, which is also representative of the stiff roof case as the soft and stiff roof cases show very similar results. A plastic shear strain value greater than 0.02 indicates that the material is in its residual state. Such large extents of yielding can be a sign of improper mine (pillar) design and might lead to global failure during the retreat mining process. As seen in Figure 2.9 and Figure 2.10, the soft roof case experiences more yield as highlighted by the top right pillar. In the soft roof case, the mentioned pillar has reached its residual state, whereas in the stiff roof case the mentioned pillar is still able to take on more load.

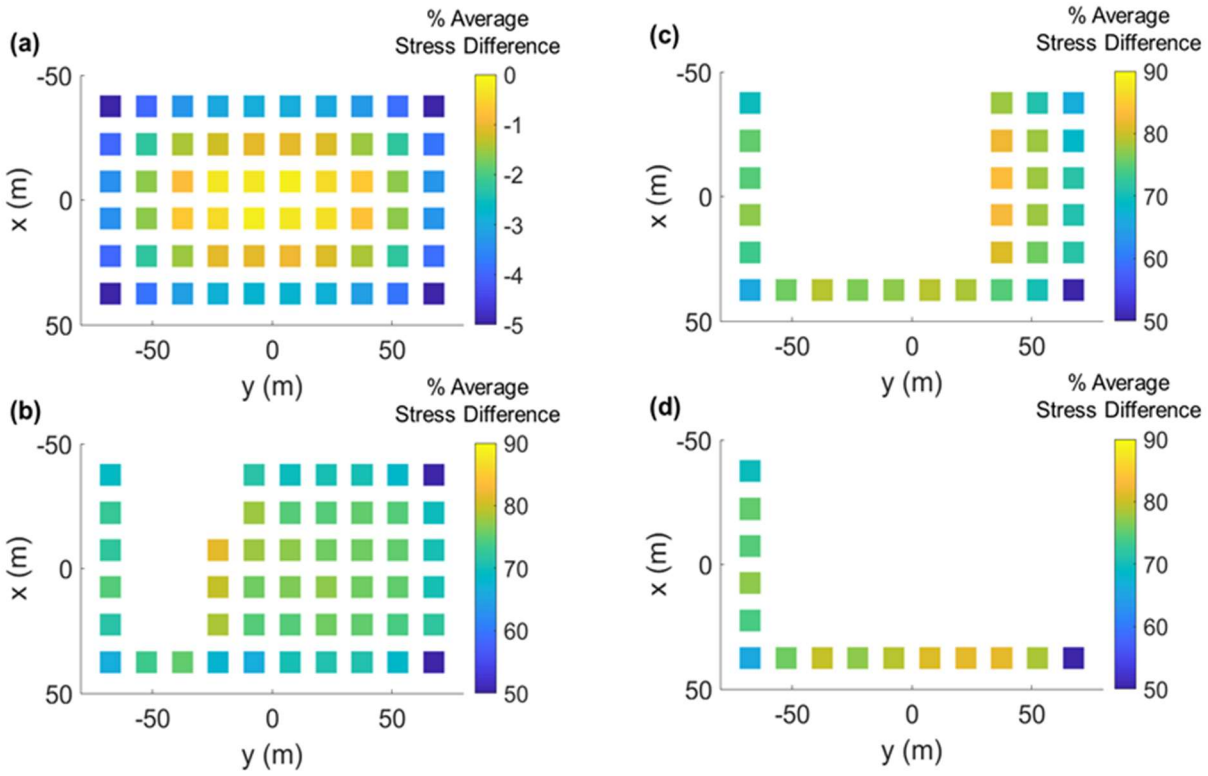

Figure 2.7: Stress comparison between Case 3I Stiff and Case 3E Stiff: (a) Stress percent difference prior to pillar removal. (b) Percent difference for pillar removal at stage i2j4. (c) Percent difference for pillar removal at stage i5j7. (d) Percent difference after all pillars are removed from the panel. Note that the color bar is different in Figure 2.7 (a). This is due to the small range reflected in the figure that does not lie within the range of (b), (c), or (d).

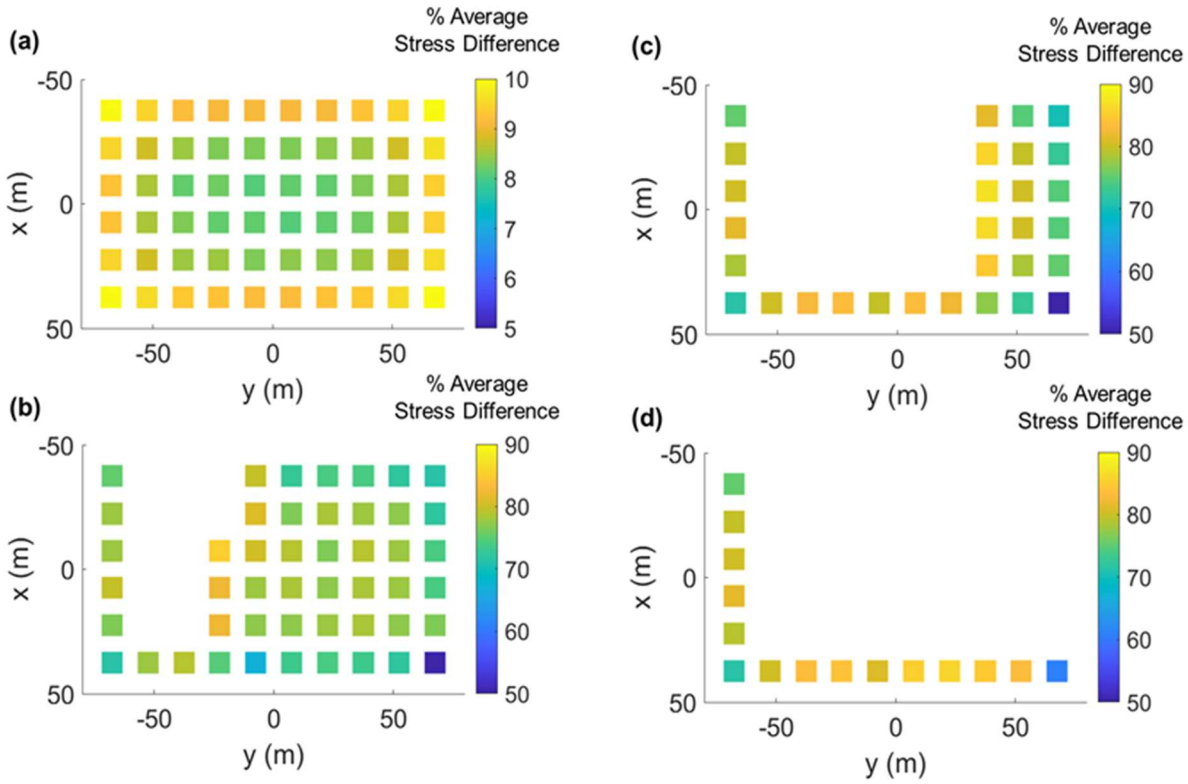

Figure 2.8: Stress comparison between Case 3I Soft and Case 3E Soft: (a) Stress percent difference prior to pillar removal. (b) Percent difference for pillar removal at stage i2j4. (c) Percent difference for pillar removal at stage i5j7. (d) Percent difference after all pillars are removed from the panel. Note that the color bar is different in Figure 2.8 (a). This is due to the small range reflected in the figure that does not lie within the range of (b), (c), or (d).

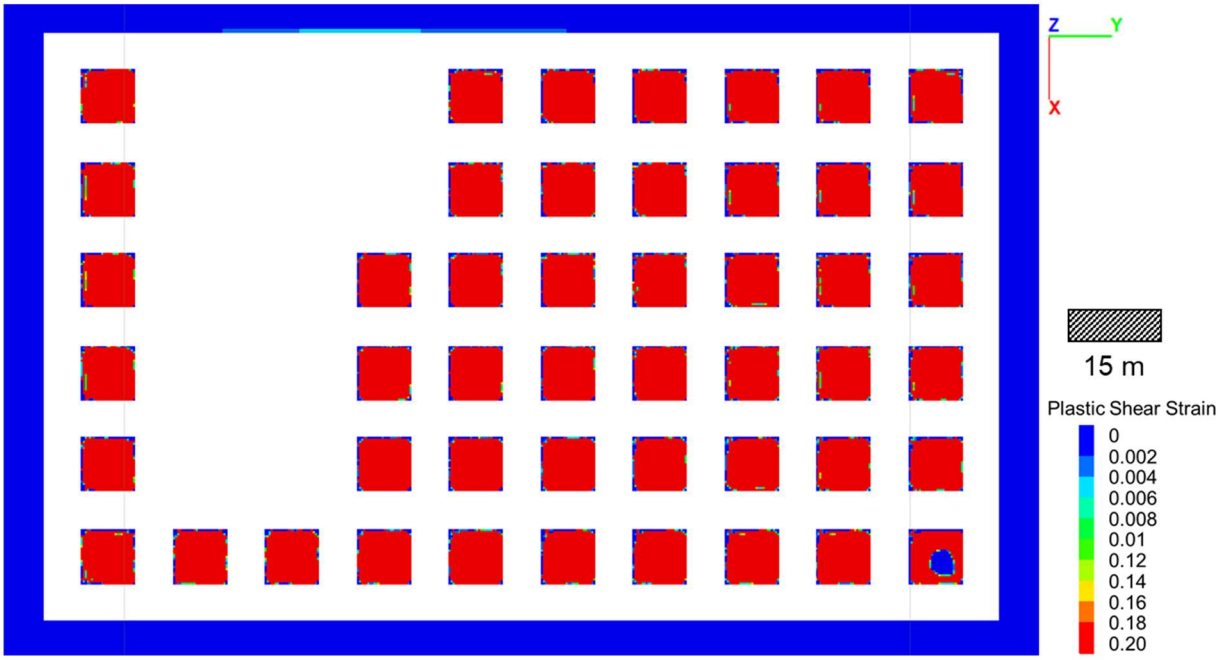

Figure 2.9: Plastic shear strain within each pillar at the i2j4 retreat extraction stage for Case 3I Soft.

2.3.5.2.2 W/H of 6

Like the W/H = 3 case, the W/H = 6 case also was minimally impacted by the pillar removal sequence. Thus, the results shown correspond to the cases where one pillar was removed at a time.

Figure 2.10 represents the percent difference between Case 6I Stiff and Case 6E Stiff. Figure 2.11 shows the same results for Case 6I Soft and Case 6E Soft. Similarly to the W/H = 3 cases, the development load stress conditions (initial room and pillar) are relatively insensitive to the use of an elasto-plastic strain-softening constitutive model.

During the retreat mining process, stresses in Case 6I Stiff and Soft differ upwards of 15% from those in Case 6E Stiff and Soft. The stress difference is due to the partial yielding of the pillars adjacent to the excavated area in the elasto-plastic strain-softening model. As pillars

are removed, the adjacent pillars take on more load, resulting in yielding at the pillar edges. The pillars don't fully yield, and as a result, load shedding onto surrounding pillars is minimal.

As in the W/H = 3 cases, the soft roof case appears to have the stresses shed further away from the yielding pillars near the excavated area. However, this is a consequence of considering the elastic and elasto-plastic strain-softening cases together in terms of a difference metric rather than individually; this will be discussed in greater detail in Section 2.3.6.

Examining the model in FLAC^{3D} confirms the limited nature of the W/H=6 pillar yield. It can be seen that at the i2j4 retreat extraction stage, yielding in the pillars occurs along the outer edges of the pillars adjacent to the extracted area. The plastic shear strain values within the pillars, in the soft roof case, are shown in Figure 2.12 and also is representative of the stiff roof case. Yield is limited to pillars nearest to the excavated area, and only the edges of the pillars have yielded for both the soft and stiff roof case.

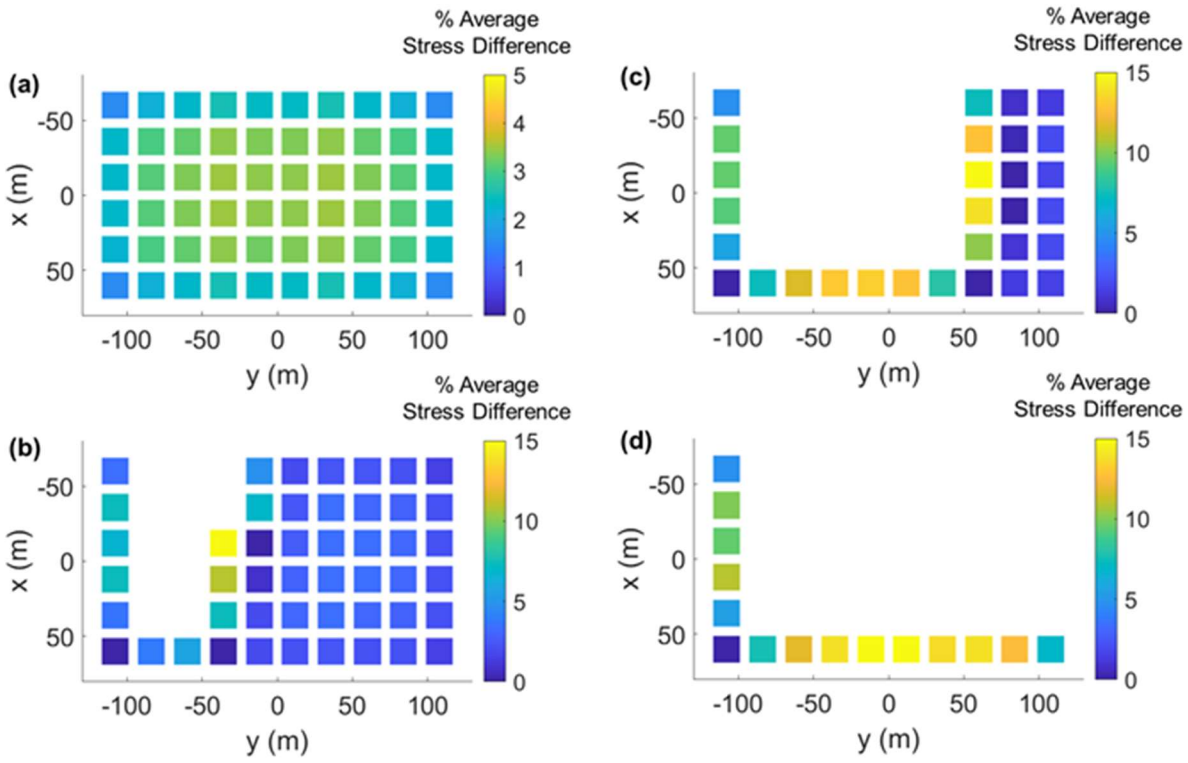

Figure 2.10: Stress comparison between Case 6I Stiff and Case 6E Stiff: (a) Stress percent difference prior to pillar removal. (b) Percent difference for pillar removal at stage i2j4. (c) Percent difference for pillar removal at stage i5j7. (d) Percent difference after all pillars are removed from the panel. Note that the color bar is different in Figure 2.10 (a). This is due to the small range reflected in the figure that does not lie within the range of (b), (c), or (d).

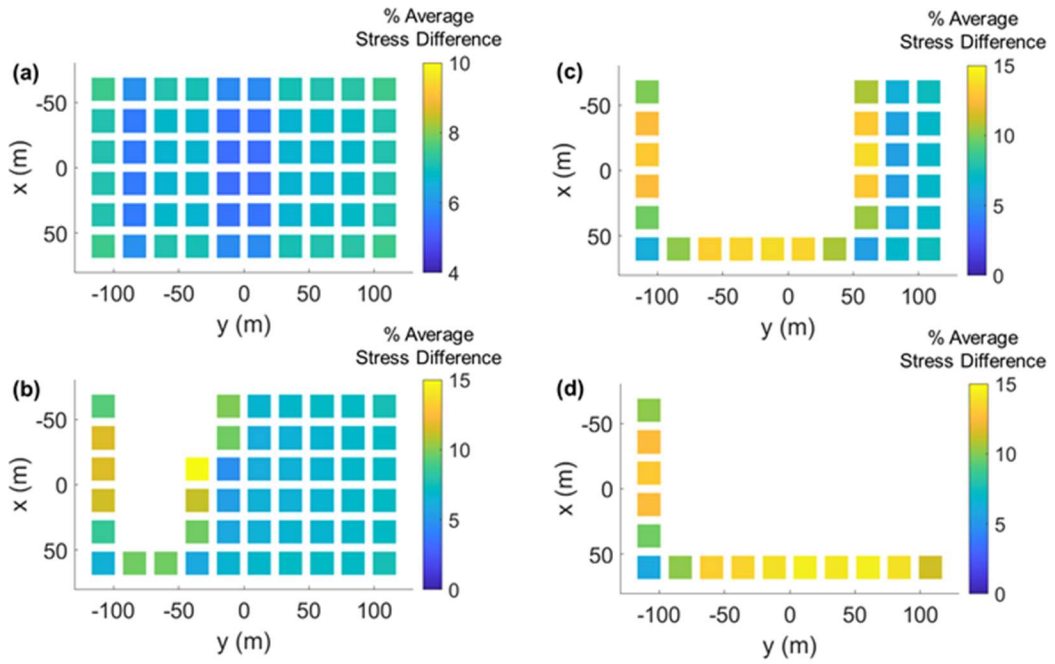

Figure 2.11: Stress comparison between Case 6I Soft and Case 6E Soft: (a) Stress percent difference prior to pillar removal. (b) Percent difference for pillar removal at stage i2j4. (c) Percent difference for pillar removal at stage i5j7. (d) Percent difference after all pillars are removed from the panel. Note that the color bar is different in Figure 2.11 (a). This is due to the small range reflected in the figure that does not lie within the range of (b), (c), or (d).

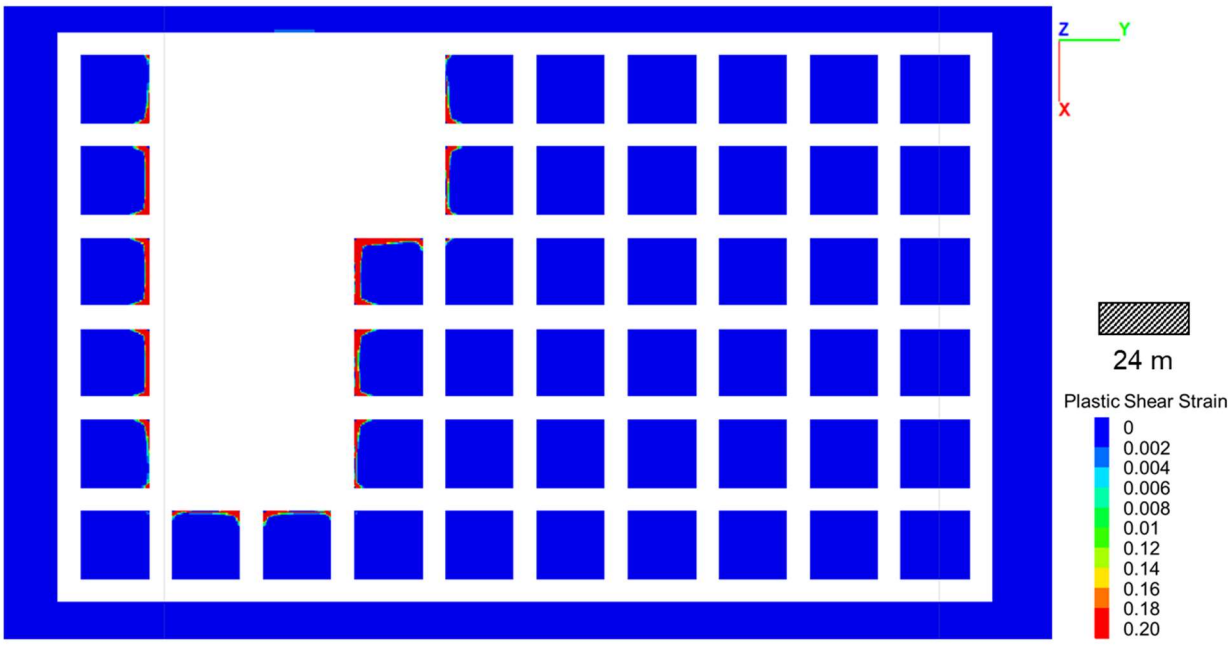

Figure 2.12: Plastic shear strain within each pillar at the i2j4 retreat extraction stage for Case 6I Soft.

2.3.6 Discussion and Conclusions

From the results of the various models that were run as a part of this study, it can be seen that modeling with elastic properties may result in incorrect pillar stress estimations. Prior to removal of any pillars, there is minimal % average stress difference between the elasto-plastic strain-softening and elastic model. Thus, the impact of modeling the development stage as elastic or elasto-plastic strain-softening is insignificant (although this will be specific to the geomining conditions considered). However, as the retreat process commences, the differences between the elastic and elasto-plastic strain-softening models become significant. As pillars are removed, the elastic models begin to incorrectly estimate the pillar stresses. This is because stresses start shedding to surrounding pillars. It is important to note that only the final equilibrium stress results were considered. With this in mind, it makes sense that the differences between the elastic and elasto-plastic strain-softening increase during retreat operations because the pillar load-carrying capacity is lower in the elasto-plastic strain-softening cases due to yield. However, it is expected that the maximum stress experienced in any given pillar during the transient load transfer process is actually greater in the elasto-plastic strain-softening cases. This is because the given pillar will be taking on load from adjacent yielded pillars before the given pillar itself yields. As a result, the elastic models may be optimistic in some cases, as they fail to explicitly capture the potential for cascading failure to develop in the pillar array. Thus, the elasto-plastic strain-softening models have the potential to provide a more realistic representation of stresses in pillars.

Besides the elastic versus elasto-plastic strain-softening model differences, the greatest influence observed was that of the W/H pillar ratio. In the case of W/H = 3 pillars, the stresses

differed in excess of 75%, whereas, for W/H = 6 pillars the stresses rarely differed between the elastic and elasto-plastic strain-softening cases by more than 15%. The primary reason is that pillar yield is impacted by the W/H ratio of the pillar (see Figure 2.7 through 2.12). This is largely because the W/H ratio influences the extraction ratio, which in turn influences the resulting stresses. Additionally, there is the potential for higher W/H pillars to generate more confinement, which will suppress yield. Considering the W/H ratio as part of the TAT Equation 2.3, it can be observed how greater W/H ratios pillars are expected to have lower stresses (Pariseau, 2006).

$$\sigma = \gamma * H \left(\frac{w+h}{w}\right)^2 \quad (2.3)$$

γ is the unit weight of the rock, H is the depth, w is the pillar width, and h is the drift width. Inputting the model geometry parameters used in the W/H of 3 and 6 models, the estimated stresses as a function of γ * D are as follows:

- W/H of 3: $\left(\frac{9+5}{9}\right)^2$* γ *D
- W/H of 6: $\left(\frac{18+5}{18}\right)^2$* γ *D

TAT shows that increasing the W/H ratio (while keeping entry width constant) results in a decrease in stress within the pillar due to the decreased excavation ratio. The lower stress combined with the geometric strengthening effects associated with higher W/H pillar ratios leads to less yield throughout the retreat mining operation.

The yielding of the pillars significantly impacts the stress redistribution throughout the retreat process. Yielding of the pillars begins along the edges and then propagates towards the center of the pillar. With continued loading, the pillar attains its residual strength and is unable to take on

additional load. This causes the surrounding pillars to take on that load, thereby causing these pillars to yield.

The study shows that in retreat mining applications, the stress redistribution process is highly sensitive to the geometric and material parameters that control pillar yield. The excavation ratio, as influenced by the W/H pillar ratio in this case, influences the resulting pillar stresses and yield. Stress will redistribute beyond the excavated area as pillars yield and shed load to surrounding pillars. This was found to be significant in the modeled W/H=3 cases (higher extraction ratio).

In addition, the influence of stiff and soft roofs is notable when examining the extent to which loads are redistributed from yielding pillars. From Figure 2.7 through Figure 2.11 it appears that soft roofs (low Young's Modulus) result in greater load transfer away from the excavated area than stiff roofs (high Young's Modulus). However, as previously noted, this observation contradicts what is expected based on previous studies. This distance load distributes away from the excavated area is a result of the corresponding flexural rigidity of the roof. The less a roof is able to deflect (more flexural rigidity), the greater the distance loads can transfer. As a result, stiffer roofs should transfer stresses over greater distances than a soft roof. Because of this contradiction, the elastic and elasto-plastic strain-softening models for the W/H = 6 case were analyzed independently. The stresses at the middle of the coal seam were examined and the results are shown in Figure 2.13.

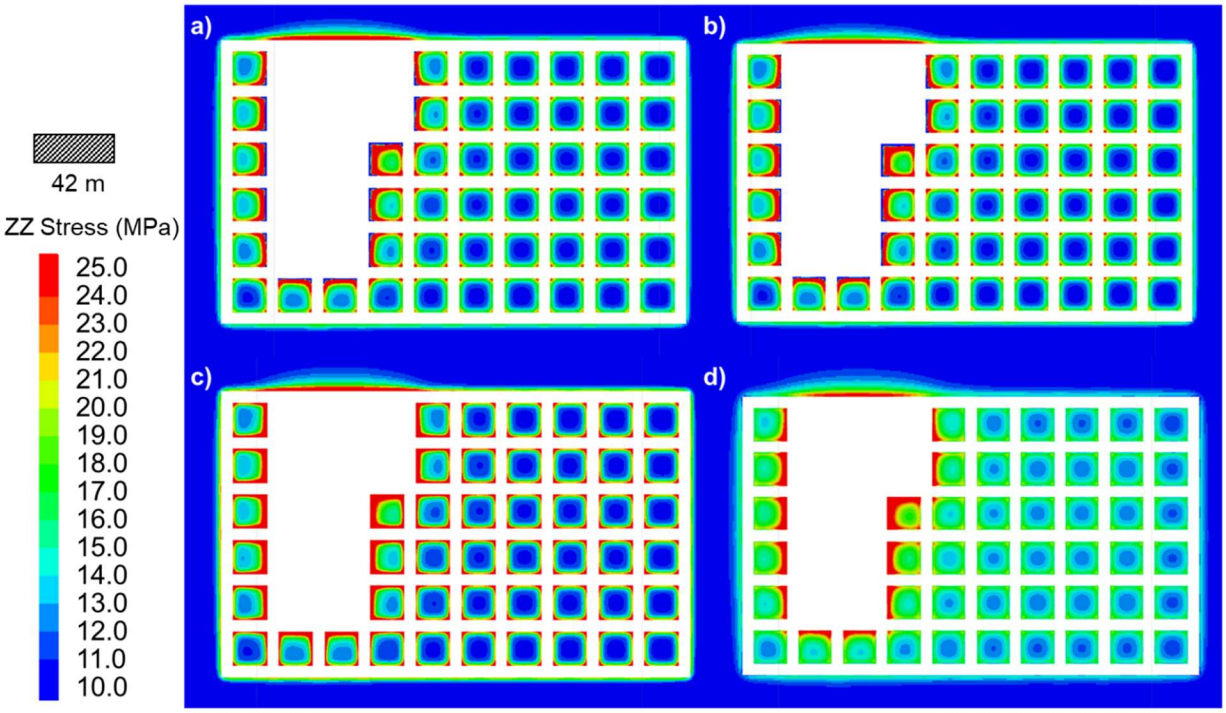

Figure 2.13: Panel stress at the i2j4 retreat extraction stage for Case 6. a) Panel stress for Case 6I Soft. b) Panel stress for Case 6I Stiff. c) Panel stress for Case 6E Soft. d) Panel Stress for Case 6E Stiff.

Figure 2.13 a) and b) show the panel stresses for the Case 6I Soft and Stiff, respectively. It is noted that there is almost no difference between the stresses in the panel. Thus, the differences in the % stress difference seen in Figure 2.10 and Figure 2.11 are associated with difference between the elastic cases. This is confirmed by Figure 2.13 c) and d) (soft and stiff roof, respectively). Figure 2.13 c) and d) have noticeably different stresses in the panel. The stiff roof case (Figure 2.13 d)) has greater stresses in the panel than the soft roof case (Figure 2.13 c)). The elastic models reflect the stiffer roof (more flexural rigidity) transferring loads over a greater distance (noted by the greater stresses). Because more overall stress is observed in the 6E Stiff pillar array, there is less of a difference in the average stress between the elastic and elasto-plastic strain-softening stiff roof case. In the 6I Soft case, greater stresses form around the active mining area, into the abutment, and around the pillar edges in the pillar array. This may be a

result of a more heterogeneous stress distribution in the 6I Soft case than the 6I Stiff case. That is why the % average stress difference is less for the stiff roof case than the soft roof case, which lead to the initial (incorrect) implication that loads traveled greater distances in the soft roof case. Additionally, it is interesting that once appreciable pillar yield occurs, the stress transfer becomes less dependent on roof properties. In other words, the well accepted concept about the influence of the roof on stress transfer is not universal, and may only apply in cases where pillar behavior is predominantly elastic.

With all this in mind, predictions of pillar stresses made using elastic models may not be sufficient in some cases. The elastic cases fail to explicitly capture the potential for cascading failure to develop in the pillar array. In contrast, elasto-plastic strain-softening models consider the dynamic interaction between stress and strength as pillars yield during retreat mining operations. The capability of capturing yield progression is pertinent in understanding the stresses within a pillar, load transfer during mining operations, and predicting potential pillar failure.

By performing this preliminary study of a generic room and pillar mine, the influences of material properties, pillar W/H ratio, and roof stiffness on stress re-distribution during the retreat mining process have been examined. Models implementing elastic and elasto-plastic strain-softening pillar behavior were considered. The differences between the elastic and elasto-plastic strain-softening models were more significant for lower W/H ratios (greater extraction ratio). In these cases, pillars experienced more yield and transferred more load onto surrounding pillars and abutments. In addition, load transfer greatly differed in the elastic cases depending on roof properties in contrast to the elasto-plastic strain-softening cases, highlighting how stress transfer becomes less dependent on roof properties once substantial pillar yield occurs.

2.4 Conclusions

This chapter summarizes the existing state of knowledge regarding pillar mechanics and pillar design, with particular emphasis on coal mining. Extensive prior research has been performed focused on individual mining system components that impact retreat mining (i.e. retreat method, roof/pillar interaction, blasting influences, material properties, gob, etc.). However, relatively little research has been performed focusing on the retreat phase of room and pillar mining. Research has mainly focused on individual components of retreat mining (i.e. gob behavior, roof/floor influences). Additionally, prior research often relies on simplified methods (e.g. analytical methods or elastic numerical models). Thus, more research is needed considering the full range of potential ground behavior, which can be achieved using three-dimensional numerical models.

With this in mind, a preliminary study was conducted using FLAC^{3D} to create a numerical model of a generic room and pillar mine. The study examined the combined influences of material properties (elastic versus elasto-plastic strain-softening), pillar W/H ratio, and roof stiffness. The importance of elasto-plastic strain-softening cases was highlighted in the preliminary study. The differences between the elastic and elasto-plastic strain-softening cases became significant once retreat operations commenced. Stresses in the elasto-plastic strain-softening cases reduced and were lower than in the elastic cases. This is due to the reduced load-carrying capacity as a result of yielding within the pillar array. As a result, elasto-plastic strain-softening cases were able to capture the potential for failure to occur within the pillar array, whereas elastic cases were not. Thus, the elasto-plastic strain-softening models are able to provide a potentially more realistic representation of stresses in the pillar array allowing for

improved understanding of mining operations that can lead to improved mine design considerations.

CHAPTER 3

MINE C CASE STUDY AND MODEL CALIBRATION

3.1 Mine C Case Study Goals

Research that examines retreat mining as a whole has the potential to advance the current state of knowledge regarding pillar mechanics and pillar stability. A calibrated numerical model that reflects site observations and takes into account the different components of a retreat mine (i.e. gob, depillaring sequence, retreat method) can serve as a starting point for future research efforts. For example, investigations of the impact of depillaring sequences, retreat method, remnant pillar influences, etc. could be examined at the panel or mine scale. As part of this thesis, an in-mine case study and model calibration were performed to investigate global and local stress re-distribution that occurs during retreat mining.

3.2 Mine C Site Information

3.2.1 Regional Geology

Mine C is a room and pillar coal mine located in the Western U.S. The local geology is a part of the San Juan Basin. The San Juan Basin encompasses parts of Utah, Colorado, Arizona, and New Mexico, and has an approximate area of 21,600 square miles (Figure 3.1). In the area of interest, the formations of the San Juan Basin are all sedimentary rocks of Late Cretaceous age. The Late Cretaceous age encompassed many transgressions and regressions of shallow seas. The rocks mainly consist of transgressive and regressive marine shore-zone sediments that were deposited in shallow seas that encroached into the San Juan Basin area from the northeast, and nonmarine clastic deposits from source areas southwest of the basin (Craig, 2001). Figures 3.2 and 3.3 show cross-sections of the stratigraphy and the geologic units of the San Juan Basin, respectively.

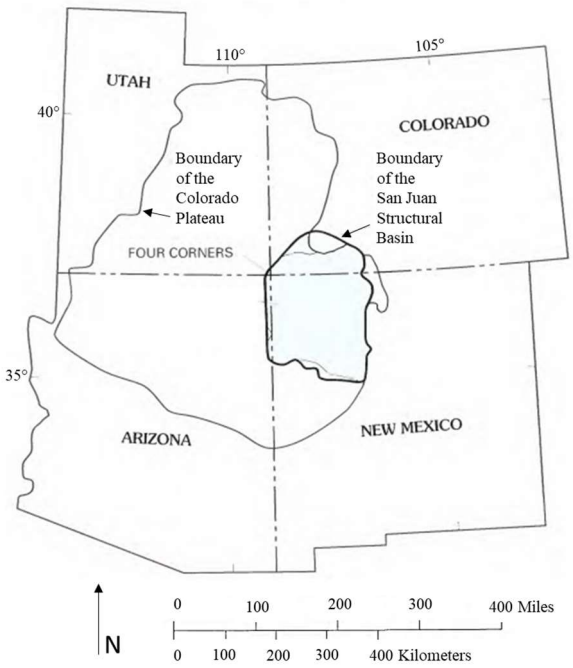

Figure 3.1: Map of the San Juan Structural Basin that makes up the local geology of Mine C (Craig, 2001).

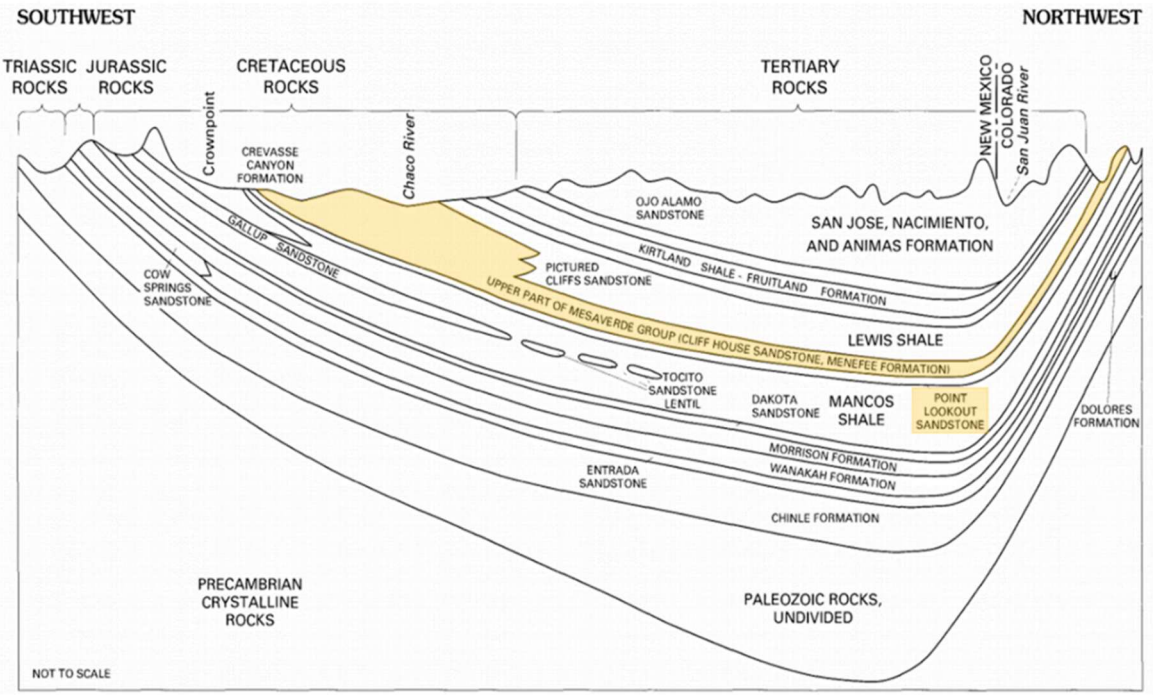

Figure 3.2: Stratigraphic cross-section of the San Juan Basin (Craig, 2001). The highlighted sections show the units that make up the regional geology of Mine C.

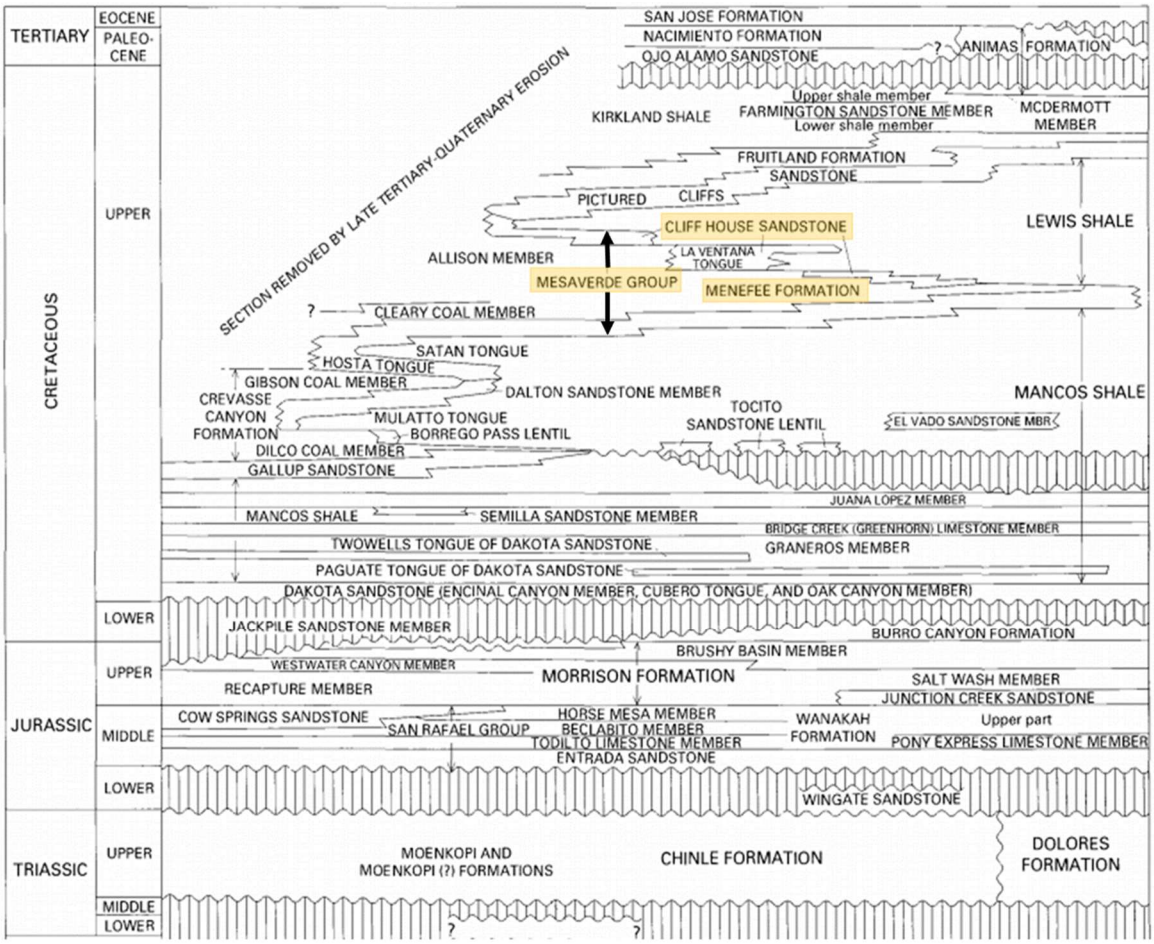

Figure 3.3: Geologic units of the San Juan Basin (Craig, 2001). The highlighted sections show the units that make up the regional geology of Mine C.

Predominant formations of the San Juan Basin, local to Mine C, are part of the Mesaverde Group. The Mesaverde Group consists of the Point Lookout Sandstone, the Menefee Formation, and the Cliff House Sandstone.

The Point Lookout Sandstone is the lowermost formation of the Mesaverde Group. The formation conformably overlies the Mancos Shale throughout the basin. The Point Lookout Sandstone typically consists of light-gray, thickly to very thickly bedded, very fine to medium grained, locally cross bedded sandstone. Thin interbeds of dark marine shale can be found, especially in the lower part of the formation. The Menefee Formation overlies the Point Lookout

Sandstone, with some local interfingering at the contact. The formation consists of interbedded and repetitive sequences of variably thick sandstone, siltstone, shale, claystone, carbonaceous shale, and coal beds. Lastly, the Cliff House Sandstone overlies the Menefee Formation, with some interfingering, and is the uppermost formation of the Mesaverde Group in the San Juan Basin. The Cliff House Sandstone consists of several sandstone fingers of varying thicknesses and areal extents. The Cliff House Sandstone generally consists of tan, light brown, or yellowish brown, thick to very thick bedded and locally cross-bedded sandstone with calcite or silica cement and clay matrix (Craig, 2001).

3.2.2 Mine C Layout and Sequencing Information

In context of the Mine C case study, the focus is on the Main Panel. In this panel, depillaring operations were performed and pillar stability was monitored by installing instruments into one of the pillars to understand the resulting pillar behavior associated with depillaring. Figure 3.4 shows the Mine C map, which includes the completed depillaring of the Main Panel area as of 03/06/2018 (the date on which the instrumented pillar was mined out). The mine map provides the date on which the different pillars were extracted from this panel. The location of the instruments are also indicated by the red lines in Figure 3.4.

The cut sequence Mine C utilized for their depillaring operation was based on the Outside Lift retreat method. With this cut sequence, Mine C employs two support systems. System 1 (shown in Figure 3.5) used 4 MRS units throughout the operation and timbers to create a breaker row to help control gob movement. System 2 (shown in Figure 3.6), on the other hand, used 2 MRS units and posts and timber to create multiple breaker rows.

Figure 3.4: Mine C map of the panel area to be modeled.

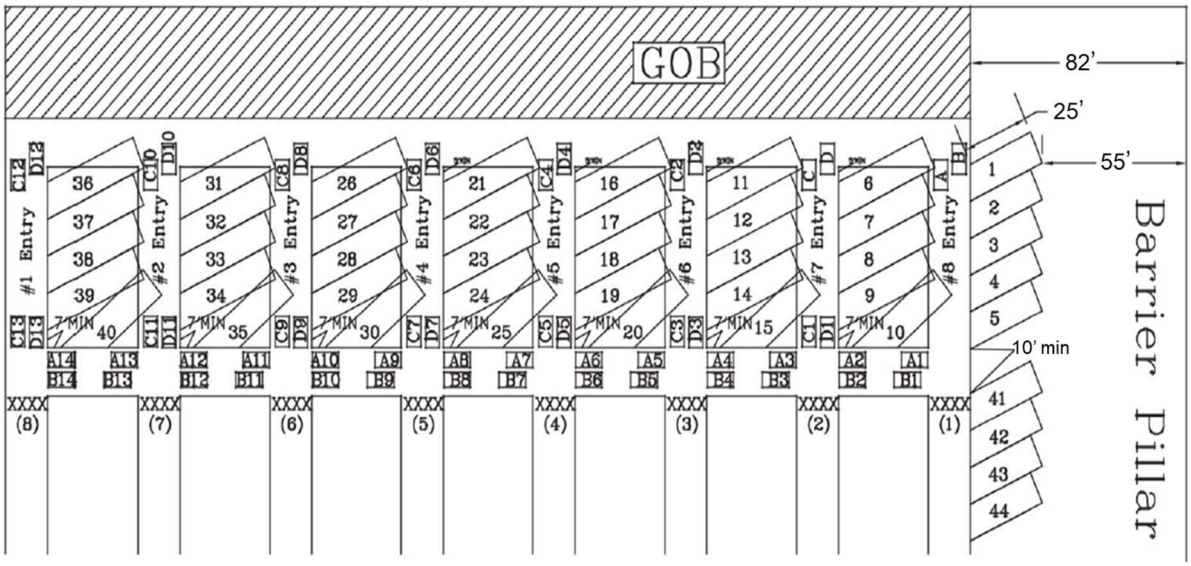

Figure 3.5: Cut sequence for support design system 1 with 4 MRS units and a timber breaker row.

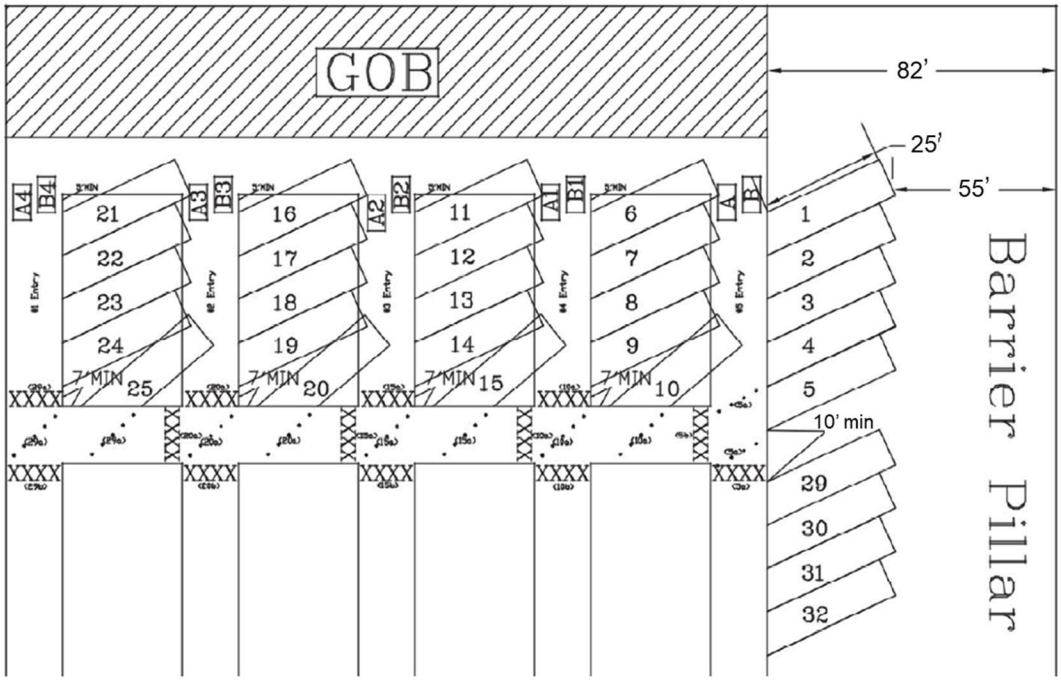

Figure 3.6: Cut sequence for support design system 2 with 2 MRS units and multiple timber breaker rows.

3.3 Instrumentation of Mine C

To understand how pillars react to depillaring, instrumentation was installed in Mine C. In October 2017, three extensometers and one borehole pressure cell (BPC) were installed in a pillar located in the Main Panel, between X-cut 9 and 10 (shown in Figure 3.4). The extensometers were 6 anchored, with the anchors located 0.406 m, 0.711 m, 1.016 m, 1.626 m, 2.540 m, and 4.572 m from the borehole collar. The head was 0.203 m long and recessed into the pillar to avoid damage during production operations. Two of the extensometers were installed in the cross-cut (Figure 3.7), while the stress cell and one extensometer were installed in the entry (shown by the small red lines in Figure 3.4). Other geometric details of the instrumented site can be found in Figure 3.8.

Depillaring operations concluded in the Main Panel in March 2018. The instrumented pillar was extracted on March 6th around 10 AM.

Figure 3.7: The two extensometers installed in the cross-cut. The heads were ultimately fixed to the borehole mouth using wooden wedges.

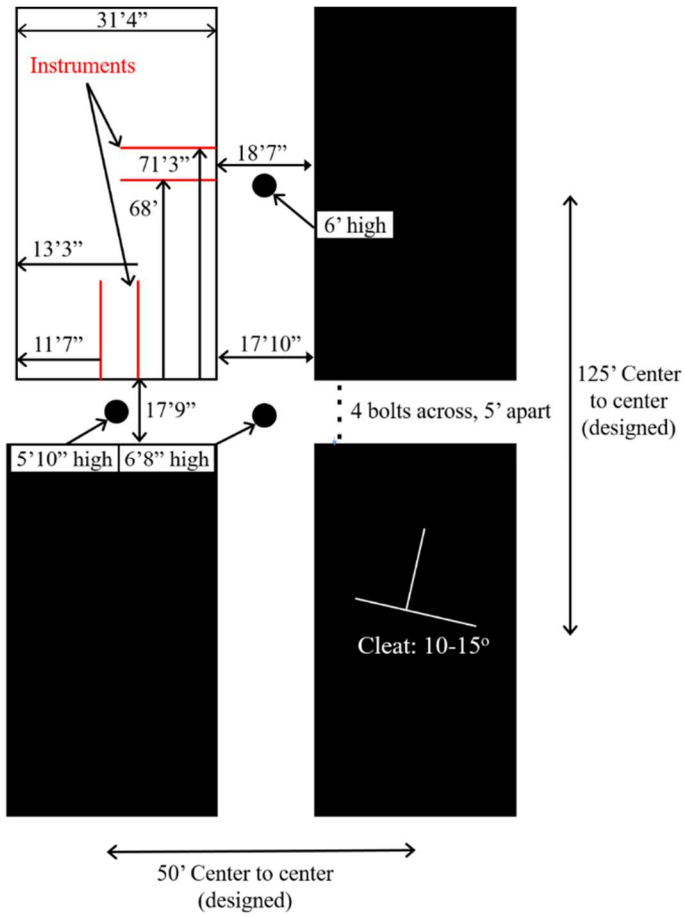

Figure 3.8: Instrumentation layout at Mine C.

3.3.1 Field Measurements and Interpretation

The displacements recorded by the three extensometers are shown in Figure 3.9. Gaps in the displacements recorded by the extensometers are represented by dotted lines. The graphs display movement relative to the innermost anchor (4.572 m into the pillar), which was assumed to be approximately stationary. Additionally, the data beyond Anchor 2 have been excluded, as movements at those locations were negligible (<1 mm). These data indicate minimal fracture development occurred in the rib along the cross-cut until March 6th (Figure 3.9 a and b). However, the rib along the entry showed substantial deformation, with movements on the order of 20 mm (Figure 3.9 c). This was likely due the extraction sequence leading up to the

instrumented pillar. Pillars on the entry side of the instrumented pillar were removed prior to 03/06, whereas pillars on the cross-cut side of the instrumented pillars were not removed. This resulted in a greater concentration of load on the entry side of the instrumented pillar than the cross-cut side, since there were coal pillars on the cross-cut side with which to share load.

Due to the substantial deformation on the rib along the entry, further analysis of this data was performed. The time window for Figure 3.9 c was shortened to February 26th – March 6th, and the resulting plot is shown in Figure 3.10. Results were zeroed with respect to the displacement recorded on 02/26 as a result of the extended time period of "missing" data, to reduce uncertainty in displacement interpretations. After 02/26, each arrow indicates a substantial increase in displacement. These increases in displacements correspond with the extraction of neighboring pillars according to the depillaring sequence performed on-site (seen in Figure 3.11). The exact times at which each pillar was mined are unknown. Accordingly, the times pillars were mined (per Figure 3.11) were inferred according to the jumps in the extensometer data and the known pillar extraction dates. After 02/26, significant increases in extensometer displacement appear to correspond to extraction of pillars near to the instrumented pillar (within approximately two pillars away). When pillars further away were mined, minor increases in displacements were typically observed. This suggests that the load transfer resulting from the removal of a pillar extends a distance of approximately two pillar widths.

The depth of softening along the entry from February 6th – March 6th is shown in Figure 3.12; the depth of softening is the depth of significant displacements which are significantly more than would be predicted by elasticity theory. Significant fracturing occurred within the first 0.4 m of the rib up to March 5th. The depth of softening increased to 0.7 m with the extraction of the adjacent pillar on March 6th, just before the removal of the instrumented pillar.

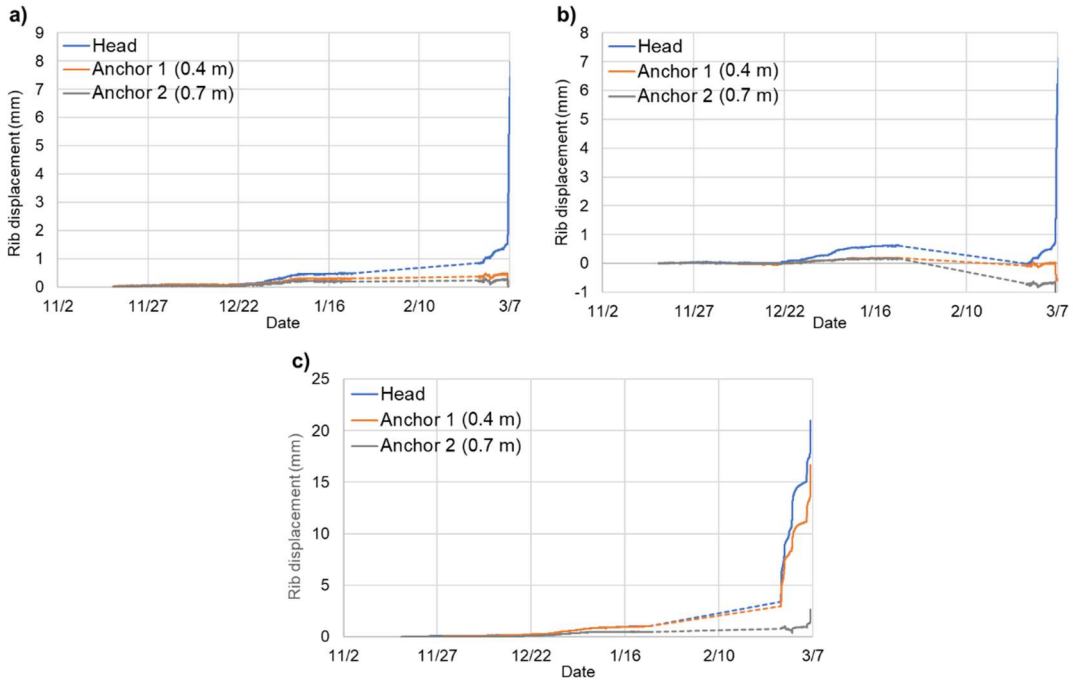

Figure 3.9: Extensometer measurements from November 2017 - March 2018 for the extensometers located (a and b) in the cross-cut, and (c) in the entry. Anchor 1 was located 0.4 m from the rib and anchor 2 was located 0.7 m from the rib. The dotted line indicates a gap in recorded displacements.

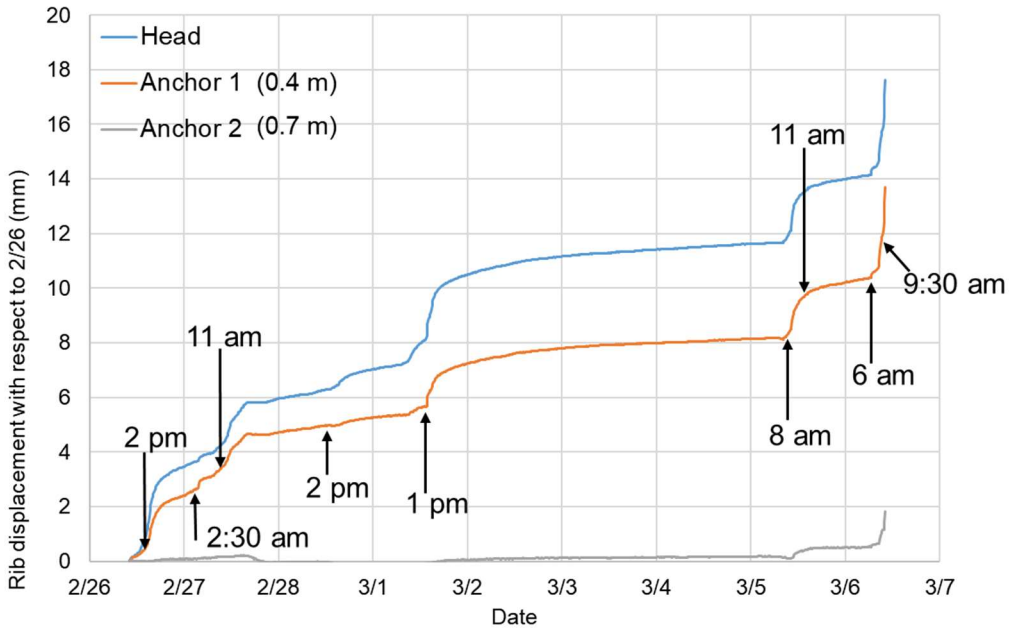

Figure 3.10: Measurement from the extensometer located in the entry for the period February 25th - March 6th. The arrows show the jumps in displacement recorded by the extensometer. Anchor 1 was located 0.4 m from the rib and anchor 2 was located 0.7 m from the rib.

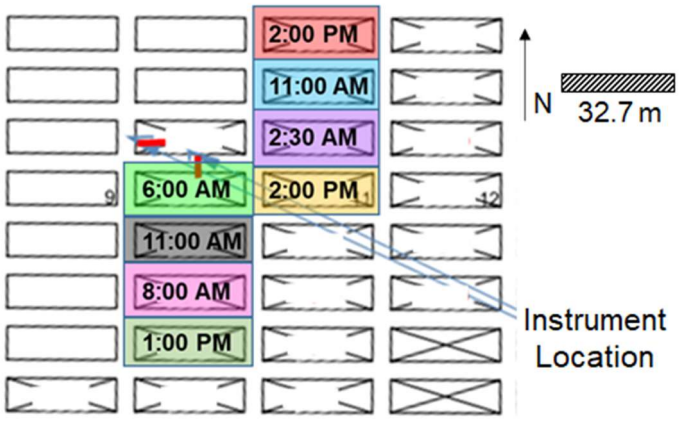

Figure 3.11: Depillaring sequence and time a pillar was removed as recorded by the extensometer data.

The shape of the displacement profile is convex within the first 0.4 m of the rib. This is common in brittle rock masses where discrete slabs form along the outer edges of the pillar. In this case, it can be inferred that the slab is approximately 0.4 m thick and is primarily displacing as a single unit (refer to the relatively small difference in the displacement magnitude between the leftmost two data points up to February 28th). Following this point, there was a rapid decline in displacements as a function of distance into the pillar. The displacement difference between the leftmost two data points increased after March 1st, indicating that there might be some localized fracturing occurring within the slab itself.

The extensometers were assumed to function properly as the cross-cut extensometers both behavior in a similar function. If the extensometers were not functioning properly, different behavior would have likely been recorded. Additionally, jumps in displacements observed in the entry displacements correlate to the extraction of pillars, which is expected.

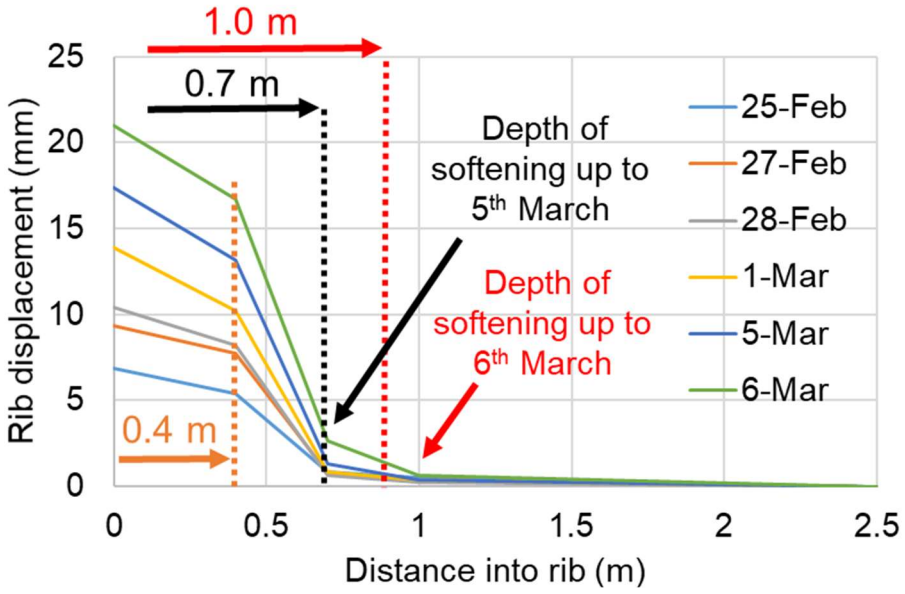

Figure 3.12: Depth of softening as recorded by the extensometer along the entry for different dates (February 25th - March 6th).

The region over which stress changes are observed in a pillar increases in proportion to the depth of fracturing. Given the shallow depth of softening (~1 m (3.3 ft)) in this case, it was not surprising that the BPC, which was located 3.57 m (11.7 ft) from the rib, did not record any significant change in stress (< 1 MPa). This was confirmed from one of the FLAC^{3D} models by examining the vertical stress profile across the width of the instrumented pillar on 03/05 (stage 9). In this model, the distance (from the pillar edge) over which some stress perturbation occurred was noted to be about ~2 m.

3.4 Model Development

The numerical model for Mine C was developed using basic information regarding the site and geological parameters that were provided by the mine. The coal is that of the Menefee Formation. It was assumed that the portion of the overburden for which borehole data were not available was composed of the Cliff House Sandstone. Material parameters were based on data

provided by the site, where possible. Any parameters not provided were based on the associated properties of the corresponding Mesaverde group rocks and relevant literature.

3.4.1 Model Stratigraphy

The main overburden and underburden included many thin interbeds which needed to be combined into broader-scale units to avoid generating too many zones in the model. Thus, the overall model stratigraphy was simplified in order to ensure the ability of the model to run fast enough to allow for parameter calibration to be performed. The implemented model stratigraphy reflects the lithology provided in the site's roof control plan (Figure 3.13).

The overall, simplified, model consists of four distinct layers and three material types: sandstone (overburden and underburden), shale with sandstone (immediate roof and floor), and coal. The overburden extends from surface (0 m) to -90.1875 m. The immediate roof is 2.3125 m thick, extending from -90.1875 m to -92.5 m. This is underlain by the 3 m coal seam from -92.5 m to -95.5, followed by a 0.9 m immediate floor from -95.5 to -96.4 m. The underburden is 23.6 m thick, extending from -96.4 m to -120 m. The stratigraphy implemented in the model can be seen in Figure 3.14.

3.4.2 Model Topography

Topography was not implemented into the model (i.e. the ground surface was modeled as flat). Examining the topography in Google Earth with the Main Panel overlaid on the topography, it was observed that there was approximately 20 m difference between the lowest and highest surface elevation. The ground surface was modeled using a coal seam depth corresponding to the area of lowest coverage.

3.4.3 Coal Seam and Overall Model Geometry

The coal seam geometry was built based on the provided mine map. To ensure all relevant mine elements around the instrumented pillar were considered, the entire panel was modeled (Main Panel and the Sub-Mains). The Sub-Mains are the set of excavations oriented 85º from the entries in the Main Panel (see Figure 3.4). The regular pillars are 9.55 m x 32.7 m, and the drifts are 5.4 m wide. All irregular pillar dimensions were determined using the mine map and scale. The Main Panel has a length of 335.95 m. The width varies due to the different orientation of the Sub-Mains. The Sub-Mains also has a length of 395.95 m and a width of 109.5767 m. Some assumptions and simplifications had to be made when representing the coal seam geometry for in model (Figure 3.4): (1) the pillar dimensions in the Sub-Mains that are cut off in the mine map (Figure 3.4) were assumed to be of similar dimensions as the pillars seen before the map cuts off; (2) the two large-angled pillars in the Main Panel (see Figure 3.4) were simplified to be rectangular; (3) small adjustments were made to barrier pillar in the Main Panel and the boundary between the Main Panel and the Sub-Mains to better align the gridpoints of the pillars and drifts within the panel. The model coal seam geometry can be seen in Figure 3.15 (compare to Figure 3.4).

The overall model dimension is dependent on the panel and the modeled abutment area. The abutments were extended 75 m beyond the coal seam. As a result, the entire model extends 485.95 m (x-direction), 691.611 m (y-direction), and 120 m (z-direction) (Figure 3.16).

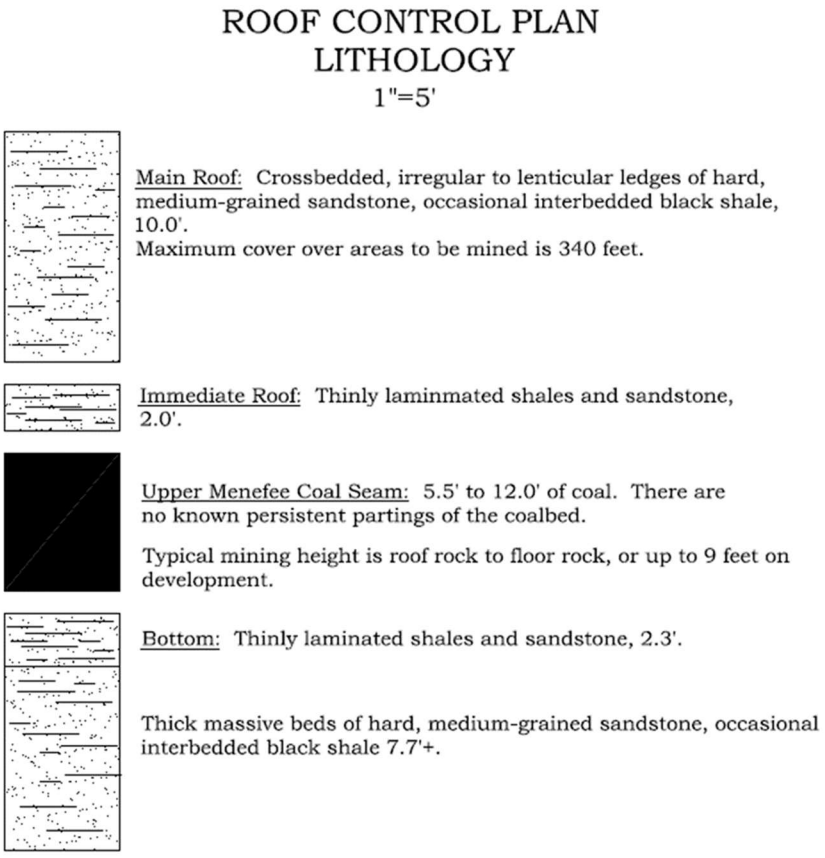

Figure 3.13: Lithology assumed in Mine C's roof control Plan.

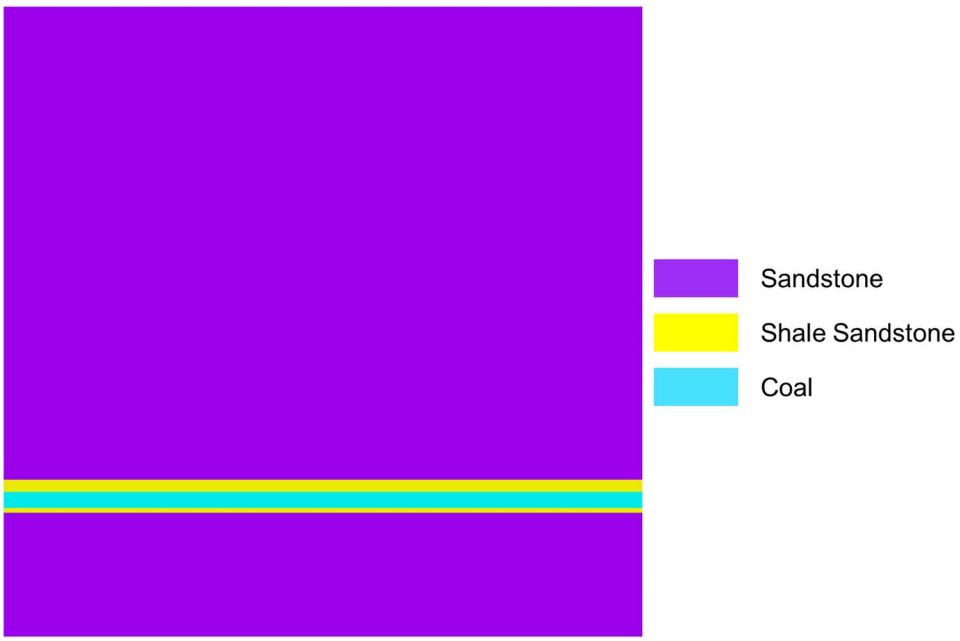

Figure 3.14: Model stratigraphy.

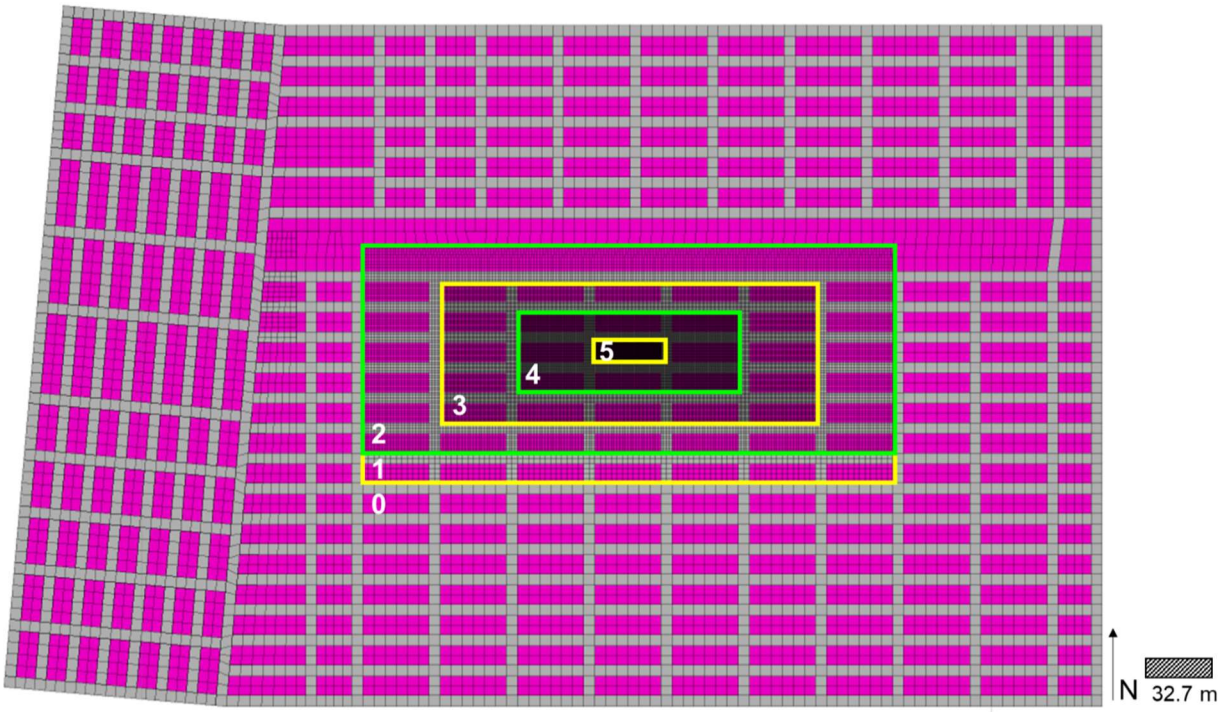

Figure 3.15: Coal seam geometry with the instrumented pillar outlined in yellow. Labels correspond to the mesh densification levels discussed in Section 3.4.4.

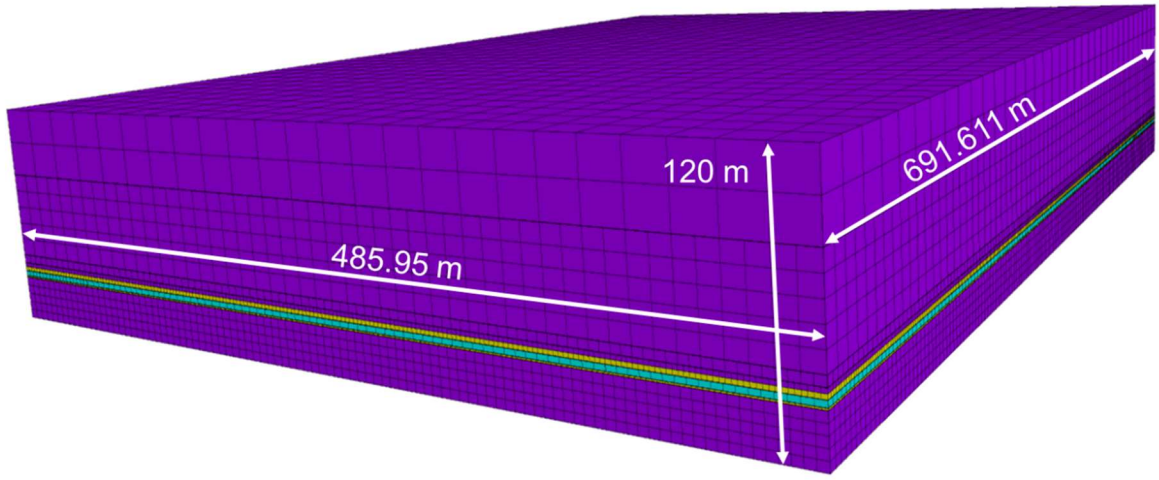

Figure 3.16: Overall model extents.

3.4.4 Model Mesh

The model mesh was developed in three parts: coal seam, overburden/immediate roof, and immediate floor/underburden. The coal seam mesh size was chosen based on the pillar size (9.55 m x 32.7 m) and the drift size (5.4 m). For majority of the Main Panel and Sub-Mains, the pillar mesh size was 4.775 m x 5.45 m x 3 m in the x, y, z direction, respectively, and the drift mesh size was 5.4 m x 5.45 m x 3 m in the x, y, z direction. The mesh was densified in the region surrounding the instrumented pillar. Densification was performed five times, the fifth densification being the instrumented pillar area (Figure 3.15). During densification, it was ensured that all zones maintained similar edge lengths in all directions. Table 3.1 lists the mesh dimensions corresponding to each level of densification. The finer mesh in the region of the instrumented pillar allows damage to be resolved to a scale comparable to the extensometer data.

The overburden and underburden mesh sizing becomes coarser moving away from the coal seam. The overburden starts at a 20 m mesh size and grades down to 2.5 m just above the immediate roof. The immediate roof uses a 2.5 m mesh size away from the pillar of interest. The immediate roof mesh size overlying the densified coal seam area was reduced to promote more uniform flow of stresses between the roof and the coal seam. The immediate floor mesh mirrors that of the immediate roof. The mesh reduces from the 2.5 m down to 0.156 m x 0.156 m x 0.145 m, just above and below the instrumented pillar (Figure 3.17).

Table 3.1: Mesh element dimensions in the coal seam.

Densification Level	x (m)	y (m)	z (m)
0	4.775	5.450	3.000
1	2.388	2.725	3.000
2	1.194	1.363	1.500
3	0.597	0.681	0.750
4	0.298	0.341	0.375
5	0.149	0.170	0.188

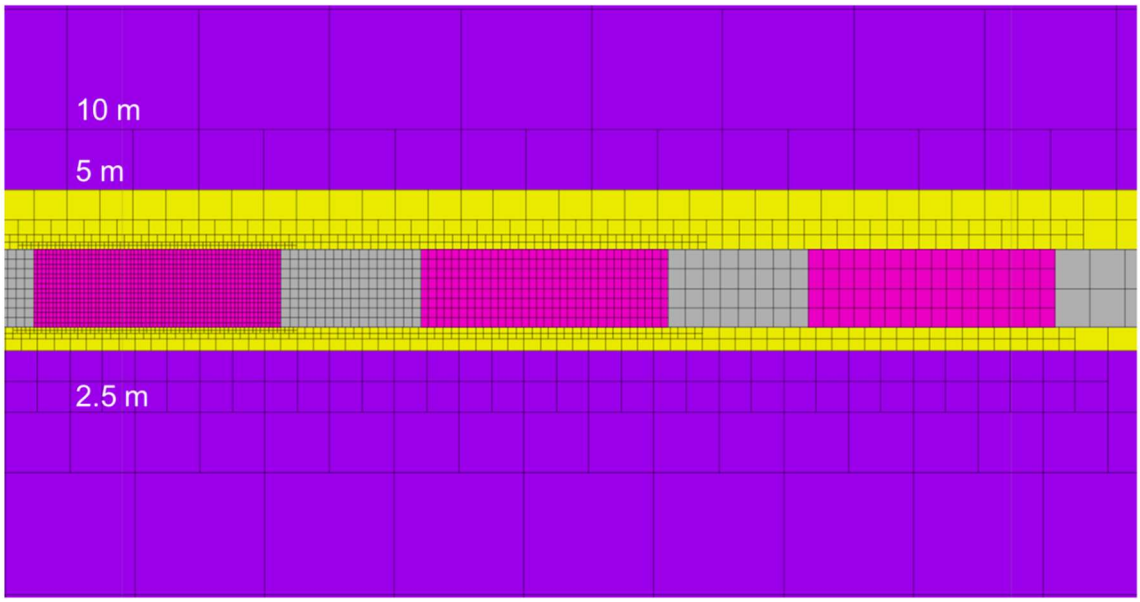

Figure 3.17: Immediate roof and floor densification.

A mesh sensitivity test was not performed. This is because regenerating a different mesh, unlike in 2D models, is not a trivial task and has the potential to lead to issues that can affect model stability (e.g. issues with attachment of nodes between regions of differing mesh sizes). However, the implemented model mesh is believed to be appropriate given the model scale based on comparison to previous studies:

- Walton et al. (2015) used mesh elements of 0.3125 m in the pillar of interest in the developed FLAC^{3D} numerical model calibrated to data from the Creighton mine, in Sudbury, Canada.
- Sears et al. (2018) developed a mine model in FLAC^{3D} to model coal rib response during bench mining using mesh elements of length 0.25 m in the x and y direction and 0.15 m in the z direction for the pillar of interest; the model was successfully calibrated and reflected site conditions.
- Mohamed et al. (2018) calibrated a numerical model to data from a coal mine using FLAC^{3D}, where mesh element dimensions were set not to be greater than 0.3 m in the x, y, or z direction; as in this study, the mesh elements were graded away from the pillar of interest, becoming more coarse.
- Sinha and Walton (2018) utilized mesh elements edge length 0.166 m in a FLAC^{3D} model used to investigate the effect of width to height ratio on the strength of pillars, validating the use of the new progressive S-shaped yield criterion.

With all this in mind, the element size chosen for the pillar of interest reflects the lower end element sizes from the literature review (0.166 m and 0.15 m). The mesh edge lengths in the pillar of interest were 0.149 m, 0.170 m, and 0.188 in the x, y, and z directions, respectively.

3.4.5 Pillar-Roof/Floor Interfaces

The implementation of a discontinuum interface can have important impacts on simulated ground behavior in numerical models. Studies suggest the interfaces that typically exist at the top and bottom of a coal seam have a significant impact on resulting pillar strength (Iannacchione, 1990; Perry et al., 2013). The interface slip mechanism between the coal seam and the

surrounding strata can impact the extent and pattern of stresses and deformations in a coal pillar; the presence of these interfaces effectively weakens coal pillars) (Iannacchione, 1990).

Interfaces between the pillar and roof and floor strata were initially included in the Mine C model. However, after extensive testing, the interfaces were found to be improperly modeling the interaction (stress transfer) between the roof/floor and the coal seam, leading to numerical instability. Thus, the interfaces were removed such that the model reflected a simplified continuum attachment between roof/floor and the coal seam. Since discontinuous slip was not allowed between the roof/floor and the coal seam, the calibrated coal properties obtained can be considered to represent lower bound strength values (to offset the lack of a weakening effect associated with interfaces).

3.4.6 Initial Material Properties

Data available from the site includes laboratory tests of the sandstone, mudstone, and mudstone with sandstone bands from the overburden, as well as the results from the initial ARMPS analysis. The UCS values of the overburden and underburden were obtained from the laboratory tests. The unit weight of the overburden was provided in the ARMPS analysis and was used to estimate the density of the overburden and underburden. Since limited data on material properties were available from the site, the majority of the properties used in the model were based on calibrated properties for similar rocks suggested by Esterhuizen et al. (2010), Tulu et al. (2017) and Sinha (2020). Properties were assigned to the overburden, immediate roof, immediate floor, underburden, coal, supports, and gob. All materials were modeled as inelastic, except the supports and gob. The use of inelastic materials in this case is important to allow for yield propagation to be modeled, as the purpose of the model is to understand stress re-

distribution and load transfer. The initial parameter values applied to the model will be discussed in this section, but ultimately the parameters were modified as part of the calibration process.

Parameters for the overburden, immediate roof, immediate floor, and underburden were selected from Tulu et al. (2017), who modified the suggested rock elastic, intact strength, and bedding strength properties from Esterhuizen et al. (2010). Esterhuizen et al. (2010) estimated typical field-scale parameters for a variety of rocks based on laboratory testing and numerical model calibration. Tulu et al. (2017) provides matrix and ubiquitous joint parameters for three rock types: sandstone, limestone, and shale. Since all material except the coal seam is a variant of sandstone (sandstone or interbedded sandstone), the parameters defined by Tulu et al. (2017) for sandstone were implemented in the model. Within the sandstone category, Tulu et al. (2017) sub-divided parameters based on uniaxial compressive strength (UCS). When the UCS value for a given unit available from Mine C laboratory tests matched the value for a set from Tulu et al. (2017), this set of parameters was used directly. Whenever the UCS value fell between values from Tulu et al. (2017), parameters were obtained via linear interpolation. At Mine C, the sandstone unit has a UCS value of 25 MPa, and the shale-sandstone has a value of 13 MPa, which is consistent with the expected strength relationship that sandstone is stronger than shale. Because the rockmasses modeled include both matrix (intact rock) and prominent joints (bedding planes, laminations, etc.), a strain-softening ubiquitous constitutive model was assigned to the overburden, immediate roof, immediate floor, and underburden. The initial properties used in the model are reported in Table 3.2 to two significant digits.

Table 3.2: Parameters for the overburden, underburden, immediate roof, and immediate floor.

Overburden and Underburden		**Immediate Roof and Immediate Floor**	
Matrix Parameters	**Value**	**Matrix Parameters**	**Value**
Young's Modulus (GPa)	9.7	Young's Modulus (GPa)	8.0
Density (kg/m3)	2600	Density (kg/m3)	2600
Friction Angle (°)	25	Friction Angle (°)	25
Peak Cohesion (MPa)	5.1	Peak Cohesion (MPa)	2.6
Yield Cohesion (MPa)	0.51	Yield Cohesion (MPa)	0.26
Peak Tensile Strength (MPa)	1.5	Peak Tensile Strength (MPa)	0.75
Yield Tensile Strength (MPa)	0.15	Yield Tensile Strength (MPa)	0.075
ε^{ps} from yield to peak	0.0050	ε^{ps} from yield to peak	0.0050
Ubiquitous Parameters	**Value**	**Ubiquitous Parameters**	**Value**
Cohesion (MPa)	0.41	Cohesion (MPa)	0.23
Friction Angle (°)	6.2	Friction Angle (°)	5.0
Tensile Strength (MPa)	0.14	Tensile Strength (MPa)	0.078

The properties assigned to the coal reflect the Cohesion-Weakening-Frictional-Strengthening (CWFS) strength model (Figure 3.18). The application of the CWFS model should be restricted to the surficial portions of a pillar, where failure occurs predominantly via brittle fracturing (Hajiabdolmajid et al., 2002; Sinha, 2020). Deeper within the pillar, where confinement is high, extensile fracturing is suppressed, causing the failure to occur in a shear mode. It is known that coal is a highly brittle material (Hajiabdolmajid et al., 2002; Sinha, 2020), and given the surficial nature of the damage inferred from the extensometer measurements, the use of a CWFS strength model is considered appropriate. Conventional yield criteria (i.e. Hoek-Brown and Mohr-Coulomb), based on laboratory tests or field observations where the mode of failure was primarily shear, have been shown to be incapable of numerically simulating the brittle rock damage process (Martin, 1997; Martin et al.,1999; Hajiabdolmajid et al., 2002). It was this inability of shear yield criteria to model the brittle behavior of intact rock that led to the development of the CWFS model (Hajiabdolmajid et al., 2002; Hajiabdolmajid et al., 2003). The

initial cohesive strength of the CWFS model is defined by the crack initiation (CI) threshold and the mobilized frictional strength is defined by the spalling limit. The CI threshold is relatively insensitive to changes in confining stress (Martin, 1997; Diederichs, 1999) and is exceeded by the spalling limit beyond the black dotted line (Figure 3.18). To the left of the black dotted line, following yield, the strength degrades from the CI threshold to the spalling limit which corresponds to brittle fracture propagation. To the right of the black dotted line, hardening occurs from the CI threshold to the spalling limit. At these higher confinements, crack growth is stunted, and more stress is necessary to induce the interaction and coalescence of microcracks (greater stress intensity at the crack tip). Ultimately, the CWFS strength model simulates the degradation of cohesion and mobilization of friction with damage at a rate controlled by the critical plastic shear strain.

Initial CWFS coal properties (see Table 3.3) reflect those from Sinha (2020) who calibrated the parameters to match the Mark-Bieniawski pillar strength equation (Mark and Chase, 1997). The resulting coal parameters applicable to the CWFS model are listed in Table 3.3. Additional parameters to define the coal seam are listed in Table 3.4. These parameters were determined from Esterhuizen et al. (2010) and Tulu et al. (2017). In order to implement the CFWS strength model in FLAC^{3D}, the strain-softening constitutive model was applied.

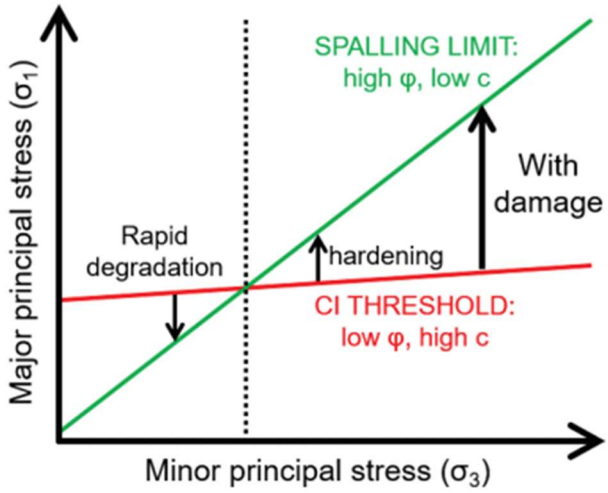

Figure 3.18: Components of the CWFS strength model (Sinha, 2020).

Table 3.3: Parameters for a new yield criterion for coal, fitted to the Mark-Bieniawski pillar strength equation (Sinha 2020).

Parameters	Values
Initial Cohesion (MPa)	6
Initial Friction Angle (º)	0
Final Cohesion (MPa)	0.1
Final Friction Angle (°)	50
ε^{ps} from initial to final	9
Dilation Angle (°)	15
Initial Tensile Strength (MPa)	1.5
Final Tensile Strength (MPa)	0
εps for Tensile Strength	0.001

Table 3.4: Additional parameters to define the strength parameters of the coal seam.

Parameters	Values
Young's Modulus (GPa)	3.0
Density (kg/m^3)	1200
Poisson's Ratio	0.25

The critical ε^{ps} value is mesh-size dependent and needs to be adjusted to the mesh size of the modeled coal seam. Sinha (2020) obtained the value of 9 millistrains when using a 0.25 m

mesh size. Because mesh size and the critical ε^{ps} value are inversely related (Itasca, 2016), the critical ε^{ps} value was scaled according to the effective edge length of each zone (in the Mine C model) as determined based on the cube root of zone volume. Per Sinha (2020), the initial assumption was that the critical ε^{ps} value for any given zone denotes the strain over which both friction angle and cohesion change from their initial to final values (Table 3.3).

The, the critical ε^{ps} value for dilation angle is determined by Equation 3.1, which is also a function of the critical ε^{ps} value assigned to the friction angle table. The purpose of using Equation 3.1 is to ensure that the dilation angle value is always less than the friction angle (a requirement in FLAC^{3D}).

$$\varepsilon^{ps}\ dilation = \frac{\varepsilon^{ps}\ friction\ angle}{Peak\ Friction\ Angle}\ x\ Peak\ Dilation \tag{3.1}$$

3.4.6.1 Modeling Roof Support

Supports that are modeled follow the provided cut sequence and support layouts (Figure 3.5), although the breaker row was not modeled (as explained in Section 3.4.7).

To model the MRS units, zones that reflect the canopy area of the MRS units used at Mine C were assigned an elastic modulus and stress value that are representative of the MRS unit. The elastic modulus defines how stresses will increase in MRS with additional convergence and the initial vertical stress value simulates the active setting pressure of the unit. To determine the elastic modulus and initial stress values of the MRS units, the canopy area, setting pressure and % setting pressure reduction, and stiffness must be known. Values were determined from the MRS 50-110 Fletcher unit specification (Burgess, 2021) as well as from the work of Barczak and Gearhart (1997). Table 3.5 lists the known parameters of the MRS unit used at Mine C. These

parameters were used to calculate the initial stress of the zones representing the MRS units as well as the MRS Young's Modulus based on Equation 3.2 and Equation 3.3.

The MRS units were assigned to zones based on the known canopy width and length. The site employs four MRS units at the pillar being extracted (two above the pillar and two to the left). In the model, the zones were modeled as two MRS units (side-by-side) (Figure 3.19). The zones were generated based on the canopy area of two side-by-side MRS units to accurately assign the properties associated to the MRS units (which are area dependent). In areas of coarser mesh, it was not possible for the area representing MRS units to exactly match the actual area of two MRS canopies. This resulted in a slightly larger representation of the MRS units in the model. This slight overestimation of MRS size was considered acceptable, as the MRS units have a minimal impact on stress transfer throughout the overall mine system (despite being critical for local roof stability and safety). Additionally, it should be noted that the degree of error decreases towards the instrumented pillar (area of interest), as the mesh is denser in that region.

Zones were first nulled, assigned as elastic, then assigned MRS unit properties (see Table 3.5) based on the area of two MRS canopies. Additionally, the Poisson's Ratio was reassigned to a value of zero because only vertical stress was considered (intended to eliminate expansion of the MRS zones resulting in artificial confinement of the coal zones in areas with coarse mesh).

Table 3.5: Parameters of the MRS unit utilized at Mine C.

Parameter	Value
Canopy Width (m)	1.68
Canopy Length (m)	1.98
Canopy Area (m^2) (of two MRS units)	6.640
MRS Capacity (ton)	800
Setting Pressure Reduction (%)	70
MRS Stiffness (GN/m)	0.1

$$MRS\ Initial\ Stress = \frac{\text{MRS Capacity x Setting Pressure Reduction } x \frac{907.185\ \text{kg}}{1\ ton}\ x\ 9.81\ \frac{m^2}{s}}{Canopy\ Area} \quad (3.2)$$

$$MRS\ Young's\ Modulus = \frac{\text{MRS Stiffness x Coal Seam Height}}{Canopy\ Area\ (of\ two\ MRS\ units)} \quad (3.3)$$

Table 3.6: Input parameters of the elastic zones representative of MRS units.

Parameters	Values
Poisson's Ratio	0
Initial Stress (MPa)	1.5
MRS Modulus (MPa)	45

Figure 3.19: MRS units modeled, seen by the orange zones, at the instrumented pillar.

3.4.6.2 Modeling Gob

Gob is defined as broken and caved material as a result of a mined out portion of the deposit/mine (Hartman and Mutmansky, 2002). In the case of Mine C, gob forms during the retreat mining process. As pillars are removed in a panel, gob eventually forms and is made up of broken and caved overburden material. Typically, gob forms three times the height of the coal seam (Su, 1991). This was difficult to implement because of the difference in zone sizes in the gob and roof. Sinha (2020) was able to model the gob compaction using elements covering a single seam-height in FLAC^{3D}. In this case the gob was modeled as a softer material, resulting in three times the strain that would be experienced in reality, and an equivalent total displacement. In this study, the gob was modeled in a similar fashion as Sinha (2020).

Gob was modeled using two approaches during the calibration process: (1) Gob elements were modeled using the strain-softening constitutive model with properties reflecting the strain hardening behavior that gob follows in the field. (2) Gob elements were modeled as elastic (a simplification from Approach 1). Approach 1 has been utilized by Esterhuizen et al. (2010) and Tulu et al. (2017) in modeling gob response in longwall mining applications. Approach 2 simplifies the gob behavior represented in Approach 1 to a linear stress-strain relationship, which is only valid over relatively small strains. Therefore, Approach 2 cannot be applied in longwall mining cases where panels are large and therefore large strains are experienced in the gob. The advantage of Approach 2 is that it depends only on a single parameter (Gob Young's Modulus) and results in faster model run time.

For both approaches, the creation of gob was identical. Zones that were assigned as gob were first nulled to simulate the excavation of material, followed by reassigning these zones as either elastic or strain-softening depending on the approach implemented. In both cases, the gob

was assigned a low stiffness value such that the gob will only pick up appreciable load if large amounts of deformation occur. Parameters used to define the gob were obtained from Tulu et al. (2017). The parameters chosen reflect gob behavior from a strong overburden. The distance gob forms from the active pillar being removed was based on approximate field observations during a field visit. Specifically, the gob was noted to form approximately one pillar length away from the active extraction area. It is important to note that this observation was made at a different panel and no observations of the gob were made at the Main Panel. Despite the uncertainty associated with the gob formation process in the Main Panel specifically, the gob was modeled one pillar length away from the abutments and active extraction area based on the observations at a different mine panel.

Approach 1 assigns the strain-softening constitutive model to gob zones based on the work of Esterhuizen et al. (2010). This approach varies cohesion as a function of critical plastic shear strain, in order to obtain a hardening response (Esterhuizen et al., 2010b). The friction angle and tensile strength of all gob zones were set to zero. Cohesion (half of the major principal stress for zero friction angle) was defined for multiple critical plastic shear strain values that were representative of the hyperbolic gob hardening curve that is well-established in the literature (Figure 3.20) (Tulu et al., 2017). As previously mentioned, the strain was tripled to account for the softer behavior of gob required in order to model the gob the height of the coal seam, as opposed to the conventional height (three times the coal seam). To reflect this softening effect, the hyperbolic curve was adjusted and the new curve is referred to as the softened gob curve. As gob zones were assigned, all stress components but the vertical stress were initialized to zero to force the gob to be loaded in uniaxial compression. This causes plastic shear strain to develop as a result of inelastic deformation in the vertical direction (overburden loading) (Sinha

2020). Parameters that define the strain hardening behavior of the gob (Table 3.7) were taken directly from Tulu et al. (2017) and reflect the parameters associated with a strong overburden.

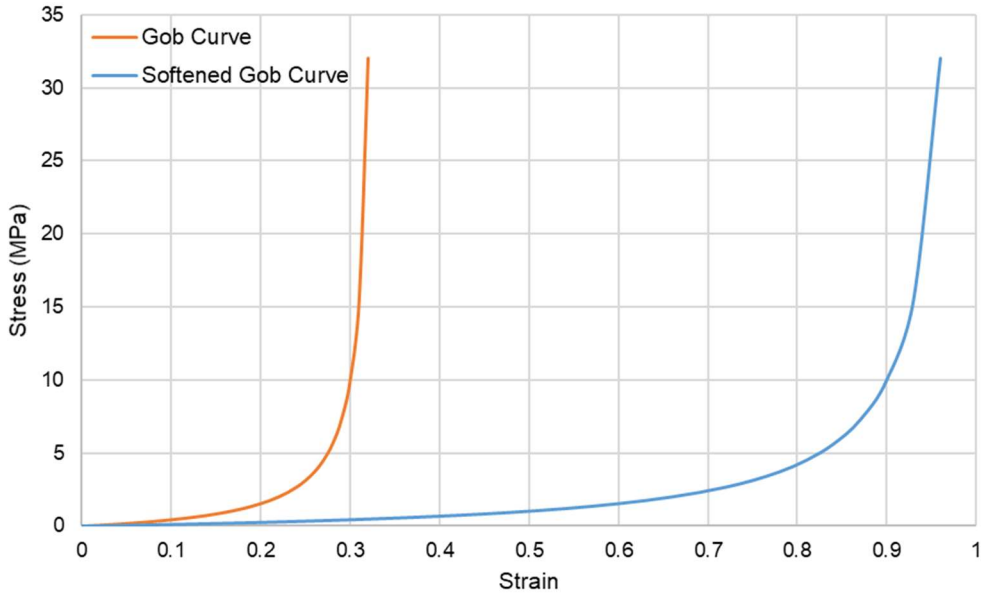

Figure 3.20: Hyperbolic gob curve.

Table 3.7: Gob strain-softening parameters.

Parameter	Value
Young's Modulus (MPa)	10
Poisson's Ratio	0
a (MPa)	7.24
b	0.33

As previously mentioned, Approach 2 is a simplification of Approach 1 (Esterhuizen et al. (2010) gob model). In this case, the gob behavior is controlled by the assigned Young's Modulus. The initial Young's Modulus assigned to the gob (Gob Young's Modulus) was determined using the gob softening curve (Figure 3.20). The Gob Young's Modulus can be determined from the gob curve using the stress strain relationship (Equation 3.4). An initial Gob Young's Modulus was chosen to reflect the stress-strain values before the stresses significantly

increase in the gob curve/softened gob curve. The resulting Gob Young's Modulus from the original gob curve was ~10 MPa (considering stress and strain values of 2 MPa and 0.22, respectively) and from the gob curve after softening to account for the gob being modeled as only having the height of the coal seam was ~3.5 MPa (considering stress and strain values of 2.6 MPa and 0.72, respectively). Ultimately, an initial Gob Modulus of 5 MPa was assigned to the gob.

$$Gob\ Young's\ Modulus = \frac{\sigma_1}{\varepsilon_1} \tag{3.4}$$

where, σ_1 is the axial stress and ε_1 is the axial strain.

Preliminary tests were performed using Approach 1 and Approach 2. It was found that the difference between the two approaches was negligible for the Gob Modulus values tested and the emergent range of strain that occurred in the model. As a result, Approach 2 was used to model the gob, as the simplification resulted in only one parameter to be altered and improved model run times.

3.4.7 Model Sequencing and Gob Development

The extraction sequence modeled was based on the dates the pillars were extracted on site (Figure 3.21). This active mining area where extraction occurs is referred to as the active mining area. The extraction sequence modeled removes one pillar at a time. However, in order to reduce model run time, the model was only solved to equilibrium at specific points in the extraction sequence. These points were determined based on when deformation was seen in the extensometer data. The majority of displacements occurred as pillars close to the instrumented pillar were removed. As a result, it was important that the model was solved after each pillar removal for the pillars near the instrumented pillar. Pillars further away were removed as a

group, since almost no displacements were observed in the instrumented pillar when these pillars were removed. Ultimately, the model was solved in 10 stages (Figure 3.22). Each model solve corresponds to a specific date in the extraction sequence and time that the pillar was completely removed. The time and date at which pillars were removed relate to the extensometer data (Figure 3.10). The jumps in displacements correspond to the points in time at which pillars were removed. These times were then related to when a pillar was removed in the model. Displacements were only considered for the solved stages once equilibrium was reached, as the FLAC^{3D} model did not incorporate a time-dependent (e.g. visco-plastic) constitutive model. Extensometer data from the entry were then compared with the corresponding model displacement at each stage (and times at which pillars were removed) to assist with model calibration.

Support sequencing in the model follows the actual in-mine sequence per Figure 3.5. Essentially, two MRS units were placed one entry behind the pillar that was being extracted. The remaining two MRS units were placed in the cross-cut between two standing pillars (one of which is the next pillar in the extraction sequence). The placement of the MRS units at the pillar being removed can be seen in Figure 3.23. The four MRS units were moved after each pillar was removed. In addition to the MRS unit supports, the site utilizes a timber breaker row to help control and prevent gob formation into future mining areas. These breaker rows consist of two rows of timbers. As a simplification, the breaker rows were not modeled. This was considered a reasonable simplification, as timber props do not have much impact on the global stress redistribution process because of their size and low stiffness.

Prior to the start of the pillar extraction process and pillar instrumentation installation, some pillars were already removed in the Main Panel and Sub-Mains, and gob was considered to

have formed in these areas (based on the observation that gob forms at a distance one pillar length from active mining) (Figure 3.24 a). The gob development process during the extraction process is illustrated in Figure 3.24. Gob was assumed to not form in the Northeast portion of the active mining area. This is because the Northeast portion was not large enough for gob to form one pillar away from the barrier pillar (North of this region) and the solid coal pillars (South of this region). The gob that could possibly form North of the Eastern portion of the gob depicted in Figure 3.24 was not included. This is because the span in that region is not considered to be sufficient to allow for gob formation until pillars immediately South of the instrumented pillar began to be extracted; given that this extraction process began only five days prior to the end of monitoring, any gob that may have formed in that area would not have had sufficient time to compact enough to take on any practically significant amount of load.

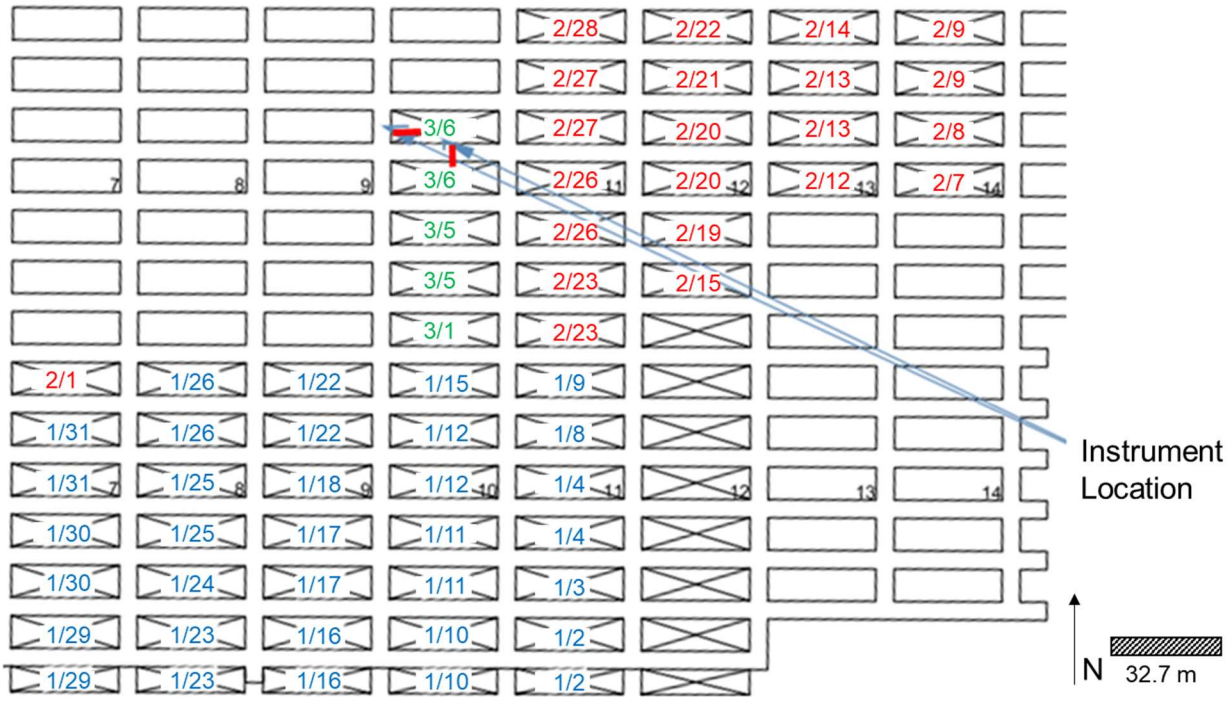

Figure 3.21: Mine C extraction sequence

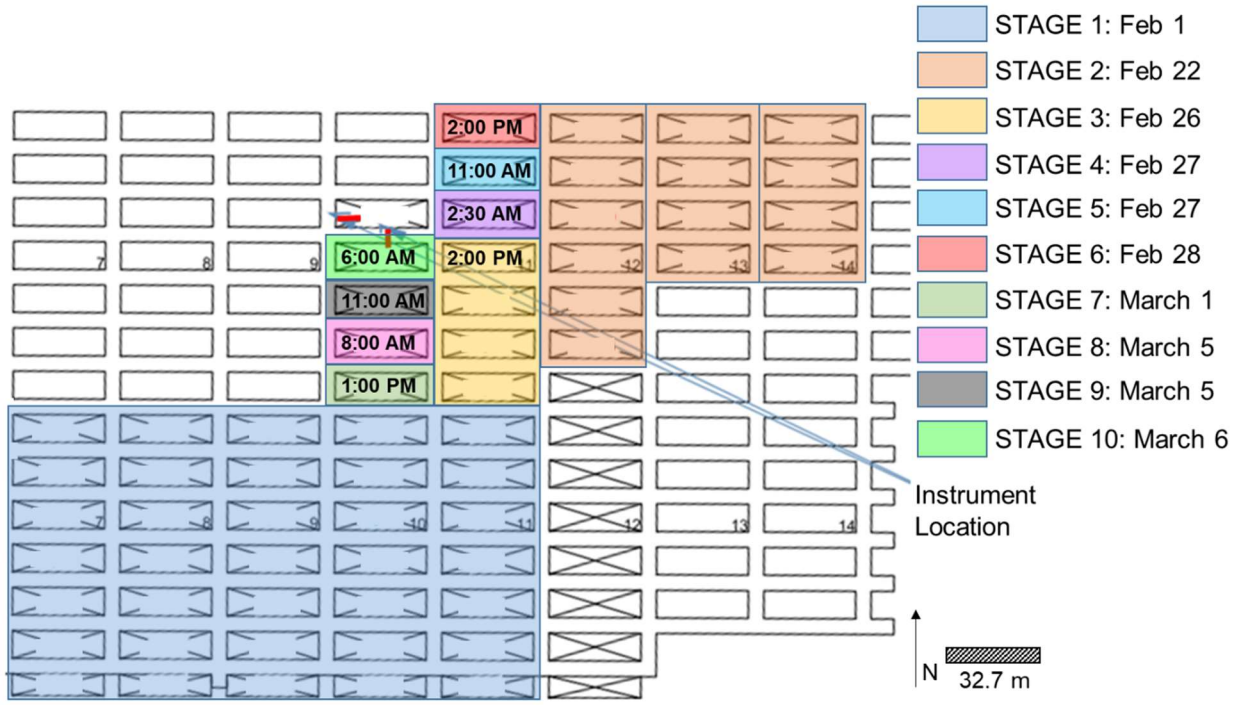

Figure 3.22: Extraction stages modeled and the associated removal date.

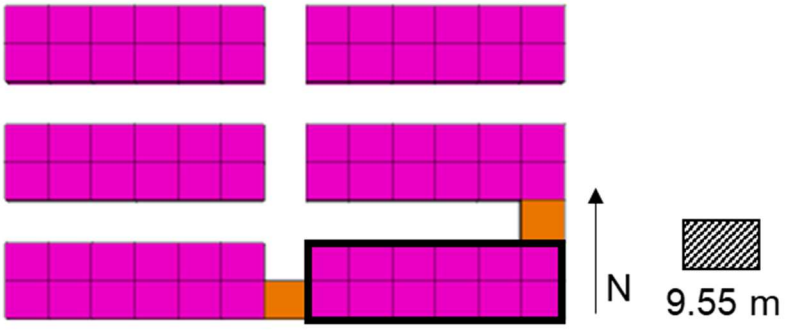

Figure 3.23: Location of the MRS units relative to the pillar being removed. The pillar being removed is outlined in black.

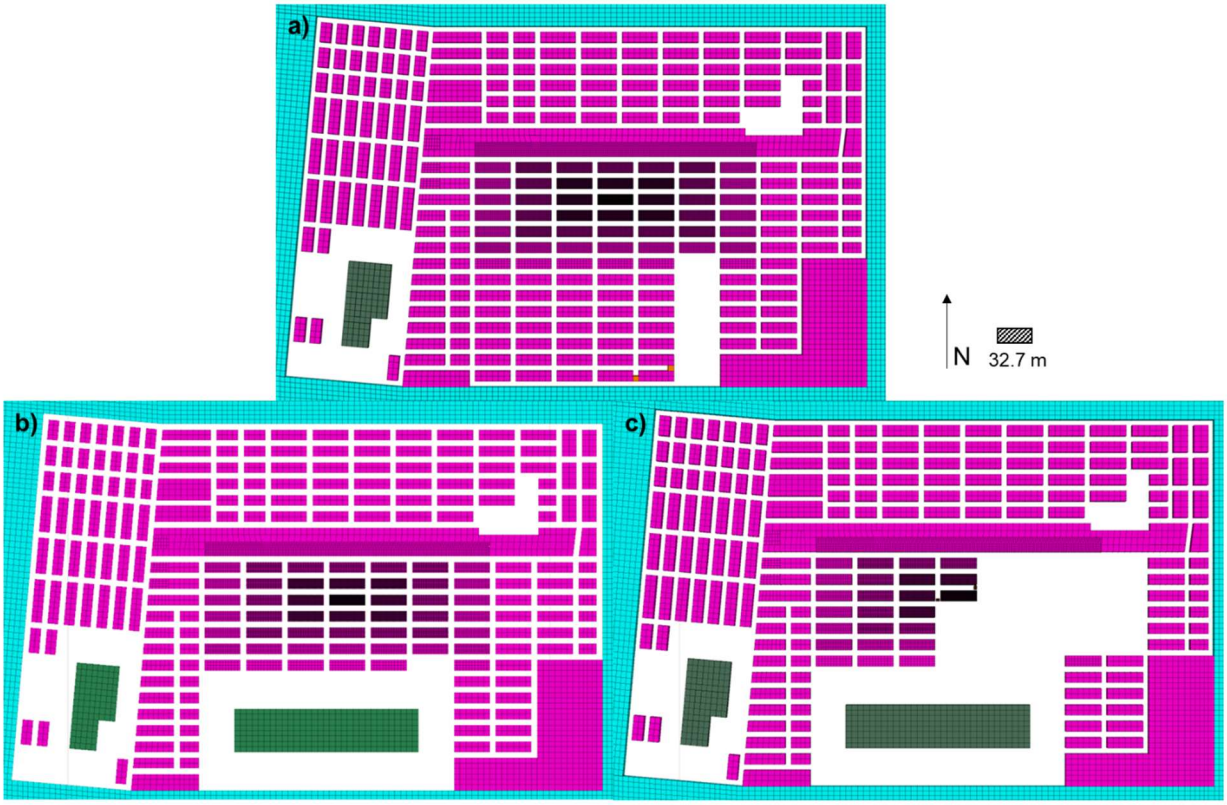

Figure 3.24: Gob development throughout the retreat process. a) Layout prior to the instrumentation of the pillar and retreat operations. b) Gob development after February 1 (stage 1). c) Gob development immediately prior to the removal of the instrumented pillar (stage 10).

3.5 Model Calibration

After the development of the numerical model, the calibration process was performed. The model was calibrated to match the extensometer data presented in Section 3.3.1. The parameter sets that were most uncertain and therefore modified most during calibration were the coal seam parameters; the roof/floor parameters were also adjusted slightly during calibration. The parameters defining the supports were not modified, as these are well-defined. Lastly, gob parameters were only minimally adjusted, as "typical" gob stress-strain behavior is reasonably well constrained in the literature (Esterhuizen et al., 2010b; Tulu et al., 2017).

To compare the results from the model to the extensometer data, displacements at identical anchor points were extracted after each model stage, as well as after the initial model stage corresponding to the point of extensometer installation (the baseline for evaluation of results).

3.5.1 Extracting Results from the Numerical Model for Analysis

Table 3.8 lists the locations of the grid points in the model where the displacements were queried to facilitate comparison with the field data. Entries marked with n/a are due to function issues of the installed extensometer. Thus, all model displacements were with respect to the deepest functional extensometer anchor point (5 and 6 for the entry and cross-cut, respectively).

Table 3.8: Anchor nomenclature, location in relation to the pillar rib, and corresponding coordinates of the anchor location in the model. Anchor 6 in the entry failed to function properly and hence the next deepest anchor (Anchor 5) was considered.

Anchor Number	Distance from Rib (m)	Corresponding Model Coordinates: Entry	Corresponding Model Coordinates: Cross-Cut
0 (Head)	0	44.8500, 136.05, -94	40.075, 119.7000, -94
1	0.2032	44.4436, 136.05, -94	40.075, 120.1064, -94
2	0.5080	44.1388, 136.05, -94	40.075, 120.4112, -94
3	0.8128	43.8340, 136.05, -94	n/a
4	1.4224	n/a	n/a
5	2.3368	42.3100, 136.05, -94	n/a
6	4.3688	n/a	40.075, 124.2720, -94

Once the displacement data were exported from FLAC^{3D}, they were then imported into Excel. First, the displacement values at each anchor point were zeroed with respect to 2/26 (stage 3). Then, entry displacements were zeroed with respect to anchor 5 point (anchor X – anchor 5), while cross-cut displacements were with respect to anchor 6 point (anchor X – anchor 6), matching how the extensometer data was processed. The displacements for each model solve stage were also zeroed in the same fashion. The resulting displacements at each anchor point for

each corresponding extraction date (except at 03/06) were plotted against the extensometer data collected onsite. Displacements occurring on 03/06 were not considered as part of the calibration due to the uncertainty with when the pillar before the instrumented pillar was removed in relation to the extensometer data. Through a comparison between the plotted model and extensometer displacements, it was determined whether a given model could be considered calibrated. If not, input parameters were then modified and the process continued until calibration was accomplished.

3.6 Model Calibration and Key Parametric Influences

As mentioned in Section 3.4.6, the coal seam parameters were modified the most, followed by the roof/floor parameters. Prior to any modifications, the model results with the initial parameters and gob formation as shown in Figure 3.24 were examined. This model did not converge, as severe roof yield and numerical instability occurred in the north area of the active mining area after stage 3 (02/26). As a result, it was necessary to increase roof stability. Specifically, stronger ubiquitous joint properties were required, as majority of the roof yield was observed to occur through ubiquitous joint yield. As a result, the roof/floor properties were strengthened to reflect the parameters associated with a UCS of 60 (main roof/floor) and UCS of 40 (immediate roof/floor) from Tulu et al. (2017). Although these UCS values are significantly greater than what the lab data suggests, the UCS values themselves are not what was observed to control the roof behavior in the models. Again, it was most important to increase the ubiquitous joint strength parameters (tied to the UCS values) relative to those provided by Tulu et al. (2017). The increase in the roof strength and stiffness promotes greater load transfer through the roof and greater roof stability.

The initial model was re-run with the increased roof/floor strength and the results can be seen in Figure 3.25. Instrumented pillar displacements were minimal and did not occur until immediately before the instrumented pillar was removed. These results indicated the need for parameter modifications in order to promote displacements to occur earlier in the depillaring sequence and reduce the depth of softening to separate the displacements observed at the different anchor points.

Some modifications were made to the Gob Modulus to understand its impact on the system. The Gob Modulus was observed to affect the degree of inelastic strain occurring in the pillars adjacent to the gob. However, the Gob Modulus had minimal influence on the point at which yield initiates (no impact on increasing displacements earlier on in the retreat sequence). Given that the Gob Modulus was relatively well constrained, this parameter was ultimately kept constant in the final stages of calibration. Additionally, the inclusion of additional gob areas (north of the gob shown in Figure 3.24) was tested. It was concluded that the presence of these gob areas would only have a marginal impact on the pillar damage and displacement (given the relatively low loads they were observed to carry and the limited differences observed in pillar displacements).

The main model parameters modified during the calibration process were the coal properties. Modifications were targeted to increase displacements starting at stage 4 (02/27) relative to those presented in Figure 3.24 while promoting the localization of yield between anchor 1 and anchor 2. This is because the depth of softening dictates the differences between the displacements simulated (and observed) at different anchor point locations. Modifications to the final/initial cohesion, final/initial friction angle, and peak dilation angle were made.

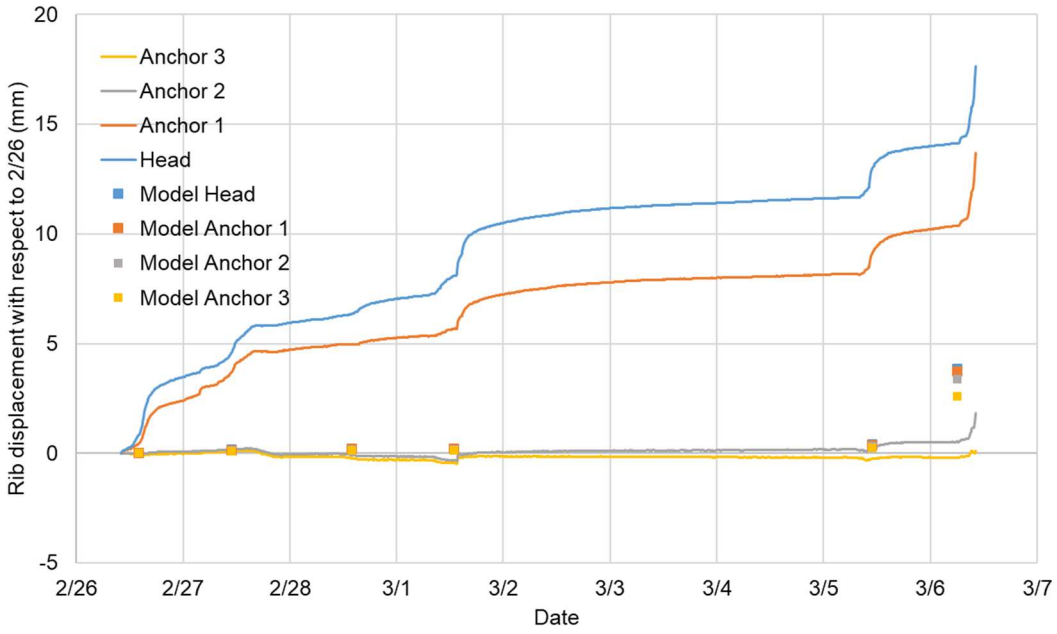

Figure 3.25: Calibration results from initial parameter values and increased roof/floor strength.

The initial cohesion defines the crack initiation strength of the coal. This parameter represents the primary control on the initiation of fracturing (when yield starts to occur within a pillar). The final (or "residual") cohesion also impacts the strength of the pillar. A higher final cohesion increases the pillar strength, reducing the propagation of yield within the pillar after its initiation. The initial friction angle represents a secondary control on the initiation of fracturing, as it defines the slope of the crack initiation envelope in principal stress space. The final (or "mobilized") friction angle, which defines the spalling limit, is the primary control on the depth of softening that occurs within a pillar. The dilation angle controls the relative proportions of plastic maximum principal strain (ε_3^P) and plastic minimum principal strain (ε_1^P) (Vermeer and De Borst, 1984). By increasing the dilation angle, ε_3^P (which manifests as horizontal displacements at the rib) can be increased for a given value of ε_1^P. In the context of the numerical model, this impacts the displacements occurring within the yielded portions of the pillar. Lastly, throughout the calibration process, the importance of the critical ε^{ps} value on the model was

observed. The critical ε^{ps} value is important in controlling the pillar damage process, as it controls the rate of coal strength degradation. A larger value results in slower pillar degradation and a smaller value results in faster pillar degradation. During the calibration process, the critical ε^{ps} value was reduced to promote the propagation of yield, ultimately increasing observed displacements. Although different values of critical ε^{ps} values for friction angle and cohesion were considered during calibration per Walton (2019), ultimately, it was determined that the use of a single critical ε^{ps} value for both strength components was appropriate.

Figure 3.26 compares simulated pillar damage results for different combinations of the aforementioned parameters tested during the calibration process. Table 3.9 lists the parameters for the model cases presented in Figure 3.26. When the observed plastic shear strain is greater than 100%, this indicates zones fully in the final (residual) state. Greater plastic shear strains represent greater degrees of damage in the model. The associated yield state within the instrumented pillar is shown at stage 10 (03/06) to compare with the plastic shear strain at stage 10 (03/06). The yield state visually suggests more severe pillar damage and instability in the pillar than in reality (as illustrated by the depth of softening in the extensometer data). Certain zones towards the edges of the pillar have large plastic shear strains (some greater than the critical plastic shear strain), and as a result these zones have reached their final (residual) state (plastic shear strain > critical plastic shear strain). Zones within the central portion of the pillar have not reached their final state, and as a result, these zones are able to take on more load until their final state is reached. As zones reach their final state, the modeled displacements are impacted and can be observed through the depth of zones into the pillar that have reached their final state (similar to the depth of softening). Model 5 had a limited depth of softening and was not consistent with interpretations from the extensometers. Model 2 had greater depth of

softening than Model 1, however the extent was not representative of that inferred from extensometer measurements. Model 1, Model 3, and Model 4 all have depths of softening that are more consistent with the extensometer measurements. During calibration, it was apparent that different combinations of the parameters have significant impacts on the extent of yield occurring in a pillar, ultimately impacting the depth of softening (important in the calibration process). Parameters continued to be modified until a calibrated model, with displacement results (and therefore corresponding yield extents) approximately in agreement with the extensometer data were obtained.

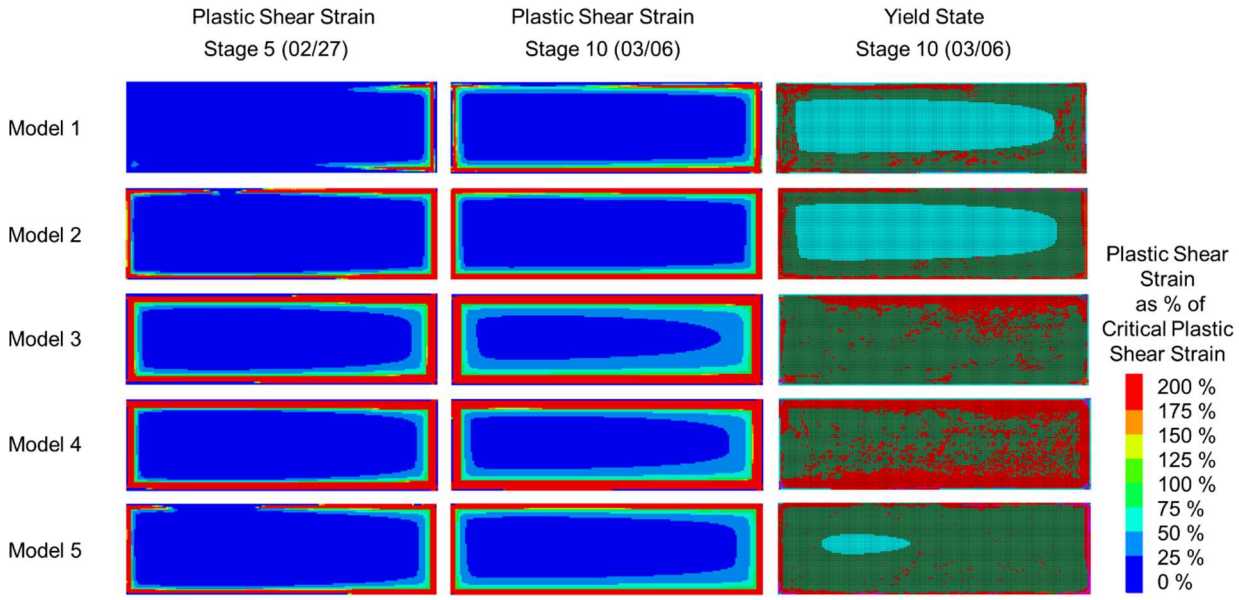

Figure 3.26: Plastic shear strain, in terms of % critical plastic shear strain, at mid-height of the instrumented pillar for five models with varying coal parameters (see Table 3.9) at stage 5 (02/27) and stage 10 (03/06). Yield state at mid-height of the instrumented pillar for five models with varying coal parameters at stage 10 (03/06).

Table 3.9: Parameters associated with the model results presented in Figure 3.26.

Coal Parameters	Model 1	Model 2	Model 3	Model 4	Model 5
Initial Cohesion (MPa)	2.3	2.3	2.5	3	3
Initial Friction Angle (°)	15	15	0	0	0
Final Cohesion (Mpa)	0.1	0.05	0.05	0.05	0.05
Final Friction Angle (°)	60	65	55	55	65
ε^{ps} from intial to final	0.0040	0.0013	0.0010	0.0010	0.0010
Dilation Angle (°)	40	40	40	50	40

3.7 Calibrated Model Results

Results from the model case with the best agreement with the extensometer observations (referred to as the "calibrated model") can be seen in Figure 3.27 and the associated parameters are listed in Table 3.10 and Table 3.11. The unconfined strength (UCS) of the coal corresponding to the parameters listed in Table 3.10 is 6 MPa. This matches the 6.2 MPa field UCS of coal (Mark and Barton, 1997) used in the U.S. Although the final friction angle value for coal in the calibrated model is higher than might be expected in a classical strain-softening model, this is because the final CWFS parameters control the simulated development of spalling fractures in the coal pillars. In other words, the final parameters are not a reflection of the intact coal strength, and the final friction angle (after friction mobilization) is not equivalent to the friction angle obtained from a compression test. Physically, the high friction angle demonstrates how sensitive the extensile fracturing process is to confining stress (on the right side of the black dotted line (Figure 3.18)); an incremental increase in confinement results in a dramatic increase in the driving stress (σ_1) required for spalling fractures to propagate. Note that in general, the spalling limit is considered to correspond approximately to line defined by σ_1/σ_3=10-20 in principal stress space, which corresponds to a friction angle of 55°-65° (Kaiser et al., 2000;

Diederichs, 2007). A final friction angle (spalling limit) of 55° is therefore consistent with this established range.

The displacement results shown in Figure 3.26 illustrate that the model displacements are broadly consistent with the displacement trends from the extensometer data. A jump in displacement occurs at stage 4 (02/27) as the stresses were observed to shed further onto the entry-side of the instrumented pillar; in contrast, at stage 3 (02/26) stresses were shed closer to the cross-cut inby side of the instrumented pillar. Thus, displacements were not observed to significantly increase until significant plastic shear strain was observed at the instrument location (which did not occur until stage 4). Additionally, the dilatancy (displacement difference) between the head and anchor 1 and between anchor 2 and anchor 3 is approximately correct. This indicates that the modeled distance of softening into the pillar is between anchor 1 and anchor 2, as it should be. However, dilation between the head and anchor 1 is greater than observed in the extensometer measurements. Therefore, although the calibrated model reasonably approximates the damage and displacement trends observed in the field data, it is likely that other parameter combinations exist that may more accurately replicate the field data.

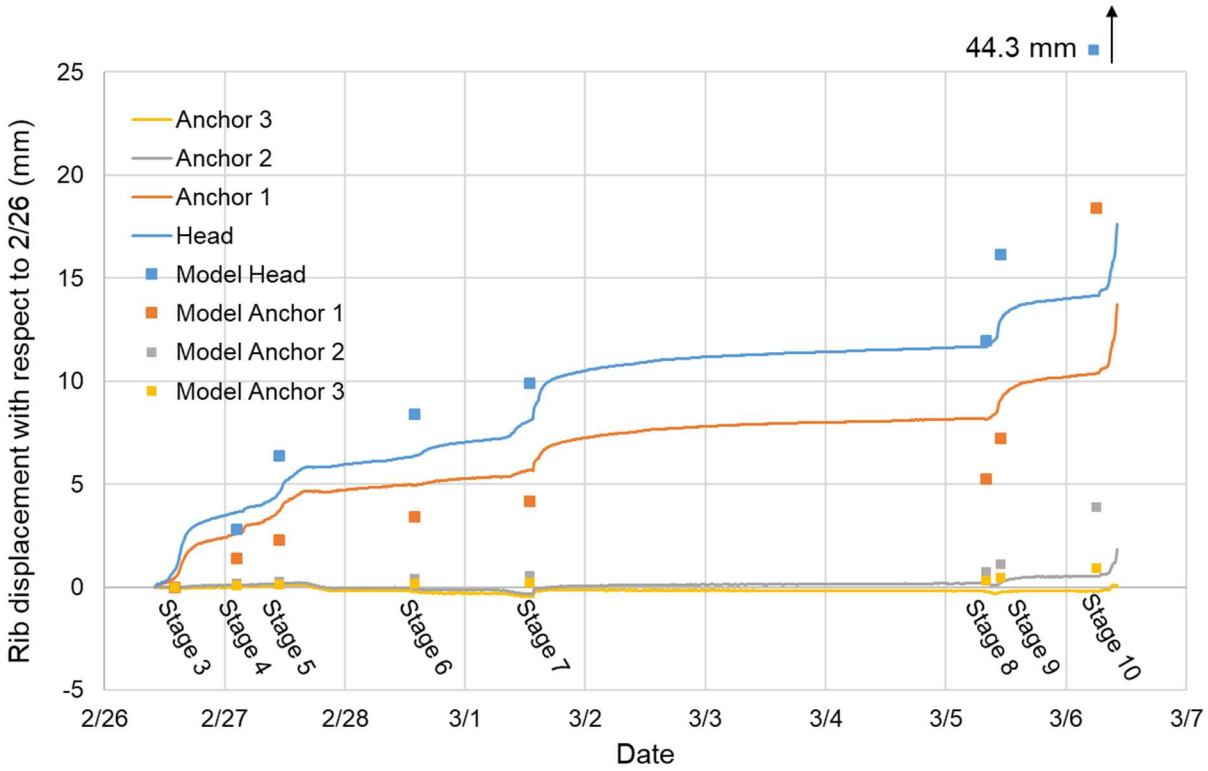

Figure 3.27: Calibration results from the best calibrated model.

Table 3.10: Coal seam parameters associated with the best calibrated model. For other zone sizes, the ε^{ps} was varied per the approach discussed in Section 3.4.4.

Material Parameters	**Values**
Initial Cohesion (MPa)	3
Initial Friction Angle (º)	0
Final Cohesion (MPa)	0.1
Final Friction Angle (°)	55
ε^{ps} from initial to final (instrumented pillar)	0.001
Peak Dilation Angle (°)	50
Initial Tensile Strength (MPa)	1.5
Final Tensile Strength (MPa)	0
ε^{ps} for Tensile Strength	0.001
Gob Modulus (MPa)	5

Table 3.11: Overburden and underburden parameters associated with the calibrated model.

Overburden and Underburden		**Immediate Roof and Immediate Floor**	
Matrix Parameters	Value	Matrix Parameters	Value
Young's Modulus (GPa)	14.74	Young's Modulus (GPa)	11.88
Density (kg/m^3)	2594	Density (kg/m^3)	2594
Friction Angle (°)	25	Friction Angle (°)	25
Peak Cohesion (MPa)	10.05	Peak Cohesion (MPa)	7.39
Yield Cohesion (MPa)	1.005	Yield Cohesion (MPa)	0.739
Peak Tensile Strength (MPa)	3.48	Peak Tensile Strength (MPa)	2.32
Yield Tensile Strength (MPa)	0.348	Yield Tensile Strength (MPa)	0.232
ε^{ps} from yield to peak	0.005	ε^{ps} from yield to peak	0.005
Ubiquitous Parameters	**Value**	**Ubiquitous Parameters**	**Value**
Cohesion (MPa)	2.44	Cohesion (MPa)	1.78
Friction Angle (°)	7	Friction Angle (°)	7
Tensile Strength (MPa)	0.35	Tensile Strength (MPa)	0.23

Given that a reasonably calibrated model was established, the evolution of stresses and yield can be examined in the model throughout the depillaring sequence. The evolution of vertical stress in the coal seam can be seen in Figure 3.28. Stresses were seen to increase in areas next to the gob. About 3 to 4 pillars North of the gob, stresses were reduced at the outer boundary of the pillar. This indicates increased load onto the pillars beyond the pillars adjacent to the gob resulting in the edges of the pillar yielding. When retreat operations commenced in the Northern portion of the active mining area, stresses were observed to increase inby (gob side) in a diagonal line from the pillar being removed. This highlights the stress redistribution that occurs approximately 1 pillar outby of the active mining area. Minimal changes were observed in pillars in the Main Panel outside of the active mining area as well as the pillars within the active mining area that were near the abutments and barrier pillar.

The vertical stress evolution within the instrumented pillar is shown in Figure 3.29. The stress evolution shows a reduction in stress along the pillar edges, indicating a loss of strength.

Conversely, stress in the center of the pillar increases throughout the retreat process, reflecting the development of pillar confinement and corresponding strengthening of the core. Throughout the retreat process, the stress within the gob was observed to increase by approximately 0.2 MPa between the first (stage 1) and last stage (stage 10). This highlights the limited role of the gob in taking on load as the retreat process continues away from the gob. Specifically, the removal of the pillars in the Northern active mining area had minimal impact on the gob loads. This suggests that the loads shed as a result of the depillaring process were transferred onto the adjacent pillars (as noted by the increase in stress in these pillars) and minimal load was spread to the gob (indicated by the minimal changes in the maximum stress observed within the gob).

The stress influence of the retreat mining activities appears to not extend past the abutment and barrier pillar. It is intuitive that yield and stress undergo minimal changes throughout the retreat process near the abutment. The large, solid, abutment was able to take on significant load, creating less stress concentration on the nearby pillars and resulting in no observed yield. Likewise, the barrier pillar was observed to perform in a fashion similar to the abutment. The barrier pillar acts to separate the active mining area from the North portion of the Main Panel. In the case of Mine C, the lack of stress redistribution and yield development near and beyond the barrier pillar, implies that the design of the barrier pillar is adequate. Ultimately, the evolution of stress and yield beyond the active mining area was observed to be minimal due to the presence of the abutment and the barrier pillar.

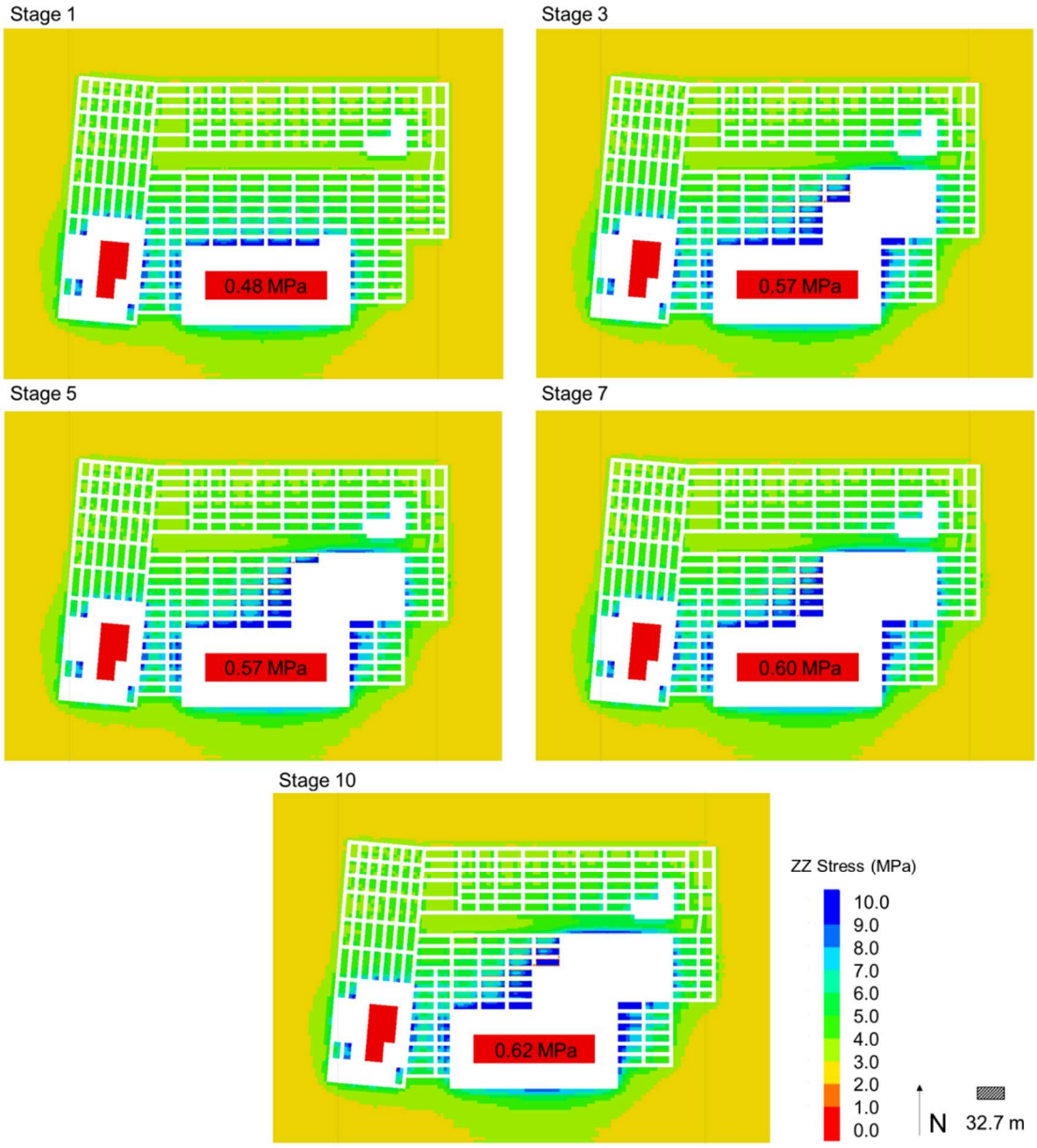

Figure 3.28: Vertical stress evolution, at coal seam mid-height, throughout the retreat process at stage 1, stage 3, stage 5, stage 7, and stage 10. The maximum observed stress within the gob.

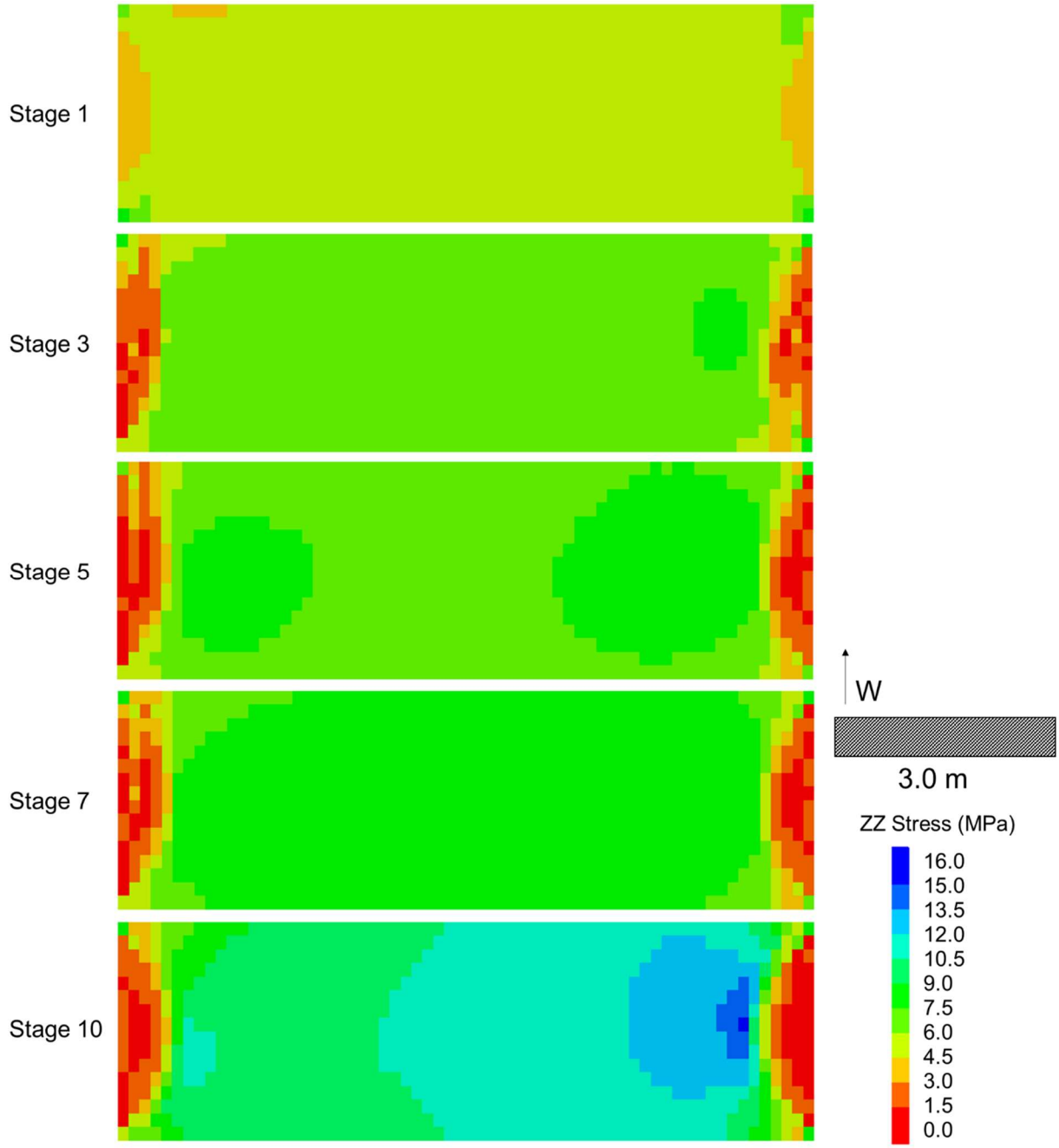

Figure 3.29: Vertical stress evolution throughout the instrumented pillar at stage 1, stage 3, stage 5, stage 7, and stage 10. The instrumented pillar is presented as a longitudinal section a cross-section.

3.8 Comparison of Modeling Results with ARMPS

A summary of an ARMPS analysis for the Sub-Mains and the Main Panel was provided by Mine C. The ARMPS stability factors for the Sub-Mains were calculated to be 3.64 and 2.50 for the developmental phase and retreat phase, respectively. The Main Panel, the area of interest, was calculated to have stability factors of 3.22 and 2.19 for the developmental phase and the retreat phase, respectively. Referring to the pillar stability equation (Equation 2.1) the calculated results suggest that the pillar design is adequate. Specifically, the pillar's predicted strength is greater than the predicted load the pillar is expected to take on, and thus ARMPS predicts that pillar failure is unlikely. This is consistent with the instrumentation data presented in Section 3.3.1 and the modeling results presented in Section 3.7. Significant plastic shear strain was observed in the Main Panel along the outer boundaries of the pillars. As previously noted, this indicates the depth of softening in the pillars is shallow. Additionally, the stress evolution in the instrumented pillar (Figure 3.29) shows the loss of strength at the pillar edges and the development of pillar confinement and corresponding strengthening of the core. Thus, the models reflect that there was no total loss of load carrying capacity of the pillars, indicating stability of the Main Panel. Overall, both the ARMPS analysis and modeling efforts suggest that the pillars in the Main Panel should be stable during retreat mining, as was observed on site.

3.9 Discussion

Throughout the development and calibration of the numerical model of Mine C, many lessons were learned. Many practical factors must be considered during the process of developing a numerical model for calibration purposes. Main considerations include the following: total number of zones, interfaces, and gob development. The total number of zones has a direct impact on the run time of the numerical model. An excessive number of zones will

result in unreasonable run time. The 1 million zone threshold was deemed “practical” by Klemetti et al. (2019, 2020) which aligns with the number of zones used in this model (~1.2 million zones). Interfaces were excluded from the model due to the improper interaction (stress transfer) between the roof/floor and the coal seam. Without the presence of an interface, the coal properties were artificially weakened to obtain similar pillar weakening affects as a result of interfaces. Thus, obtained coal parameters reflect lower bound strength values.

During the calibration process, it was determined that the specific spatial distribution used to model the gob did not have a significant impact on the model results. It was found that modeling gob formed in relatively small panels do not require a complex gob model to simulate the gob hardening response (typical of large scale panels) as proposed by Esterhuizen et al. (2010) and Tulu et al. (2017). From a practical perspective (i.e. for future modeling activities), it is valuable to note that the use of a gob spatial distribution based on approximate field observations and the use of a linear elastic gob constitutive model were found to be sufficient to achieve reasonable model results.

3.10 Conclusions

A calibrated numerical model of a retreat panel at Mine C was developed evaluate pillar mechanics and pillar stability in the context of retreat mining operations. The calibrated model accounted for the main components of a retreat mine (i.e. gob, depillaring sequence, roof supports). During the development of the numerical model, it was found that the complexities of gob development in small retreat panels (as compared to longwall panels) can successfully be simplified based on field observations and the use of elastic properties. Throughout the calibration process, the coal parameters were the main parameters adjusted. Various combinations of the parameters that define the CWFS strength had varying impacts on the model

results. Parameters were adjusted to match the extensometer data that reflects the depth of softening and displacements occurring within the instrumented pillar. It was found that a lower critical ε^{ps} value was essential to inducing the onset of inelastic displacements at the right time in the depillaring sequence. Modifications to the friction angle, cohesion, and dilation angle were necessary to adjust displacement magnitudes and depth of softening to match the extensometer data.

A calibrated model was established and the implications of retreat mining at the local and mine scale were investigated. At stage 1, it was observed that greater load was distributed approximately 3 to 4 pillars North of the gob area. Throughout the retreat operations, stress was shed to the pillars outby of the pillar being removed. This resulting in the stress evolving in a diagonal manner as seen in Figure 3.28. Pillar yield was observed to form in a similar manner. As retreat operations continued, yield and stress evolution was found to progress in a diagonal fashion with respect to the pillar being removed. However, stress and yield change was minimal in areas near the abutment and barrier pillar and outside the active mining area. Thus, it was concluded that the Main Panel (consisting of the study area) represents an adequate design that was capable of isolating the impacts of the retreat operations within the active mining area from pillars outside of the panel. The model results are consistent with field observations and the ARMPS analysis that predicted pillar stability during retreat mining.

CHAPTER 4

CONCLUSIONS AND FUTURE WORK

4.1 Conclusions

This thesis focused on advancing the understanding of retreat mining, specifically in underground coal room and pillar mines. FLAC^{3D} was utilized to perform this research. The research involved a preliminary study to evaluate stress re-distribution in a generic coal room and pillar retreat mine. The core research focused on developing a numerical model for Mine C, a coal room and pillar mine in the Western U.S, and calibrating the model to match field extensometer data.

The preliminary study investigated the influence of model type (elastic versus inelastic), pillar W/H ratio, and roof stiffness during retreat operations. The model type had significant impacts on model results and interpretation. The differences between the elastic and inelastic cases became significant once retreat operations commenced. Stresses in the inelastic cases dropped and were lower than in the elastic cases. This is due to the reduced load-carrying capacity as a result of yielding within the pillar array. Accordingly, inelastic cases were able to capture the potential for cascading failure to occur within the pillar array, whereas elastic cases were not. Thus, the inelastic models are able to provide a potentially more realistic representation of stresses in the pillar array allowing for improved understanding of mining operations that can lead to improved mine design considerations. The impact of pillar W/H ratio on stress-redistribution during retreat operations was also evaluated. Higher W/H ratios lead to lower stresses (due a lower extraction ratio); combined with the geometric strengthening effects associated with higher W/H pillar ratios, such pillars experience less yield throughout the retreat mining operation. The yielding of pillars impacts stress re-distribution. The more a pillar yields,

the less load the pillar will be able to take on, and the more load that will be shed onto the surrounding pillars. Yield propagates from the outside boundary of the pillar and moves towards the center of the pillar. Pillar yield and load shedding was found to be extreme in the lower W/H case (higher extraction ratio). An interesting finding of the preliminary study was the influence of roof stiffness on stress redistribution. It was found that once appreciable pillar yield occurs, the stress transfer throughout the pillar array becomes less dependent on roof properties. This suggests that well-accepted conceptions about the influence of the roof on stress transfer based on elasticity theory are not universal, and may only apply in cases where pillar behavior is predominantly elastic.

The preliminary model highlighted the importance of modeling complex retreat operations as inelastic in order capture yield progression within the mine and pillar array. As a result, an inelastic numerical model was developed to simulate retreat operations that occurred at Mine C. The development of the model incorporated the primary aspects of a retreat operation (i.e. gob, depillaring sequence, roof support, etc.) and was calibrated to extensometer data collected on site. During calibration of the model it was found that the gob development has little significance on the model results. For practical purposes and future modeling activities, the use of a gob spatial distribution based on approximate field observations and the use of a linear elastic gob constitutive model were found to be sufficient to achieve reasonable model results. After model calibration, results were evaluated to examine the global influence of retreat operations. It was found that initial load transfer occurred about 3 to 4 pillars away from the gob, highlighting the effect of the pressure arch. As retreat operations continued, load was distributed in a diagonal fashion in relation to the pillar being extracted; this is related to the specific geometric configuration of retreat operations at Mine C. Stress and yield were more centralized

around the extraction area and continued to develop throughout the retreat process. It was concluded that geometry of the Main Panel that makes up the study area represents an adequate design capable of isolating the impacts of the retreat operations (within the active mining area) from pillars outside of the panel.

4.2 Recommendations for Future Work

The completion of this thesis resulted in a preliminary calibration of a numerical model of Mine C. Despite the good agreement between the model results and extensometer data, it is recommended that additional parameter combinations be tested until a better agreement is reached. Additionally, it is recommended that modifications be made to the numerical model setup itself to mitigate the limitations imposed by simplifications implemented in this thesis. One of the biggest limitations of the current model is the exclusion of topography, given the relatively shallow depth of mining. Additionally, further attempts to incorporate interfaces into the model should be made. These model changes will require further adjustments to the coal parameters to match the extensometer data. However, the resulting coal parameters will likely reflect more realistic pillar strength properties than the current coal parameters determined through calibration.

Using a calibrated Mine C, it is recommended that an investigation of depillaring sequencing be performed. The purpose of such an investigation would be to evaluate how mine stability is impacted by the sequence pillars are removed during the retreat process. Optimal sequences can be determined as well as identifying areas of stress concentration in the mine. These areas can signify areas of concern that may require additional supplemental support or monitoring to assess possible damage and/or failure. Additionally, an investigation on remnant pillars is proposed. Remnant pillars will improve stability as a portion of the pillar is left as

support. This will impact the composition of the gob, as small portions of coal pillars will be intermixed with the gob. Such a study would help demonstrate the influence of remnant pillars on the retreat mining process. Lastly, it was noted that Mine C has two support designs. The calibrated model also provides a unique opportunity to directly compare the two support designs implemented in the same mining environment, as well as to further evaluate the impact of support design on retreat mining and stress re-distribution. The barrier pillar and the overall mine design was observed to have a significant influence on the impacts of retreat mining. As such, an investigation on barrier pillar design and the overall mine design could be performed to observe the implications regarding stress redistribution and yield evolution within the pillar array.

The calibrated Mine C model can also be used to perform a local bonded block model (BBM) study, using the stress paths from the FLAC^{3D} model. The BBM study can better simulate the local failure processes. As a result, the impact of supports can be investigated.

REFERENCES

Bai, Q. S., Tu, S. H., Zhang, X. G., Zhang, C., and Yuan, Y. (2014). Numerical modeling on brittle failure of coal wall in longwall face—a case study. *Arabian Journal of Geosciences*, *7*(12), 5067–5080.

Barczak, T. M., and Gearhart, D. F. (1997). Full scale performance evaluation of mobile roof supports. *Proceedings: New Technology for Ground Control in Retreat Mining, NIOSH IC, 9446*, 99–126.

Bieniawski, Z. T. (1984). Rock Mechanics design in mining and tunneling.

Brady, B. H. G., and Brown, E. T. (1993). *Rock mechanics: for underground mining*. Springer science & business media.

Burgess, T. (2021). *Personal Communication on May 17,2021*.

Chase, F. E., Mark, C., and Heasley, K. A. (2002). Deep Cover Pillar Extraction in the U.S. Coalfields.

Craig, S. D. (2001). *Geologic Framework of the San Juan Structural Basin of New Mexico, Colorado, Arizona, and Utah with Emphasis on Triassic through Tertiary Rocks* (Vol. 1420). US Geological Survey.

Das, M. N. (1986). Influence of width/height ratio on post-failure behaviour of coal. *International Journal of Mining and Geological Engineering*, *4*(1), 79–87.

Diederichs, M. S. (1999). *Instability of hard rock masses: the role of tensile damange and relaxation.* Ph.D. Thesis. University of Waterloo, Waterloo.

Diederichs, M. S. (2007). The 2003 Canadian Geotechnical Colloquium: Mechanistic interpretation and practical application of damage and spalling prediction criteria for deep tunnelling. *Canadian Geotechnical Journal,* 44(9), 1082-1116.

Du X., Lu J., Morsy K., and Peng S. (2008). Coal pillar design formulae review and analysis. In *Proceedings of the 27th International Conference on Ground Control in Mining*, 153–160.

Esterhuizen, E., Mark, C., and Murphy, M. M. (2010a). The ground response curve, pillar loading and pillar failure in coal mines. In *Proceedings of the 29th International Conference on Ground Control in Mining, ICGCM,* 19-27.

Esterhuizen, E., Mark, C., and Murphy, M. M. (2010b). Numerical Model Calibration for Simulating Coal Pillars, Gob and Overburden Response. In *Proceeding of the 29th International Conference on Ground Control in Mining, Morgantown, WV*, 46–57.

Esterhuizen, G. S., and Mark, C. (2009). Three-dimensional modeling of large arrays of pillars for coal mine design. In *Proceedings of the International Workshop on Numerical Modeling for Underground Mine Excavation Design,* 37-46.

Feddock, J. E., and Ma, J. (2006). Safety: a review and evaluation of current retreat mining practice in Kentucky. In *Proceedings of the 25th International Conference on Ground Control in Mining, Morgantown, West Virginia University, USA*, 366–373.

Frith, R., and Reed, G. (2017). Coal Pillar Design When Considered a Reinforcement Problem Rather Than a Suspension Problem. In *Proceedings of the 36th International Conference on Ground Control in Mining*, 1–11.

Gale, W. J. (1996). Geological Issues Relating to Coal Pillar Design. In *Symposium on Geology in Longwall Mining.*, 185–191.

Gale, W. J. (1998). The Application of Field and Computer Methods for Pillar Design in Weak Ground. In *Proceedings of the International Conference on Ground Control in Mining and Underground Construction, Wollongong*, 243–261.

Gale, W. J., and Hebblewhite B. K. (2005). Systems Approach to Pillar Design; Module 1-pillar design Procedures. *Final Report, 1.*

Galvin, J. M. (2016). *Ground engineering - principles and practices for underground coal mining*. Springer.

Ghasemi, E., Ataei, M., Shahriar, K., Sereshki, F., Jalali, S. E., and Ramazanzadeh, A. (2012). Assessment of roof fall risk during retreat mining in room and pillar coal mines. *International Journal of Rock Mechanics and Mining Sciences*, *54*, 80–89.

Ghasemi E., and Shahriar K. (2012). A new coal pillars design method in order to enhance safety of the retreat mining in room and pillar mines. *Safety Science*, *50*(3), 579–585. https://doi.org/10.1016/j.ssci.2011.11.005

Hajiabdolmajid, V., Kaiser, P. K., and Martin, C. D. (2002). Modelling brittle failure of rock. *International Journal of Rock Mechanics and Mining Sciences*, *39*(6), 731–741.

Hajiabdolmajid, V., Kaiser, P.K., and Martin, C.D. (2003). Mobilised strength components in brittle failure of rock. *Geotechnique,* 53(3), 327-326.

Heasley, K. A. (1998). Numerical Modeling of Coal Mines with a Laminated Displacement-Discontinuity Code.

Hill, D., Canbulat, I., Thomas, R., and van Wijk, J. (2008). Coal pillar loading mechanisms and progress in pillar design. In *27th International Conference on Ground Control in Mining*, 235–240.

Holland, C. T. (1973). Mine Pillar Design. *SME Mining Engineering Handbook, 1,* 13-8.

Hartman, H. L., and Mutmansky, J. M. (2002). *Introductory Mining Engineering*. John Wiley & Sons.

Iannacchione, A. T. (1990). The effects of roof and floor interface slip on coal pillar behavior. In *Rock Mechanics Contributions and Challenges: Proceedings of the 31st US Symposium*, 153–160. CRC Press.

Itasca. (2016). *FLAC 3D Hoek-Brown PAC Model Versionv6*. Itasca Consulting Group. Minneapolis, Minnesota.

Kauffman, P. W., Hawkins, S. A., and Thompson, R. R. (1981). *Room and Pillar Retreat Mining: A Manual for the Coal Industry*, (Vol. 8849). US Department of the Interior, Bureau of Mines.

Kaiser, P. K., Diederichs, M. S., Martin, D., Sharp, J., Steiner, W. (2000). Invited keynote: underground works in hard rock tunnelling and mining. *Proceedings of GeoEng2000,* Melbourne, 841-937.

Klemetti, T. M., Van Dyke, M. A., Compton, C. S., Tulu, I. B., Tuncay, D., and Wickline, J. (2019). Longwall Gateroad Yield Pillar Response and Model Verification – A Case Study. In *53rd US Rock Mechanics/Geomechanics Symposium.* American Rock Mechanics Association.

Klemetti, T. M., Sears, M., and Tulu, I. B. (2017). Design concerns of room and pillar retreat panels. *International Journal of Mining Science and Technology*, *27*(1), 29–35.

Klemetti, T. M., Van Dyke, M. A., Tulu, I. B., and Tuncay, D. (2020). A case study of the stability of a non-typical bleeder entry system at a U.S. longwall mine. *International Journal of Mining Science and Technology*, *30*(1), 25–31.

Madden, B. J. (1991). A re-assessment of coal-pillar design. *Journal of the Southern African Institute of Mining and Metallurgy*, *91*(1), 27–37.

Maleki, H. (2017). Coal pillar mechanics of violent failure in U.S. Mines. *International Journal of Mining Science and Technology*, *27*(3), 387–392.

Mark, C., and Barton, T. (1996). The uniaxial compressive strength of coal: Should it be used to design pillars? In *Proceedings of the 15th International Conference on Ground Control in Mining. Golden, CO: Colorado School of Mines*, 61–78.

Mark, C., Chase, F., and Pappas, D. (2003). Reducing the risk of ground falls during pillar recovery. *National Institute for Occupational Safety and Health, Pittsburgh*.

Mark, C. (2007). The Evolution of Intelligent Coal Pillar Design: 1981-2006. *25th International Conference on Ground Control in Mining*.

Mark, C. (2009). Deep cover pillar recovery in the US. In *Proceedings of the 28th International Conference on Ground Control in Mining* , 1–9.

Mark, C. (2010). Pillar Design for Deep Cover Retreat Mining: ARMPS Version 6 (2010). In *Proceedings of the 3rd International Workshop on Coal Pillar Mechanics and Design*, 104–120.

Mark, C., and Barton, T.M. (1997). Pillar design and coal strength. *Proceedings of the New Technology for Ground Control in Retreat Mining,* NIOSH IC 9446, 49-59.

Mark, C., and Chase, F. E. (1997). Analysis of Retreat Mining Pillar Stability (ARMPS). *Proceedings of the New Technology for Ground Control in Retreat Mining, NIOSH IC 9446*, 17–34.

Mark, C., and Iannacchione, A. T. (1992). Coal Pillar Mechanics: Theoretical Models and Field Measurements Compared. *Proceedings of the Workshop on Coal Pillar Mechanics and Design. Pittsburgh, PA: US Department of the Interior, Bureau of Mines, IC*, *9315*, 78–93.

Martin, C.D. *The strength of massiv Lac du Bonnet granite around underground openings.* Ph.D. Thesis, University of Manitoba, Canada.

Martin, C.D., Kaiser, P.K., and McCreath, D.R. (1999). Hoek-Brown parameters for predicting the depth of brittle failure around a tunnel. *Canadian Geotechnical Journal,* 36(1), 136-151

Mohamed, K. M., Rashed, G., Sears, M. M., and Van Dyke, M. A. (2018). Calibration of Coal-mass Model Using In-Situ Coal Pillar Strength Study. *ARMA Preprint,* (18-075).

NIOSH. (2021). *Mine and Mine Worker Charts*. Centers for Disease Control and Prevention (CDC). Retrieved June 3, 2021, from https://wwwn.cdc.gov/niosh-mining/MMWC#disasters

NIOSH. (2010). *Research Report on the Coal Pillar Recovery Under Deep Cover*. https://www.cdc.gov/niosh/mining/works/coversheet1533.html

Pariseau, W. G. (2006). Pillars in stratified ground. In *Design Analysis in Rock Mechanics,* 277–289. CRC Press.

Perry, K., Unrug, K., Harris, K., and Raffald,i M. (2013). Influence of Roof/Floor Interface on Coal Pillar Performance. In *Proceedings of the 32nd International Conference on Ground Control in Mining*, 53–59.

Salamon, M. D. G., and Munro, A. H. (1967). A study of the strength of coal pillars. *Journal of the Southern African Institute of Mining and Metallurgy, 68(2),* 55-67.

Sears, M. M., Rusnak, J., Van Dyke, M., Rashed, G., Mohamed, K., and Sloan, M. (2018). Coal rib response during bench mining: A case study. *International Journal of Mining Science and Technology*, *28*(1), 107–113.

Sheorey, P., Das, M. N., Bordia, S. K., and Singh, B. (1986). Pillar strength approaches based on a new failure criterion for coal seams. *International Journal of Mining and Geological Engineering*, *4*(4), 273–290.

Sheorey, P. R., Das, M. N., Barat, D., Prasad, R. K., and Singh, B. (1987). Coal pillar strength estimation from failed and stable cases. In *International Journal of Rock Mechanics and Mining Sciences & Geomechanics Abstracts*, *24*(6), 347–355. Pergamon.

Sinha, S. (2020). *Advancing continuum and discontinuum models of brittle rock damage and rock-support interation*. (Doctoral dissertation, Colorado School of Mines).

Sinha, S., and Walton, G. (2018). A progressive S-shaped yield criterion and its application to rock pillar behavior. *International Journal of Rock Mechanics and Mining Sciences*, *105*, 98–109.

Sinha, S., and Walton, G. (2020). Modeling behaviors of a coal pillar rib using the progressive S-shaped yield criterion. *Journal of Rock Mechanics and Geotechnical Engineering*, *12*(3), 484–492.

Steed, C., Roberts, D., Pitman, W., and Carvalho, J. (). Pillar Optimization for Initial Design and Retreat Recovery. *22nd International Conference on Ground Control in Mining*, *Morgantown, WV,* 86–94.

Su, D. W. H. (1991). Finite Element Modeling Of Subsidence Induced By Underground Coal Mining: The Influence Of Material Nonlinearity And Shearing Along Existing Planes Of Weakness. In *Proceedings of the 10th International Conference on Ground Control in Mining*, *Morgantown* 287–300.

Su, D. W. H., and Hasenfus, G. J. (1999). Coal Pillar Strength and Practical Coal Pillar Design Considerations. In *Proceedings of the Second International Workshop of Coal Pillar Mechanics and Design, Pittsburgh, PA, US Department of the Interior, Bureau of Mines*, 155–163.

Tulu, I. B., Esterhuizen, G. S., Mohamed, K., and Klemetti, T. M. (2017). Verification of a calibrated longwall model with field measurements. In *51st US Rock Mechanics / Geomechanics Symposium*.One Petro.

Tulu, I. B., Heasley, K. A., and Mark, C. (2010). A comparison of the overburden loading in ARMPS and LaModel. In *Proceedings of the 29th International Conference on Ground Control in Mining*, 28–37. West Virginia University.

Tuncay, D., Tulu, I. B., and Klemetti, T. M. (2020). Analysis of ARMPS2010 database with LaModel and an updated abutment angle equation. *International Journal of Mining Science and Technology*, *30*(1), 111–118.

Tuncay, D., Tulu, I. B., and Klemetti, T. M. (2021). Verification of 3D Numerical Modeling Approach for Longwall Mines with a Case Study Mine from the Northern Appalachian Coal Fields. *Mining, Metallurgy and Exploration*, *38(1),* 447-456.

Van Der Merwe, J. N. (1990). The extraction safety factor concept in high-extraction coal mining. *Journal of the Southern African Institute of Mining and Metallurgy, 90(11)*, 303-306.

Vermeer, P. A., and De Borst, R. (1984). Non-associated plasticity for soils, concrete and rock. *HERON*, *29*(3), *1984*.

Walton, G. (2019). Initial guidelines for the selection of input parameters for cohesion-weakening-friction-strengthening (CWFS) analysis of excavations in brittle rock. *Tunnelling and Underground Space Technology*, *84*, 189–200.

Walton, G., Diederichs, M. S., and Punkkinen, A. (2015). The influence of constitutive model selection on predicted stresses and yield in deep mine pillars – A case study at the Creighton mine, Sudbury, Canada. *Geomechanics and Tunnelling*, *8*(5), 441–449.

Yaghoobi, M., Rafiee, R., and Najafi, M. (2019). Comparing the "Modified Split and Fender" and "Shortwall" Methods for the Pillar Recovery in Room and Pillar Coal Mining Using A 3D Finite Difference Modeling in Tabas Central Coal Mine, Iran. *Journal of Aalytical and Numerical Methods in Mining Engineering*, *8*(17), 27–37.

Zhang, P., Heasley, K. A., Research, G., and Keith, A. (2013). Initial results from implementing a laminated overburden model into ARMPS. In *Proceedings of the 32nd International Conference on Ground Control in Mining/Morgantown, West Virginia,* 239-247.

Zingano, A., and Weiss, A. (2019). Subsidence over room and pillar retreat mining in a low coal seam. *International Journal of Mining Science and Technology*, *29*(1), 51–57.

Zipf, R. K. (2001). Toward Pillar Design to Prevent Collapse of Room-and-Pillar Mines. In *108th Annual Exhibit and Meeting, Society for Mining, Metallurgy and Exploration, Denver, CO, 26-28 February.*

Zipf, R. K., and Mark, C. (1997). Design Methods to Control Violent Pillar Failures in Room-and-Pillar Mines. *Transactions of the Institution of Mining and Metallurgy-Section A-Mining Industry*, *106*, A124.

APPENDIX A

PERMISSION FROM PUBLISHERS AND CO-AUTHORS

ELSEVIER LICENSE
TERMS AND CONDITIONS

Aug 07, 2021

This Agreement between Miss. Rahel Dean-Pelikan ("You") and Elsevier ("Elsevier") consists of your license details and the terms and conditions provided by Elsevier and Copyright Clearance Center.

License Number	5123720767812
License date	Aug 07, 2021
Licensed Content Publisher	Elsevier
Licensed Content Publication	International Journal of Rock Mechanics and Mining Sciences
Licensed Content Title	Assessment of roof fall risk during retreat mining in room and pillar coal mines
Licensed Content Author	Ebrahim Ghasemi,Mohammad Ataei,Kourosh Shahriar,Farhang Sereshki,Seyed Esmaeil Jalali,Ahmad Ramazanzadeh
Licensed Content Date	Sep 1, 2012
Licensed Content Volume	54
Licensed Content Issue	n/a
Licensed Content Pages	10
Start Page	80
End Page	89

Type of Use	reuse in a thesis/dissertation
Portion	figures/tables/illustrations
Number of figures/tables/illustrations	2
Format	both print and electronic
Are you the author of this Elsevier article?	No
Will you be translating?	No
Title	Numerical Modeling of Pillar Stress Redistribution During the Retreat Mining Process
Institution name	Colorado School of Mines
Expected presentation date	Aug 2021
Portions	Figure 1, Figure 2

GENERAL TERMS

2. Elsevier hereby grants you permission to reproduce the aforementioned material subject to the terms and conditions indicated.

This is a License Agreement between Rahel Dean-Pelikan ("User") and Copyright Clearance Center, Inc. ("CCC") on behalf of the Rightsholder identified in the order details below. The license consists of the order details, the CCC Terms and Conditions below, and any Rightsholder Terms and Conditions which are included below.

All payments must be made in full to CCC in accordance with the CCC Terms and Conditions below.

Order Date	07-Aug-2021	**Type of Use**	Republish in a thesis/dissertation
Order License ID	1139035-1	**Publisher**	PERGAMON PRESS,
ISSN	0148-9062	**Portion**	Image/photo/illustration

LICENSED CONTENT

Publication Title	International journal of rock mechanics and mining sciences & geomechanics abstracts	**Rightsholder**	Elsevier Science & Technology Journals
		Publication Type	Journal
Article Title	Room and pillar retreat mining. A manual for the coal industry : Kaufman, P W; Hawkins, S A; Thompson, R R US Bureau of Mines report IC 8849, 1981, 228P : Kaufman, P W; Hawkins, S A; Thompson, R R US Bureau of Mines report IC 8849, 1981, 228P	**Start Page**	59
		Issue	3
		Volume	19
Date	12/31/1972		
Language	English		
Country	United Kingdom of Great Britain and Northern Ireland		

REQUEST DETAILS

Portion Type	Image/photo/illustration	**Distribution**	United States
Number of images / photos / illustrations	1	**Translation**	Original language of publication
Format (select all that apply)	Print, Electronic	**Copies for the disabled?**	No
Who will republish the content?	Author of requested content	**Minor editing privileges?**	Yes
Duration of Use	Life of current edition	**Incidental promotional use?**	No
Lifetime Unit Quantity	Up to 499	**Currency**	USD
Rights Requested	Main product		

NEW WORK DETAILS

Title	Numerical Modeling of Pillar Stress Redistribution During the Retreat Mining Process	**Institution name**	Colorado School of Mines
		Expected presentation date	2021-08-12
Instructor name	Rahel Dean-Pelikan		

ADDITIONAL DETAILS

Order reference number	N/A	**The requesting person / organization to appear on the license**	Rahel Dean-Pelikan

REUSE CONTENT DETAILS

Title, description or numeric reference of the portion(s)	Figure 2	**Title of the article/chapter the portion is from**	Room and pillar retreat mining. A manual for the coal industry : Kaufman, P W; Hawkins, S A; Thompson, R R US Bureau of Mines report IC 8849, 1981, 228P : Kaufman, P W; Hawkins, S A; Thompson, R R US Bureau of Mines report IC 8849, 1981, 228P
Editor of portion(s)	N/A	**Author of portion(s)**	N/A
Volume of serial or monograph	19	**Issue, if republishing an article from a serial**	3
Page or page range of portion	4	**Publication date of portion**	1981-12-31

Permission to use Figures from Dissertation in M.Sc. Thesis Inbox ×

Rahel Dean-Pelikan <rdeanpelikan@mymail.mines.edu>
to Sankhaneel

Hi Neel,

I am emailing to request permission to use Figure 1.3 in my thesis.

Thank you,

Rahel Dean-Pelikan

Sankhaneel Sinha
to me

Hi Rahel,

Thank you for the email. I grant you permission to use the figure.

-Sankhaneel.

•••

--

Sankhaneel Sinha, Ph.D.
Post-Doctoral Fellow
Geology and Geological Engineering
Colorado School of Mines
Golden,Colorado
https://geomech.mines.edu/

U.S. Geological Survey Response [Ticket#600002] Permission to use figures from a publication in Masters thesis. External Inbox ×

USGS Answers Incoming <answers@usgs.gov> 8:21
to me

Good morning,

USGS produced materials are public domain and may be used without permission. It is requested that proper credit is given. Please see the Copyrights and Credits page for a complete statement and citation examples.

Regards,

Will
USGS

Please take a moment to tell us how we did!

U.S. Geological Survey
Science Information Services
Toll Free 1-888-ASK-USGS
You can contact us live on Webchat Find us on Facebook and Twitter and see other USGS social media accounts.

[External] RE: Copyright Request

Hide message history

From: Gabriel Walton [mailto:gwalton@mines.edu]
Sent: Tuesday, August 3, 2021 12:41 PM
To: Peter Smeallie <peterhsmeallie@gmail.com>
Cc: Rahel Dean-Pelikan <rdeanpelikan@mymail.mines.edu>
Subject: Copyright Request

Hi Peter,

Rahel (cc'd) is an M.Sc. student who is about to defend her thesis. One of her chapters includes some material originally published as "Numerical Modeling of Pillar Stress Redistribution during the Retreat Mining Process" in the proceedings of ARMA 2020 (the publication of the material as part of the ARMA proceedings will be acknowledged in the thesis). I am writing to formally request that you, in your role as Executive Director of ARMA, grant us permission to include this material in Rahel's thesis.

Thank you in advance to your attention to this request.

- Gabe

[External] RE: Copyright Request

From: Peter Smeallie <peterhsmeallie@gmail.com>
Sent: Tuesday, August 3, 2021 2:58:25 PM
To: Gabriel Walton <gwalton@mines.edu>
Subject: [External] RE: Copyright Request

Dear Gabe,

You have ARMA's permission to use the material described below with proper attribution.

Best,

Peter